TÉCNICO LISBOA

Numerical modeling and validation of a Chemical Reactor Network for NH_3/H_2/air flames and theoretical evaluation of the Rich-Quench-Lean implementation

Francisco Manuel Freitas Mesquita Guimarães

Thesis to obtain the Master of Science Degree in

Mechanical Engineering

Supervisors: Prof. Pedro Jorge Martins Coelho
Prof. Miguel Abreu de Almeida Mendes

Examination Committee

Chairperson: Prof. José Manuel da Silva Chaves Ribeiro Pereira
Supervisor: Prof. Miguel Abreu de Almeida Mendes
Member of the Committee: Prof. Edgar Caetano Fernandes

December 2021

Acknowledgments

My thanks go, first of all, to my supervisors, Prof. Miguel Mendes and Prof. Pedro Coelho, for the help they provided me in working on this dissertation and for all the suggestions and corrections they gave me, which were of great use and benefit to me. In a very special way I also thank Rodolfo Rocha, who followed my work particularly closely and from whom I learned a lot, for the patience with which he generously gave me many hours of his time and clarified any doubts that arose.

I would like to thank Miguel Franco and Gonçalo Pacheco for the support they also gave me at various times, and for the material and information they made available to me, with great generosity; and Ana Isabel Ferreiro, for the free initiative and availability she showed in helping me work with the *Cantera* program; and Mr. Manuel Pratas, for his help in the lab work, always available to clarify questions or to lend a hand assembling something and having the material ready in time.

Thanks to all those in the *Cantera* user community who have been very prompt in answering several of my questions regarding the use of this open-source program, among them particularly Thomas Indlekofer, Steven DeCaluwe, Bryan Weber, Ray Speth, and Weiqi Ji.

I also thank my friends, several of them also in the same situation as me, who have been interested in the progress of my work and have encouraged me with great humor and often with truly useful suggestions and advice. Particularly to everyone at the Montes Claros University Residence, especially the directors, where I finished my bachelor's and master's degrees, and from where I have very fond memories and friendships.

Finally, and mainly, I thank God and entrust to Him this completed stage. And to my parents and siblings for the affection they have always shown and the attention they have paid to my work. A special mention to João Paulo, who gave me invaluable help with the time-consuming work of filling in tables and organizing the bibliographical references.

Resumo

O amoníaco (NH_3) tem surgido como um promissor combustível alternativo. A sua composição química isenta de carbono permite uma queima livre de CO_2. Baixa reactividade e emissões de NO_x e NH_3 não queimado, tóxico, são os principais problemas relativos à combustão de NH_3. Alguns inconvenientes deste combustível - fraca reactividade, baixa velocidade da chama, elevado tempo de atraso à ignição e dicícil estabilização de chama - podem ser parcialmente ultrapassados adicionando H_2. Para estudar as emissões mais importantes da combustão desta mistura - NO_x, NH_3 e H_2 - foi desenvolvido um modelo de Rede de Reactores Químicos para representar um queimador, estabilizado através do uso de corpo não fuselado e rotação de ar, para o qual existem dados experimentais sobre temperaturas e concentrações de espécies para várias chamas. O modelo foi desenvolvido tendo em conta características aerodinâmicas e geométricas do queimador e de modo a prever a temperatura, pressão, tempo de residência, espécies químicas e eficiência de combustão. O modelo é comparado com resultados experimentais e os desvios são discutidos. Há uma correcta previsão de tendências qualitativas relacionadas com a variação da potência térmica, razão de equivalência e fracção molar NH_3 no combustível. Entretanto, há imprecisões na previsão de valores absolutos de NO_x, NH_3 e H_2, sendo isso abordado. Finalmente, é incluído no modelo um estágio secundário de injecção de ar, para prever teoricamente as melhores condições para um queimador com estagiamento de ar, utilizado para diminuir as emissões de NO_x, NH_3 e H_2 mantendo uma elevada eficiência global de combustão.

Palavras-chave: Combustíveis alternativos, Amoníaco, Hidrogénio, Chama estabilizada, Rede de Reactores Químicos, Queimador de Estagiamento de ar.

Abstract

Ammonia (NH_3) has emerged as an alternative fuel for important combustion applications. Its carbon-free chemical composition allows for zero-CO_2 burning, therefore preventing from relevant greenhouse gases emissions. Low reactivity, the emission of NO_x and unburnt NH_3, which is toxic, are the biggest issues concerning NH_3 combustion. Some drawbacks of the use of NH_3 as fuel - weak reactivity, low flame speed, high ignition delay time and hard flame stabilization - can be partially overcome by adding H_2. To study the most concerning combustion emissions of this type of mixture - NO_x, NH_3 and H_2 - the Chemical Reactor Network modelling method was chosen to model a swirl and bluff-body stabilized burner, for which experimental data on temperatures and chemical species is already documented in previous works. Thus, a model of Perfectly Stirred Reactors and a Plug-Flow Reactor was developed, taking into account aerodynamic and geometric characteristics of the burner and being able to predict temperature, pressure, residence time, chemical species and combustion efficiency. The model was validated against experiments and discrepancies are addressed. It shows good agreement with experiments on predicting qualitative trends related to variation of thermal input, equivalence ratio and NH_3 mole fraction in fuel. However it fails on predicting accurately quantitative values of NO_x, NH_3 and H_2, which is discussed. Finally, the model is extended to include a secondary air injection stage, to theoretically predict optimal conditions for a Rich-Quench-Lean combustor, a method used for the decreasing of NO_x, NH_3 and H_2 emissions, while securing high overall combustion efficiency.

Keywords: Alternative fuels, Ammonia, Hydrogen, Stabilized flame, Chemical Reactors Network, Rich-Quench-Lean combustor.

Contents

List of Tables

List of Figures

Nomenclature

Acronyms

CFD	Computational Fluid Dynamics.
CRN	Chemical Reactor Network.
CRZ	Center Recirculation Zone.
dv	Dry volume.
FZ	Flame Zone.
HRR	Heat release rate.
IRZ	Inner Recirculation Zone.
LES	Large Eddy Simulation.
LZ	Lean Zone.
MFC	Mass flow controller.
ODE	Ordinary Differential Equation.
ORZ	Outer Recirculation Zone.
PC	Pressure controler.
PFR	Plug-Flow Reactor.
PFZ	Post-Flame Zone.
PSR	Perfectly-Stirred Reactor.
QZ	Quench Zone.
RANS	Reynolds-Averaged Navier–Stokes equations.
RQL	Rich-Quench-Lean.
RT	Residence time.
SNCR	Selective Non-Catalytic Reduction.

TI Thermal input.

V Valve.

Greek symbols

α Mass flow splitting coefficient.

ϵ Emissivity.

κ Thermal conductivity coefficient.

ϕ Equivalence ratio.

ρ Density.

Roman symbols

N Natural number.

U Heat transfer coefficient.

x Mole fraction.

p Pressure.

Subscripts

∞ Environment condition.

i, j, k Indexes.

avr Average.

ext Exterior.

int Interior.

ovr Overall.

pri Primary.

ref Reference condition.

sec Secondary.

Superscripts

e Experimental.

f Forward direction.

n Numerical.

r Reverse direction.

Chapter 1

Introduction

1.1 Motivation

The last few years have been marked by a growing global awareness of the ecological issue, particularly concerning the environmental impact of human action. The current energy needs of an increasingly industrialized and globalized world and the continuing challenge to achieving the best performance have sometimes neglected the negative impact of possible damage to nature, which has consequences on people's life quality. According to the International Energy Agency (IEA) [1], the growth rate of world energy demand has almost reached 14300 Mtoe in 2018, being Oil, Coal and Natural Gas the most demanded energy sources worldwide (Figure 1.1).

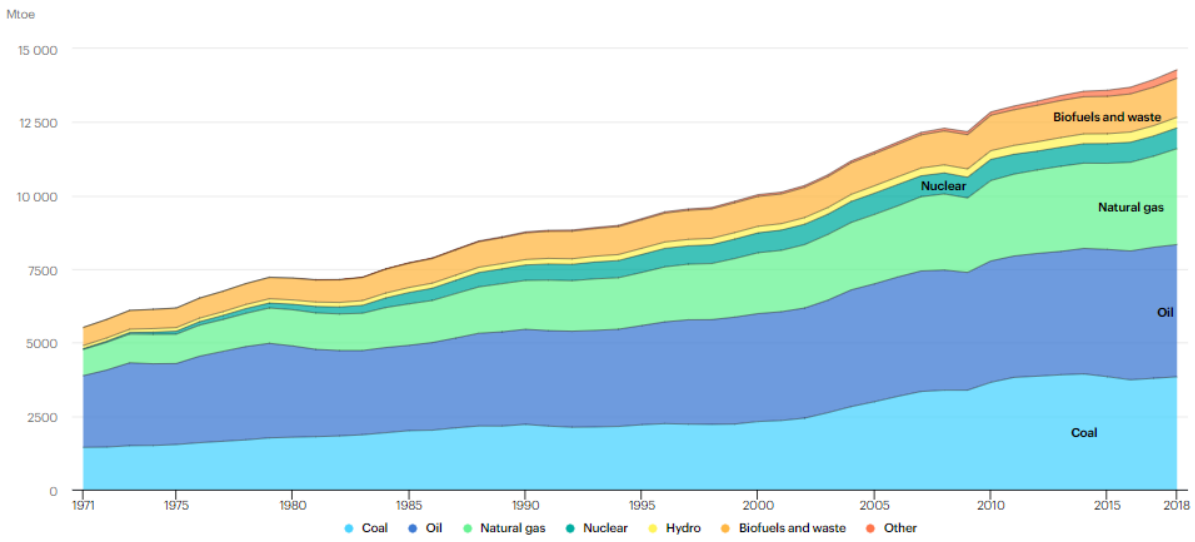

Figure 1.1: World energy outlook (1971-2018). Reprinted from [1].

Figure 1.2 shows the total final energy consumption by each sector, pointing out Industry, Transport and Residential as those with greater energy consumption, that continues to increase.

Although this growing demand and consumption of energy has as a positive cause the improvement in

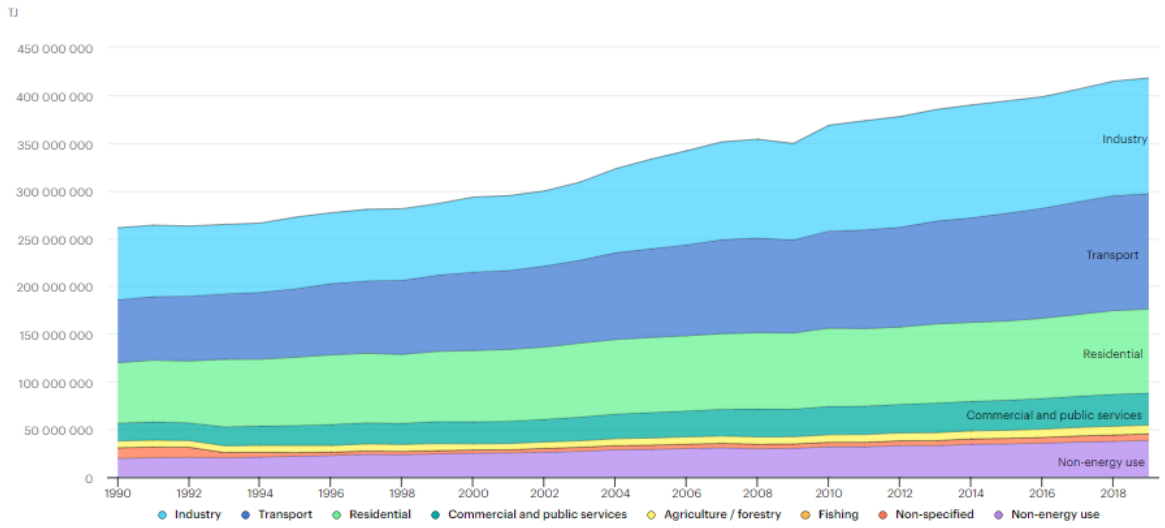

Figure 1.2: Total final energy consumption by sector. Reprinted from [1].

the quality of life of people who benefit from it, it cannot be disregarded the negative impact that obtaining and consuming these energy resources may have, in the medium or long term, on this same quality of life of people, mainly due to environmental pollution. One of today's most relevant undesirable gases is CO_2, whose large-scale emission, through the combustion of hydrocarbons that make up the vast majority of conventional fuels, seems to have, according to the majority of the scientific community [2, 3], a considerable contribution to the increase in the global greenhouse effect. According to the IEA, as shown in Figure 1.3, the sectors most responsible for CO_2 emission are prominently power generation through coal burning, Industry and Transport.

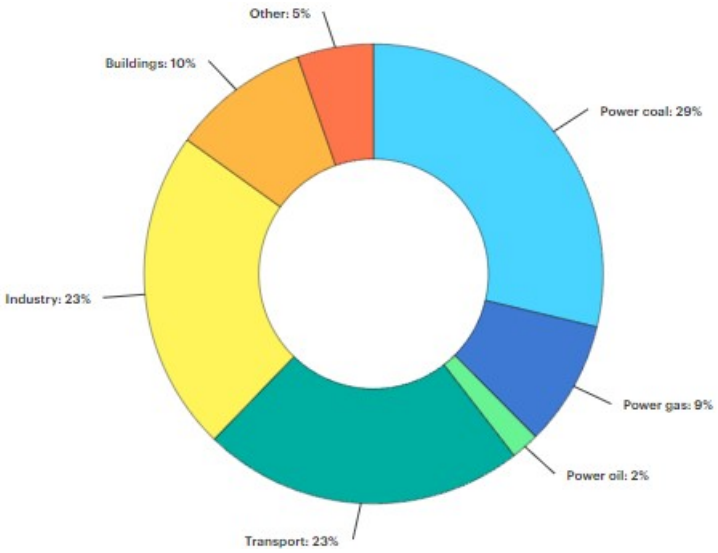

Figure 1.3: Global energy-related CO_2 emissions by sector. Reprinted from [1].

To reduce carbon emissions in energy production some alternatives have been pointed out. The renewable energy sources - wind, solar, hydro, tides, waves, and geothermal - are zero-carbon sources that show promising place on this running. However some important limitations, as it is the inconstant energy

production due to the dependence on climatic and geological conditions, have prevented the viability of this alternative of energy production. Considering the fact that combustion currently remains the main way to obtain energy, in practically all sectors of human activity, and that it is most reasonable for this trend to continue, one of the alternatives that has also attracted the attention of researchers is the use of less polluting fuels, especially in terms of carbon release pollution, thus minimizing the negative impact of this globally well-established energy source.

Table 1.1: Thermal properties and combustion characteristics of ammonia and hydrocarbon fuels. Reprinted from [4].

Fuel	**NH_3**	**H_2**	**CH_4**	**C_3H_8**
Boiling temperature at 1 atm (℃)	-33.4	-253	-161	-42.1
Condensation pressure at 25℃ (atm)	9.90	N/A	N/A	9.40
Lower heating value, LHV (MJ/kg)	18.6	120	50.0	46.4
Flammability limit (Equivalent ratio)	0.63∼1.40	0.10∼7.1	0.50∼1.7	0.51∼2.5
Adiabatic flame temperature (℃)	1800	2110	1950	2000
Maximum laminar burning velocity (m/s)	0.07	2.91	0.37	0.43
Minimum auto ignition temperature (℃)	650	520	630	450

Thus, the fuel that seems to meet the best conditions in terms of emissions is hydrogen (H_2), due to its carbon-free constitution and good combustion performance. Hydrogen meets most of the characteristics of a good fuel since it has a high calorific value, a high reactivity demonstrated by the high flame speed, a low auto-ignition temperature, very low ignition delay time and a high adiabatic flame temperature. The major disadvantages of this fuel are mainly related to storage, transportation and safety issues. The very low boiling temperature at atmospheric pressure (-252.9 ºC), combined with a low volumetric energy density, require hydrogen to be stored and transported at very high pressures, which entails large associated energy consumption and costs. Also the high reactivity of hydrogen can be a major hazard if systems leak.

Along with hydrogen, ammonia (NH_3) has also been touted as a promising alternative to fossil fuels. The use of this chemical as a fuel is not a recent discovery although interest has now resurged due to the fact that it is also carbon neutral. The major challenge in adopting ammonia as a fuel is due to certain disadvantageous combustion characteristics of this chemical: it has low calorific value, poor reactivity, low flame speed, high ignition delay time and a narrow range of flammability limits. Along with this, the toxicity of ammonia can also be a major problem if burning is inefficient or if there are leakage problems. Nevertheless, the large amount of hydrogen present in NH_3 makes it a promising H_2 carrier. Taking advantage of this characteristic, one of the solutions that have been pointed out as promoting the combustion of NH_3 is its cracking into H_2 with the consequent burning of the mixture of both fuels, thus compensating each of the fuels for the deficiencies of the other in a complementary manner. In this way it is also possible to take advantage of the great advantages of NH_3 in terms of production, storage and transport. Being NH_3 the second most produced chemical in the world (180 M tons annually) [5], especially used in fertilizers for agriculture, its storage and transport are already well established worldwide, with the appropriate infrastructures. Allied to this, the fact that the boiling temperature and

condensation pressure of NH_3 are quite similar to those of propane (C_3H_8), as shown in Figure 1.1, the storage and transportation structures used for the latter can also be used for the former [4]. The NH_3 synthesizing process used on a large scale is the well-known Haber-Bosch process, which consists of the catalytic reaction of hydrogen with nitrogen at high pressures (10-25 MPa) and not very high temperatures (450-600 ℃) [5]. Currently the hydrogen used in this process is produced through steam reforming of methane or coal gasification, which thus implies that overall, ammonia is not completely carbon neutral. However, another possibility for producing NH_3 is through electrolysis, and in this way it is possible to combine its production with renewable energy sources, mainly by taking advantage of excess energy produced by these sources [6].

Regarding the emissions issue, the main pollutant emitted by the combustion of both H_2 and NH_3 are nitrogen oxides (NO_x), both toxic and ozone-layer depleting, which are generally produced at high temperatures and in the presence of considerable amounts of nitrogen (N) and oxygen (O). Currently, research on this fuel has focused particularly on this aspect, looking for ways to decrease these emissions in order to comply with the regulations imposed and in order to make it viable to use this fuel in certain applications. The present thesis intends to be a contribution to the advancement of this work.

1.2 Literature review

1.2.1 Theoretical and experimental studies on ammonia combustion

The first known systematic study of ammonia combustion goes back to 1809, developed by W. Henry [7], who wanted to perform the decomposition of ammonia. At that time the author pointed out the difficulty of finding the correct ratios of ammonia and oxygen to attain combustion. He also mentioned the slow-burning of ammonia, described the products of combustion and indicated some visible characteristics of flame.

In the 1930s the Italian company Ammonia Casale Ltd. patented a system for the partial thermal decomposition of ammonia. Based on the later patents, a new process, named Gazamo, was developed and covered by the patents of E. Kroch and J.L. Restieau. The Gazamo process consisted of the burning of ammonia in the air, assisted by the addition of coal gas with a significant percentage of hydrogen to facilitate the ignition. This was probably the first practical application of ammonia combustion for power at a major scale, only preceded by applications of the Casale system at a smaller scale. Krock reported [8] that the first use of ammonia as a motor fuel was implemented in Belgium buses, in 1943, in the middle of World War II. The scarcity of diesel oil and other main fuels due to the wartime circumstances made it inevitable to find alternative fuels to cope with the buses' fuel needs. Some solutions were pointed out, namely using compressed coal gas and producer gas, but they were not feasible, due to the low energy density of both fuels, which furthermore required larger fuel containers. A better solution came with the adaptation of the Gazamo process to the buses' motors, using ammonia combined with coal gas to enhance combustion. Three main advantages of ammonia fuel are attested: it requires less air to burn than some main hydrocarbon fuels; the great expansion due to combustion, very desirable for internal combustion engines; the endurance to high compression rates, which prevents from the knock. The author also states that, according to the results of one year of use and thousands of miles covered, there was no power loss relative to gas-oil use, nor corrosion or an additional need for lubrication. He summarizes that great performance was achieved and also proposes the replacement of coal with hydrogen.

This successful utilization of ammonia fuel promoted the further scientific study of the characteristics of its combustion and of the main applications that could be the most appropriate for the new fuel. An important contribution to that research came in the 1960s with the Energy Depot Project promoted by the US Army, intending to find new types of fuels that could be used in the lack of petroleum supplies and thus produced at a large scale, derived from the elementary substances, air and water. Hydrogen and ammonia were pointed out as the principal ones. Some authors responded to this research proposal. In 1965, Cornelius et al.[9] [10], from Research Laboratories - General Motors Corp. developed a very thorough study on the application of ammonia in military use as fuel and tested it for spark-ignition (SI) reciprocating engines. The authors present the main issues that may be taken into account of that use since when compared with the conventional fuels, like gasoline, ammonia has a low heat of combustion, a narrow flammability range, fairly difficult ignition, and shows low flame speed. Some solutions were

presented to overcome these drawbacks: use of supercharging, high compression ratios, and partial dissociation of the ammonia before induction. Another solution that is suggested is the addition of another substance that could enhance the combustion, being hydrogen the most attractive proposal.

Starkman and Samuelsen [11] also sustained by the US Military, released in 1967 an important analysis on the ammonia fuel based on experiments developed in a Cooperative Fuel Research (CFR) engine, an instrument used to test the performance of fuels and lubricants for internal combustion engine purposes, concluding that the shorten flammability limits were primarily due to the low flame speed and that the pre-dissociation of ammonia was a key point for the successful ignition of the mixture. These authors also observed that there was more NO_x in the exhaust than expected, which could not be attributed only to the thermal NO_x formation. They concluded that the high quantities of NO_x were mainly a result of the pyrolysis of ammonia.

In the gas turbine field experiments with ammonia also started to be done and, also in 1967, Pratt et al. [12] carried out a research project, based on theoretical and experimental investigations, that aimed to understand the scaling and combustion characteristics of gaseous ammonia-fired gas turbines. They recognized that the principal problem of fueling gas turbine combustors with ammonia was its low reactivity with air when compared with hydrocarbon fuels. This led to a reduction in airflow to increase residence times and allow for proper reaction, with the negative effect of combustion efficiency loss. The solution proposed was the correct design of the combustor, with a small fuel nozzle to create an intense fuel jet in the primary zone and at least two combustors in parallel instead of only a larger one. It was also pointed out that two other important solutions can be obtained chemically, by cracking ammonia or using additives.

Still, in 1967, Verkamp et al. [13] performed experimental tests to verify minimum ignition energy, quenching distance, stability limits, and performance of an ammonia-air flame in a gas turbine burner. Minimum ignition energy and quenching distance were found to be fairly greater than the corresponding values related to propane-air flame. The stability was attained for a narrow range of equivalence ratios and at a relatively low air velocity when compared to hydrocarbon fuels. The conclusion was that ammonia could not replace the hydrocarbon fuels in the conventional gas turbine combustors. The solutions adopted to facilitate ammonia burning were those already mentioned: the pre-partial-dissociation of ammonia and the use of additives. The latter was tested using 5% concentration by volume of additives in the total fuel mixture, without improvements. On the contrary, 28% of dissociated ammonia mixture proved to present the approximately same flame characteristics as hydrocarbons, both in flame-stability apparatus and in gas turbine experiments. The conclusion was that 28% of dissociated ammonia could be used as an alternative in gas turbines optimized to conventional fuels.

The attention given to ammonia fuel during the Energy Depot period had a decline in the years that followed, largely due to the various drawbacks of operating with ammonia and its poor combustion effi-

ciency raised in the aforementioned and other similar research studies. In the 1970s and for almost two decades ammonia combustion science knew almost no advancements although ammonia continued to be used in some combustion studies about the production and reduction of NO_x [4]. After that, only in the 1990s did it attract scientists again, mostly driven by the ambition to reduce emissions and to observe the increasingly tighter restricting regulations on that matter. Since then the scientific study of ammonia combustion has been growing, following which had been referred to in the previous works and looking for ways of overcoming those challenges.

The application to internal combustion engines dominated the first stage of investigations in the revival of the field. In 2008, Reiter and Kong [14] released a paper stating the feasibility of using ammonia blended with diesel in compression-ignition (CI) engines, as a solution to carbon emissions reduction. The dual-fuel approach was the important factor to overcome the difficulty of ammonia autoignition. The only modification introduced was in the intake manifold, adding a fuel duct for ammonia, with no need to change the diesel fuel injection system. Experiments were done for some engine speeds and loads, using distinct diesel/ammonia ratios and the peak engine torque was obtained for various of these different ratios. The authors measured a maximum energy replacement by ammonia of 95% and observed the best fuel efficiency was obtained for the range of 40-80% of ammonia energy ratio. Concerning the emissions, it was shown that CO_2 was reduced with the ammonia increasing, for the same engine torque, in a relation of near proportionality with the ammonia energy ratio (Figure 1.5). Emissions of NO_x were reduced for an ammonia energy ratio lower than 60%, which the authors explained by the low flame temperature and the NO_x reduction effect by ammonia adding (Figure 1.4). Biodiesel was also used with success for different biodiesel-ammonia ratios and results showed similarity with diesel-ammonia ones.

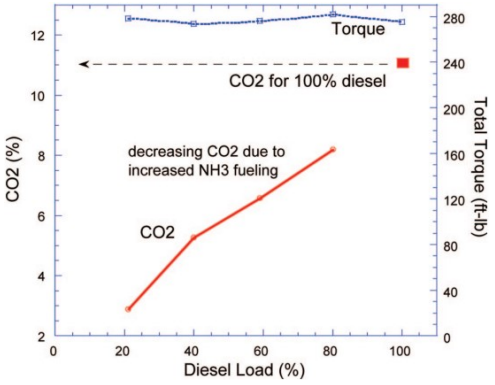

Figure 1.4: CO_2 emissions for diesel-ammonia combustion at 1000 rpm under peak torque conditions at various diesel loads. Reprinted from [14].

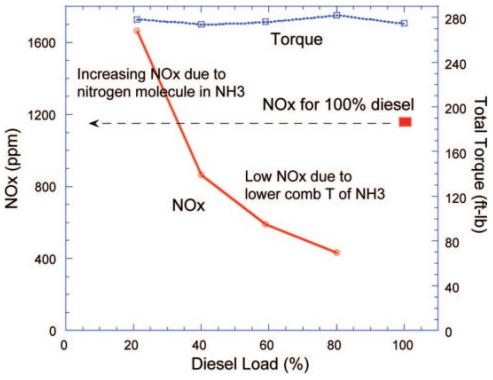

Figure 1.5: NO_x emissions for diesel-ammonia combustion at 1000 rpm under peak torque conditions at various diesel loads. Reprinted from [14].

The same authors published another article [15] in 2011 based on the previous investigations and with the same experimental apparatus, consisting of a four-cylinder, turbocharged, compression-ignition engine. This time they were especially interested in verifying exhaust emissions values for some diesel-ammonia ratios/fueling combinations in a dual-fuel approach when compared to pure diesel fuel usage for two operating conditions: operation with constant engine power for various diesel-ammonia combi-

nations and operation with different engine power for a small fixed diesel quantity and variable amounts of ammonia. The results demonstrated, for the constant power output, that both carbon monoxide (CO) and hydrocarbons (HC) were higher in flue gases for the dual-fuel usage: the main reason pointed out was the more incomplete combustion with ammonia usage, due to its lower heating value and flame temperature. On the other hand, soot emissions could be reduced when more ammonia was used, due to the lower amount of carbon presented. Low values of NO_x emissions were obtained unless the ammonia fuel energy was higher than 40% of the total fuel energy; for the latter case, the NO_x in the exhaust increased greatly due to fuel-bound nitrogen. It was also highlighted that although the overall conversion efficiency of ammonia was high, nearly 100%, the levels of ammonia presented in the flue gases were also high, ranged from 1000 to 3000 $ppmv$, which might be solutioned further after-treatment, due to the toxical characteristics of ammonia. For the variable engine power operating condition, it was observed poor fuel efficiencies and great amounts of ammonia in the exhaust. It was also verified to be a decrease of peak cylinder pressure which was explained by the lower combustion temperature of ammonia.

Morch at al. [16] investigated the use of ammonia-hydrogen blends as fuel for SI-engines by performing tests for various excesses of air and different relative amounts of ammonia and hydrogen. The authors concluded that these mixtures are a very suitable fuel for this type of engines, preferably using higher compression ratios, due to the high octane rating of ammonia and hydrogen. It is also suggested that the use of exhaust gas heat may overcome the difficulty in igniting ammonia. The authors further reported that higher NO_x values were obtained in the exhaust gas for higher hydrogen content, for an excess air ratio between 1.1 and 1.4, due to the high temperature resulting from hydrogen combustion, which strongly promotes the thermal-NO_x pathway. The solution pointed out for the reduction of NO_x emissions is the use of the SCR post-combustion process.

Ryu et al. [17] studied the possibility of using an ammonia dissociation catalyst to improve the performance of an SI-engine powered by an ammonia-gasoline fuel, by dissociating ammonia into hydrogen and consequently improving combustion. The results obtained demonstrated more effective catalyst-driven ammonia-hydrogen dissociation at low to medium ammonia flow rates, with increased engine power, reduced fuel consumption, and significantly reduced CO, HC, NH_3, and NO_x emissions.

The stationary gas turbine (GT) sector has also been attracted by the potential of ammonia blends combustion and is currently one of the most promising fields for ammonia fuel adoption. Several studies have been addressed in the last years and various are in development at the present. Laboratory-scale swirl burners are often used in these studies, as they are designed to induce a rotating, *swirling* effect in the flow that approximates GT incinerator conditions. Unlike reciprocating engines, a crucial issue for gas turbines is flame stability, due to the continuous flow nature [18]. When fueling a gas turbine with ammonia, a major complication is flame stabilization, since it is well known that ammonia is weak-reactive, with low flame speed and low heating value.

To study stabilized combustion of ammonia Meyer et al. [19] proposed and analyzed a burner with swirl vanes and self-sustained heat exchange, concluding that the recirculation induced by the swirl stabilizer device proportionates quite lower NO_x emissions and efficient combustion.

Some Japanese researchers, supported by the national project Cross-ministerial Strategic Innovation Promotion Program (SIP): "Energy Carriers", have also made important progress in this field of research, particularly concerning ammonia combustion in stationary gas turbines. A very relevant project was carried out by a research group supported by the National Institute of Advanced Industrial Science and Technology (AIST) in Japan. Iki et al. [20], in 2015, released the first approach to use a gas turbine for power generation supplied by kerosene and ammonia. A prototype diffusion-combustion micro gas turbine adapted to enable dual-fuel supply is used to perform some co-firing tests of kerosene and ammonia, starting with kerosene firing until a stable power is achieved and then the addition of ammonia at a gradually increased flow rate. The co-firing was successfully attained but it was confirmed that adding ammonia greatly increased the amounts of NO_x in the combustion products, which can be reduced, as the authors suggested, by selective catalytic reaction (SCR) at post-combustion.

In the same investigation program and based on the previous works, in 2017, Kurata et al. [21] published detailed results on the effectiveness of applying SCR for NO_x reduction, following what was presented as a solution in the aforementioned article [20]. A heat-regenerator was added to the micro gas turbine to improve ammonia combustion efficiency and flame stability, increasing inlet temperatures. NO_x emission values were lower than 10 ppm, despite the typical high NO_x emissions in this combustor type, which was stated to be a consequence/effect of SCR and regenerator application. A drawback was the requirement of large-size SCR equipment to successfully decrease NO_x emissions.

Hayakawa et al. [22] carried out an investigation on the fundamental product gas characteristics of an ammonia/air laminar flame for several equivalence ratios and increasing pressures, based on experimental and numerical studies. The experimental work was performed using a stagnation flame configuration to avoid the use of a pilot flame or chemical species to enhance flame stabilization. It was concluded from experiments that the increasing of the equivalence ratio had the positive effect of decreasing NO_x emissions. Furthermore it was also reported that the increase in mixture pressure also decreased the maximum value of the NO mole fraction. The authors also reached the conclusion that a target equivalence ratio of 1.06 should be attained for a simultaneous reduction of both NO and unburnt ammonia, which has a major relevance for the emission control in rich-lean two stage combustors.

Alongside the Japanese research group, another group at Cardiff University, has been contributing with important efforts in the field of ammonia-fueled gas turbines. After a first successful test to fuel a swirl combustor [23], designed for gas turbine studies, with ammonia and methane Valera-Medina et al. [24] tested mixtures of ammonia/hydrogen fuel, to completely avoid carbon emissions. Experiments were done with a fuel of 50:50 (vol.%) ammonia/hydrogen blend, under lean conditions, for a thermal

power around 31 kW. Flame stability was achievable for a relatively narrow range of equivalence ratio ($0.43 < \phi < 0.52$). Very high NO_x levels were obtained, in thousands of ppm for $\phi > 0.5$. Chemiluminescence tests showed qualitative evidence for the fast and earlier burning of hydrogen, very close to the burner mouth. A numerical study was also elaborated in parallel to the experimental one through the Chemical Reactor Network approach, adopting Tian's mechanism [25]. The simulation results corroborated the sooner burn of hydrogen and estimated the principal intermediate radicals and underlying reactions of the consumption of ammonia and hydrogen. The authors suggested the adoption of low-swirl burners to allow larger residence times for ammonia oxidation improvement and apply stratified hydrogen injection to , and thus improve stable operation.

The mixture of ammonia and hydrogen has become one of the most attractive fuels among mixtures of ammonia with other substances, not only because it is a carbon-free mixture but also because the high reactivity and flammability of hydrogen compensates for these poor properties in ammonia, which in turn mixed with hydrogen makes it a safer fuel. Some strategies for NO_x reduction were also projected. One of those, particularly promising for the burning of ammonia-hydrogen blend in stationary gas turbines is the Rich-Quench-Lean (RQL) configuration. This combustor concept was firstly proposed in 1980, by Mosier and Pierce [26], with the specific target of reducing NO_x emissions in gas turbines. Since then RQL gas turbines have been commercially available and also submitted to several design modifications.

Feitelberg and Lacey [27], from General Electrics, reported in 1998 a successful adaptation and operation of a RQL gas turbine combustor (RQL2) for low heating value (LHV) fuel and specially designed for low conversion of fuel-bound nitrogen into NO_x, with the additional advantage of being easily adaption for natural gas or liquid fuel supply. RQL2 was tested with LHV fuel supplied by a pilot scale coal gasification and high temperature desulfurization system. At the optimum rich stage equivalence ratio the levels of NO_x emissions were reduced by a factor of more than 3 in comparison with a standard combustor burning the same fuel, which, for 4600 $ppmv$ NH_3 in the LHV fuel corresponds to a conversion of 5% of NH_3 to NOx. They also found that NO_x emissions increased with departure from the optimal conditions.

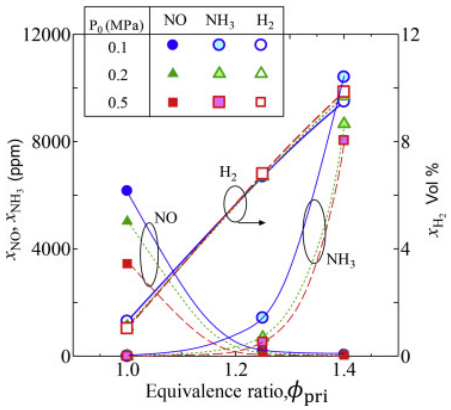

Figure 1.6: Variation in emissions of NO, NH_3 and H_2 in turbulent NH_3/air flames with equivalence ratio, ϕ, and pressure, P_0. Reprinted from [28].

Recent studies have been conducted to examine the effectiveness of staged combustion in stationary gas turbine combustors fueled by ammonia-hydrogen blend. This staged combustion did not always obey the RQL configuration pattern due to the inexistence of the quenching zone.

In 2017, Somarathne et al. [28] conducted a numerical study, using Large Eddy Simulation (LES), on the performance of a secondary air high-pressure injection to promote lower NO_x, unburnt NH_3 and H_2 emissions for premixed NH_3/air turbulent flames. The authors reported that a key factor for attaining overall minimum NO_x, NH_3 and H_2 was the equivalence ratio in the primary zone. This zone should be maintained at or slightly below the specific equivalence ratio that grants minimum emissions, without regard to secondary air injection. The little NO_x and high NH_3 and H_2 emission values characteristic from rich combustion lead to higher NO_x values but almost zero NH_3 and H3 at the exit of the secondary stage, due to the NH_3 and H2 reburning in high oxygen concentration in this later stage. The authors also found that minimal emission levels of NO_x and NH_3 were obtained for equivalence ratio of 1.2, as it is shown in Figure 1.6. With secondary air injection the study realized a drop in the NO_x level by half, while NH_3 and H_2 were completely consumed, which is presented in Figure 1.7.

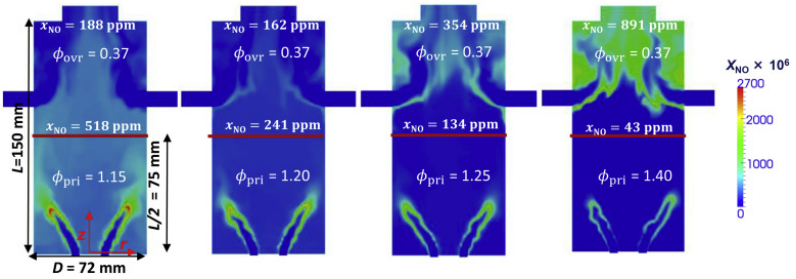

Figure 1.7: NO_x results for two-staged combustor. Reprinted from [28].

Kurata and co-workers, mentioned above in this text, have also produced important experimental research in the air-staged GT combustor field. By adapting a 50 kW micro gas-turbine (Figure 1.8), Kurata et al. [21] [29] developed a non-premixed combustor for allowing two-stage, rich-lean, NH_3/air combustion. In an initial stage of experiments [21] the authors reported successful and stable operation for a wide range of power (18.4 to 44.4 kW) and rotational speeds (70 000 to 80 000 rpm), and quite good combustion efficiency for higher power-generation operating conditions, i.e., for 80 000 rpm (89 to 96%). Regarding the emissions, the experimental results suggested the particular significance of the combustor inlet temperature (CIT) for the emission of NO_x and unburnt NH_3 as it is shown in Figure 1.9. Moreover, it was presumed that both local rich and lean regions exist in the primary zone, being the rich regions responsible for unburnt NH_3 release and lean regions, at higher temperatures, responsible for NO_x production. It was also expected that the presence of additional dilute air in the secondary combustion zone could allow unburnt NH_3 to react with NO via the selective non-catalytic reduction (SNCR) process, thus resulting in a reduction of NO.

More recently, in 2019, the same authors [29] undertook some important modifications on the two-staged combustor rig that significantly lowered NO_x emissions and increased the operating power range. Those

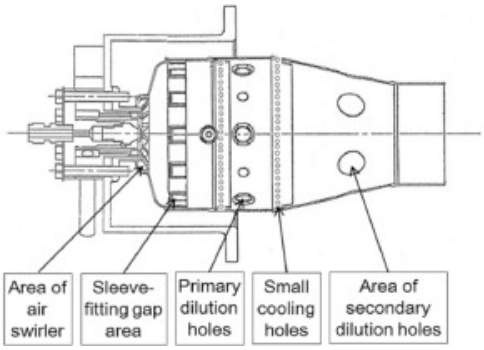

Figure 1.8: Modifications applied to the base combustor. Reprinted from [29].

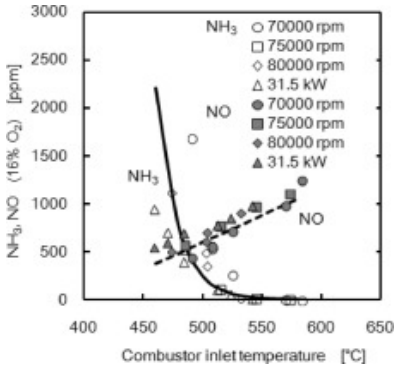

Figure 1.9: The variation of NO_x and NH_3 emissions with combustor inlet temperature for a single ammonia-fueled micro gas turbine. Reprinted from [29].

modifications were the removal of primary dilution holes, the decreasing of swirler area, the increasing of secondary dilution holes area, and the use of inclined fuel injection. The main reasons for those alterations were to avoid air dilution in the primary zone and enhance the fuel-air mixing. Experimental results corroborated the effectiveness of the newly manufactured combustor since the NO_x emissions were lowered to 337 ppm (16% O_2), about one-third of that of the base system, and also unburnt NH_3 and N_2O have simultaneously decreased.

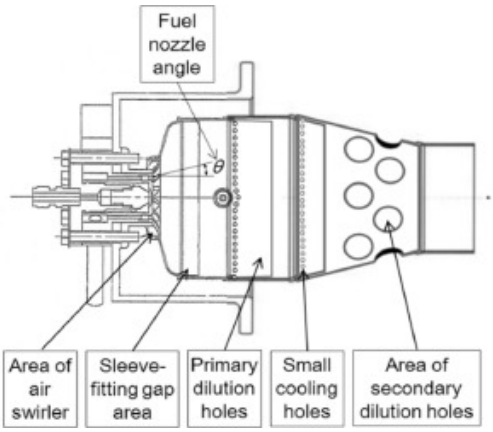

Figure 1.10: Newly manufactured combustor. Reprinted from [29].

Since the obtained levels of NO_x were still large enough to comply with the Japanese regulatory limit for NO_x emissions from gas turbines, SCR systems were required [4]. However, the large size and cost to manufacture and maintain these systems made it necessary to continue developing even lower NO_x combustors. Taking that into account, Okafor et al. [30], using the same combustor mentioned above, focused their investigation on emissions dependence on equivalence ratio, fuel injection angle, inlet temperature, and ambient pressure. In accordance with the previously mentioned studies, the authors reaffirmed the major importance of upstream equivalence ratio control to low NO_x emissions and it was obtained an optimum value of 1.1. In order to better control and assure uniformity of the upstream equivalence ratio a liner prototype was proposed, developed and implemented, with significant positive results of 42 $ppmv$ NO_x emissions and combustion efficiency of 99.5 % at an ambient pressure of 0.3

MPa and for fuel input power of 31.44 kW.

The aforementioned Cardiff University research group is also involved in investigating the RQL combustor concept. Mashruk et al. [31] performed a numerical analysis to evaluate the efficiency of an industrial-scale humidified Rich-Quench-Lean combustor using a chemical reactor network model approach. The study was performed for five of the most commonly used chemical kinetics mechanisms, and sensitivity analyses of OH and NH_3 species were performed for various points in the burner, as well as pointing out more relevant NO_x production paths predicted by the various mechanisms. The geometry of the reactor network as well as residence times for each reactor, recirculation strength, and calibration in terms of heat losses were taken from previously performed RANS simulations and experiments. The authors have theoretically demonstrated that the use of a humidified RQL combustor fueled with ammonia-hydrogen can produce exhaust gas of 99.97% water, nitrogen and oxygen, with NO_x emissions around 100 ppm at large industrial power generations.

The evolution of experimental work in the scientific field of combustion has also been accompanied by an increasing ability to simulate and computationally predict the physical and chemical phenomena that occur in the flame. The increasing improvement of computational methods and mechanisms of chemical kinetics has made it possible to achieve very satisfactory results as well as to decrease the time required for the simulations as well as the computational power requirements. The development of reliable numerical models validated by experimental results has the enormous advantages of not only allowing a deeper understanding of the combustion process, but also the possibility of obtaining adequate results without material expense or the need to set up complex experimental apparatus. One approach that has lately been used by several authors due to its low computational requirement and direct prediction of combustion chemistry is the Chemical Reactor Network (CRN) method. In contrast to the Computational Fluid Dynamics (CFD), the CRN method does not take into account differences in mixing rate and turbulence of the flows, always assuming perfect mixing. Perpignan et al. [32] propose a graphical comparison of the various methods of modeling combustion that is very illuminating to give an understanding of the most appropriate purpose of each method.

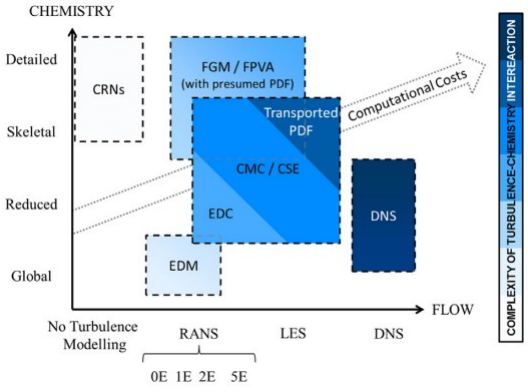

Figure 1.11: Different computational methods compared. Reprinted from [32].

One of the great challenges of the chemical reactor network architecture is the modeling of the flow pat-

tern between the various discrete reactors that approach the distinct flame zones. The flow rate in and out of each reactor can vary depending on the initial conditions, so these problem variables increase with the increase in the number of reactors used. For complex models some techniques have been used, mainly the allied use of the CRN model with CFD simulations and through experimental assessment on flow pattern characteristics.

Fichet et al. [33] developed a CRN model generated from CFD results for NO_x prediction with detailed chemistry in gas turbine combustion. A ”chemical” split and a ”physical” split to the CFD medium flow fields is proposed and performed in order to obtain homogeneous zones that can be modeled by PSRs. The ”chemical” splitting is done through mathematical laws that allow specifying the temperature ranges and equivalence ratio of the CFD grid cells. For the ”physical” division a novel method is proposed that allows to account for the complexity of any flow topology by creating a mesh based on the flow current lines. According to the authors, this splitting method dispenses with geometric or empirical criteria and can be used for any type of flow no matter how complex it is. The predicted NO_x emissions are in good agreement with the measurements, since 42.8 $ppmvd$ are predicted for 44 $ppmvd$ measured, an accuracy that is emphasized by the low value of the emissions and the short computation time, of minutes only.

Trespi et al. [34] presented a novel chemical reactor network solver, NetSMOKE, whose numerical model combines sequential-modular and equation-oriented approach for solving the global system of equations. The authors used previously available CFD simulations and measurements to accurately characterize and discretize the flow in macro-zones for the development of a simplified reactor network. The method used for refining the division of the flow into the various PSRs or PFRs was performed using experimentally obtained residence time distribution values so that the amount of fluid passing through each reactor was adjusted according to the residence time. In addition they further developed an iterative process for the refinement of the reactor network model based on a sensitivity analysis. The developed CRN model showed good agreement with the experimental data for a low computational cost.

Moving towards the end of this review, it is necessary to mention the particular importance for the present thesis of the recent works developed by the combustion research group at IDMEC - IST, University of Lisbon. Franco et al. [35] firstly presented a swirl and bluff-body stabilized burner for ammonia-hydrogen semi/quasi-premixed turbulent flames focusing on lean flame stabilization and temperature and emissions measurements and analysis. The authors did a quite detailed description on axial and radial lean flame temperature and emissions of NO and O2 in several burner points for each one of five flames with different conditions. A flame stability diagram (equivalence ratio vs volume fraction of ammonia in fuel mixture), in Figure 1.12, was also proposed from the experimental results for a power input of 1900 W, limiting the range of operability for future experimental works. A LES simulation was also conducted to assist the interpretation of experimental results (Figure 1.13).

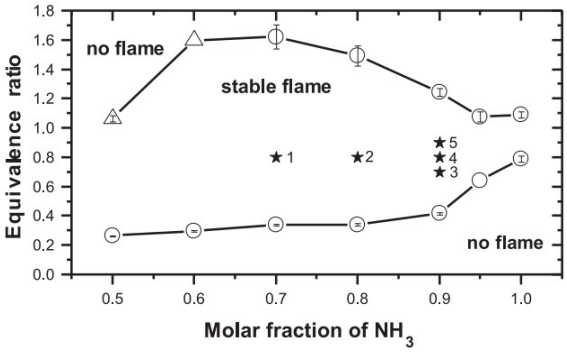

Figure 1.12: Stability flame diagram for a thermal input of 1900 W. Reprinted from [35].

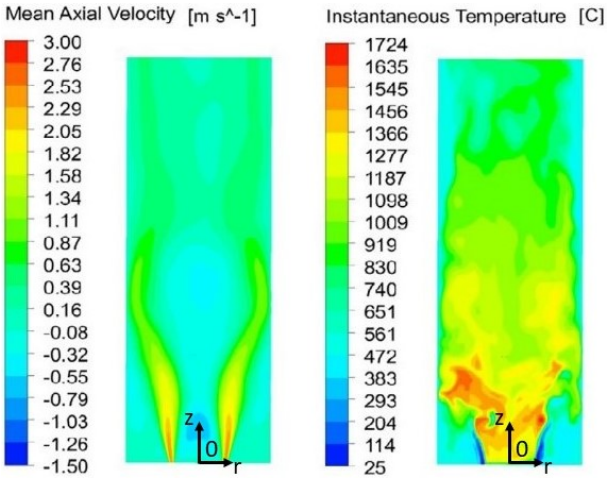

Figure 1.13: LES of flame with $\phi = 0.9$, $x_{NH_3} = 0.9$. Adapted from [35].

For some of the analyzed flames mentioned above Rocha et al. [36] conducted RANS simulations to study aerodynamics and mixing characteristics of the flow. The simulations are performed for chemistry turned off to represent isothermal flow profiles. In terms of flow fields the authors suggested the existence of three important recirculation zones, namely central recirculation zone (CRZ), inner recirculation zone (IRZ) and outer recirculation zone (ORZ), which interact with each other affecting thus the shape of the flame and the species production.

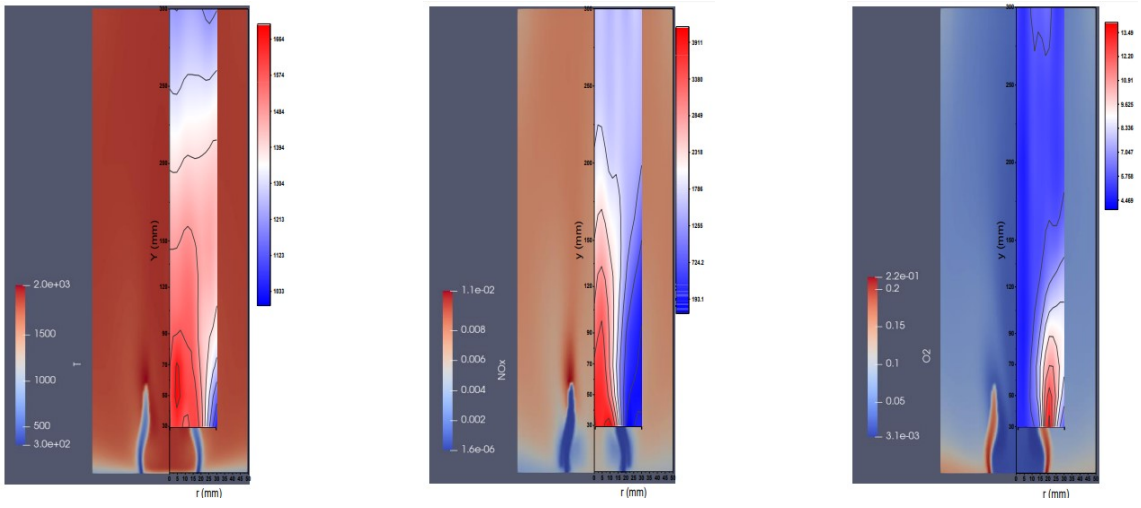

(a) (b) (c)

Figure 1.14: RANS simulation for flame with $\phi = 0.8$ and $x_{\mathrm{NH_3}} = 0.8$: (a) Temperature, (b) NO_x and (c) O_2. Reprinted from [36].

Pacheco et al. [37], using the same burner, developed some experiments on six different ammonia-hydrogen rich flames for a power input of 2800 W. A flame stability diagram (Figure 1.15) was also developed for the new power input. Temperatures were measured for several points along the combustor axis and NO_x, NH_3 and H_2 emissions were measured in the flue gases. H_2 NH_3 unburnt were detected in high concentrations in the exhaust gases, and a spontaneous secondary flame was observed above

the combustor due to unburnt reactants reburning. A numerical analysis by using a CRN simplified model was also carried out for the clarification of the involved phenomena, through rate of production analysis.

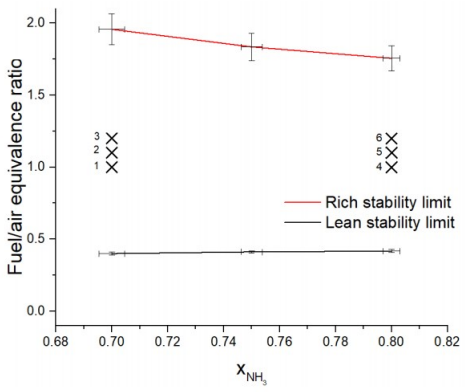

Figure 1.15: Stability flame diagram for a thermal input of 2800 W. Reprinted from [37].

1.2.2 Chemical kinetic mechanisms review for ammonia combustion

A great impulse has been given also to the development of the chemical kinetics of ammonia, blended or not with other fuels, for a fundamental understanding of the internal chemical processes that are occurring during the oxidation and that will dictate the main characteristics of the combustion of a particular fuel. Furthermore, the numerical implementation of chemical kinetics can be used to predict those characteristics, such as ignition delay times, flame speed, heat released rates, and species formation and reduction. As explained later in this thesis (Section 2.3), in terms of combustion chemistry modeling, an ideal kinetic mechanism contains all the elementary reactions taking place during the combustion process. However, there is always a trade-off between an extensively detailed model and the associated computational cost: the more detail, the more numerical processing time. Because of this trade-off between detail and computational effort, an important contribution of many researchers has been to reduce mechanisms, by suppressing less important elementary reactions to be left with the minimum number of reactions for minimal loss of accuracy in the final results, when compared to a more detailed and heavy mechanism of the same process.

Miller and Bowman [38] published in 1989 a first detailed chemical kinetics mechanism for modeling nitrogen chemistry in combustion, taking into account the various processes associated with this particular combustion, such as those of thermal and prompt NO formation, fuel nitrogen conversion, Thermal DeNO$_x$, RAPRENO$_x$, and formation and removal of NO_2 and N_2O. This first step in modeling appropriate chemical kinetics for ammonia combustion, although in certain respects outdated, has served as the basis for many other ammonia oxidation mechanisms.

Konnov and De Ruyck [39] released a chemical kinetic model with full H/N mechanism for predicting ammonia oxidation decomposition validated against experimental data for ammonia pyrolysis in shock

waves. The initially proposed mechanism has been revised and improved in subsequent publications, revising and introducing new NO formation routes [40, 41]. The full mechanism contains 129 species and 1231 reactions.

Tian et al. [25] carried out an experimental and kinetic modelling study of eleven premixed stoichiometric $NH_3/CH_4/O_2$/Ar flames at low pressure (4.0 kPa). The authors proposed a detailed mechanism, with 84 species and 703 reactions, with a particular focus on the effect of the mole ratio NH_3/CH_4 on the concentration of major species and intermediates. Some reactions proposed in literature were used to develop the presented chemical kinetic model.

Klippenstein et al. [42] studied in great detail the role of the NNH mechanism for NO formation and for predictions of the Thermal DeNO$_x$ process. The authors adapted the chemical kinetics mechanism of Miller and Glarborg [43] with the results of their investigations resulting in a mechanism with 33 species and 207 reactions.

Song et al. [44] proposed a modified mechanism from that of Klippenstein et al. [42] for better modeling of ammonia combustion at high pressures (30 and 100 bar), and medium-temperature ranging from 450 to 925 K. The updating mechanism was developed using reactions from the literature and emphasizing those more relevant for the conditions of the experiments performed, especially accounting for the role of H_2NO intermediate role for ammonia oxidation at those conditions. The investigations resulted in a mechanism with 34 species and 204 reactions.

Otomo et al. [45] started from Song et al. [44] mechanism and developed a new one for the combustion of ammonia/air and ammonia-hydrogen/air, improved with the use of important reactions including NH2, HNO, and N_2H_2. The resulting mechanism has 59 species and 356 reactions.

Nakamura et al. [46] presented a study and new chemical kinetic model particularly targeted to model low temperatures of ammonia combustion. Experiments were conducted for weak flames for rich, stoichiometric and lean regimes, at atmospheric pressure. The Miller and Bowman [38] mechanism was chosen as a starting point and some chemical models developed by other authors were adopted. A special focus was given to N_2H_x chemistry and its relevance on ammonia oxidation at low temperatures was reviewed and tested through sensitive analysis.

Glarborg et al. [47] conducted a comprehensive review on nitrogen chemistry in combustion, revising and updating the thermochemistry of the relevant nitrogen compounds, the rate parameters for the key gas-phase reactions of the nitrogen species, and the mechanisms for thermal-, prompt-, and fuel-NO, for NO formation via NNH or N_2O and for some NO reduction processes. The elaborated study resulted in a detailed mechanism with 151 species and 1397 reactions. Each subset of the mechanism was validated with experimental data.

Li et al. [48] assembled several models from the literature and developed a detailed mechanism with 128 species and 957 reactions. Two reduced chemical models were then obtained through Directed Relation Graph with Error Propagation (DRGEP) and sensitive analysis: 28 species and 213 reactions for ammonia-hydrogen and 51 species and 420 reactions for ammonia-hydrogen/methane. The studied reduction covered a wide range of conditions: $\phi = 0.5$–2.0, temperature 1000–2000 K, and pressure 0.1–5 MPa.

Stagni et al. [49] presented very recently a new chemical kinetic mechanism for ammonia oxidation. The main objective was to focus on critical conditions and unclear ammonia oxidation pathways pointed out in the available literature of kinetic models and thus a focus was put on exploring low and medium temperatures of ammonia combustion, with high oxygen concentration levels. Some intermediate species found determining for specific conditions, like H_2NO and HNO, were carefully analyzed, by performing flux and sensitive analysis. The complete kinetic mechanism was made up of 31 species and 203 reactions.

The above-mentioned chemical kinetic mechanisms are summarized in Table 1.2.

Table 1.2: Summary of chemical kinetic mechanisms.

Mechanism	Species	Reactions	Flames	Year
Miller and Bowman [38]	22	98	NH_3/O_2 and $NH_3/H_2/O_2$	1983
Konnov and De Ruyck [39]	129	1231	NH_3/air	1998
Tian et al. [25]	84	703	$NH_3/CH_4/O_2$/Ar	2009
Klippenstein et al. [42]	33	207	NH_3/O_2, $NO/NH_3/H_2O/H_2/$ and H_2/air	2011
Song et al. [44]	34	204	NH_3/air	2016
Otomo et al. [45]	59	356	NH_3/air and NH_3/H_2/air	2018
Nakamura et al. [46]	38	232	NH_3/air	2017
Glarborg et al. [47]	151	1397	CH_4, HCN, NH_3 and HNCO	2018
Li et al. [48]	28/51	213/420	NH_3/H_2/air and $NH_3/H_2/CH_4$/air	2019
Stagni et al. [49]	31	203	NH_3/He/air	2020

1.3 Objectives

The work that will be developed in this thesis is intended to be a continuation of the work already done on the current swirl and bluff-body stabilized burner in IDMEC mentioned above, fueled by a NH_3/H_2 fuel mixture. Specifically, the next important step in the improvement of this burner involves the implementation of techniques that allow for a more effective decrease in current NO_x emissions. In this sense, one of the techniques pointed out by past work [37] as probably suitable for this goal is the implementation of a Rich-Quench-Lean system in the current burner. In order to predict the effectiveness of this modification, numerical simulations should be developed in order to know in advance relevant characteristics of this system and most advantageous operating conditions. It was previously decided that the numerical studies would be done using the Chemical Reactor Network model, which, although not commonly used for simulating flames, allows the use of very detailed chemical kinetic mechanisms without large associated computational costs. This allows to perform parametric studies in a timely

manner. However, the simplifications associated with this method suggest from the outset that it may be difficult to obtain minor species results with a high level of accuracy. The evaluation of the suitability of this method will be addressed and discussed throughout the thesis.

1.4 Thesis Outline

In Chapter 2 are exposed the theoretical foundations inherent in the numerical modeling developed, particularly with regard to mathematical formulations of chemical kinetics mechanisms and chemical reactor network systems. In Chapter 3 the developed model is described in detail and the assumed assumptions and simplifications is be justified. In addition, the parametric studies are defined whose results are presented and commented in the following chapter. In Chapter 4 are presented all the results obtained, starting with the evaluation of the model by comparing its predictions with the experimental results. Then, the results of parametric studies for the theoretical case of a new RQL burner are shown and the best operating conditions according to the predicted results are discussed. In Chapter 5 are listed the main conclusions of the work done and new pathways for future research are suggested.

Chapter 2

Theoretical Background

2.1 Chemistry of ammonia-hydrogen combustion

It is of great convenience to begin the theoretical study of the ammonia-hydrogen blend combustion reaction (as is the fuel adopted for the study of this thesis) by first analyzing the overall stoichiometric reaction of the combustion of pure ammonia 2.1 given below. This reaction corresponds to what would ideally happen in chemical equilibrium [8].

$$4\mathrm{NH_3} + 3(\mathrm{O_2} + 3.76\mathrm{N_2}) \rightleftharpoons 6\mathrm{H_2O} + 15.28\mathrm{N_2} \tag{2.1}$$

A firstly evident conclusion from the analysis of this reaction is the nonexistence of carbon in the products of combustion. This is naturally due to the absence of carbon in the fuel used. Another interesting observation is the fact that, when compared to the combustion of many typical hydrocarbons, as there is no carbon dioxide production, the quantity of air needed for the complete combustion of ammonia is definitely lower.

However, the Reaction 2.2 presents an ideal case that in practice does not happen. Amounts of air other than stoichiometric, most typical in real applications, lead to the creation of other less desirable combustion products, such as NO, as it is predicted in Reaction 2.2 [8].

$$4\mathrm{NH_3} + 5(\mathrm{O_2} + 3.76\mathrm{N_2}) \rightleftharpoons 4\mathrm{NO} + 6\mathrm{H_2O} + 18.8\mathrm{N_2} \tag{2.2}$$

Although not evident from this reaction, other factors may contribute to NO_x formation, such as nitrogen dissociation at high temperatures. The analysis becomes more complex when one examines the elementary reactions that are happening within the overall process. There are several factors that have a very relevant impact on the dissociation of ammonia and other species to create undesirable products. The most relevant ones will be dealt with later in this text.

In the specific scope of this thesis the fuel under study is not pure ammonia but a mixture of ammonia-

hydrogen. In this case, the stoichiometric idealized combustion of NH_3/H_2/air is given by Reaction 2.3.

$$(1 - x_{NH_3})H_2 + x_{NH_3}NH_3 + (0.5 + \frac{x_{NH_3}}{4})(O_2 + 3.76N_2) \rightleftharpoons (1 + \frac{x_{NH_3}}{2})H_2O + (1.88 + 1.44x_{NH_3})N_2 \quad (2.3)$$

where x_{NH_3} is the volume fraction of NH_3 in the fuel mixture (Equation 2.4), which by assuming ideal gas approximation, is the same of NH_3 mole fraction in fuel.

$$x_{NH_3} = \frac{\dot{V}_{NH_3}}{\dot{V}_{NH_3} + \dot{V}_{H_2}} \quad (2.4)$$

where $\dot{V}_{NH_3}$ is the volumetric flow rate of NH_3 and $\dot{V}_{H_2}$ is the volumetric flow rate of H_2. As can be deduced from Reaction 2.3, the quantity of air necessary to completely burn the fuel increases with x_{NH_3}, achieving a maximum for pure ammonia in the fuel. Also the quantity of water and nitrogen present in the final products will increase with the increase in the volumetric fraction of ammonia.

2.2 Mechanisms for pollutants formation and reduction

As it was stated before the combustion of pure ammonia or ammonia blended with hydrogen is carbon-free. This means that neither greenhouse gases nor soot, two critical pollutants when considering hydrocarbons burning, are produced. For the case of ammonia blend combustion the two most concerning resulting pollutants are nitrogen oxides (NO and NO_2) and unburnt ammonia (NH_3).

Although the understanding of nitrogen oxides formation is presently under development and the complexity of kinetics is yet far from being completely comprehended, some theories have been proposed and corroborated by experiments. The foremost explanation processes that are concerned with pollutant formation in ammonia oxidation are the fuel nitrogen mechanism (fuel-NO), the extended Zeldovich mechanism (thermal-NO), and the nitrous oxide mechanism (N_2O-intermediate). With regard to NO_x reduction in the ammonia combustion reaction, the Thermal DeNO$_x$ mechanism is of particular interest.

2.2.1 Ammonia oxidation mechanism

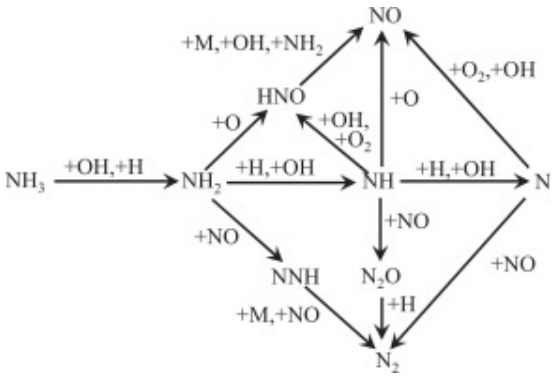

Figure 2.1: NH_3 oxidation pathway by Miller et al. Reprinted from [50].

A relevant step in ammonia oxidation comprehension was achieved with the proposal of a reaction pathway by Miller at al. [50], shown in Figure 2.1. Unburnt ammonia is largely a result of incomplete combustion although it may be also created in some minor reactions during combustion. Because of its high resistance to ignition and the low heating power ammonia oxidation is highly dependent and enhanced by the temperature and residence time increase, so the decreasing of unburnt ammonia. High concentrations of ammonia at the exhaust are not only an indicator of poor combustion efficiency but can also be a safety hazard due to the toxic nature of ammonia. The latter case requires that some methods of unburnt ammonia mitigation are adopted.

2.2.2 Fuel nitrogen mechanism

The fuel-NO mechanism is the most determining one when dealing with fuels with nitrogen in their composition. It consists of the oxidation of fuel-bound nitrogen. When dealing with ammonia oxidation, in the case of the present study, the global process follows the reaction 2.5 [8]:

$$4\mathrm{NH_3} + 5\mathrm{O_2} \rightleftharpoons 4\mathrm{NO} + 6\mathrm{H_2O} \tag{2.5}$$

The pathway presented in Figure 2.1 is also important for the understanding of fuel NO formation and reduction. It can be concluded from that pathway that the higher the O/H radical concentration (abundant concentration of oxygenated radicals O, OH, O_2) the more favored is the conversion of NH_i (i = 0,1,2) to NO, which particularly occurs for lean flames. In the case of rich flames, the decreasing of O/H radical concentration (relative abundant concentration of nitrated radicals N, NH, NH_2) promotes the pathways of NO reduction from NH_i oxidation into N_2, which is the reason for the lower levels of NO_x in the rich regime. In addition to the previous and also for the rich conditions, the relative increase of H in the flame favors the oxidation of NH_i into substantial H_2 and, then, the production of N atoms. The latter contributes to the enhancement of the extended Zeldovich mechanism [4], described next.

2.2.3 Extended Zeldovich mechanism

The thermal-NO mechanism is the most prevalent in the combustion of hydrocarbons or low-nitrogen-containing fuels at high temperatures. Nitrogen oxides are formed especially from nitrogen existing in atmospheric air, in a process that follows the global Reaction 2.6.

$$\mathrm{N_2} + \mathrm{O_2} \rightleftharpoons 2\mathrm{NO} \tag{2.6}$$

The global process can be divided into three elementary Reactions 2.7, 2.8 and 2.9, that were firstly proposed by Zeldovich [51].

$$\mathrm{O} + \mathrm{N_2} \rightleftharpoons \mathrm{NO} + \mathrm{N} \tag{2.7}$$

$$\mathrm{N} + \mathrm{O_2} \rightleftharpoons \mathrm{NO} + \mathrm{O} \tag{2.8}$$

$$\mathrm{N} + \mathrm{OH} \rightleftharpoons \mathrm{NO} + \mathrm{H} \tag{2.9}$$

The fact that quite large activation energy is necessary for the Reaction 2.7 to break the covalent N-N bond in N_2 makes this a rate-limiting reaction, very dependent on temperature, generally above 1800 K, which is a controlling factor with major importance. Two other important factors are O2 concentration and residence time, since the slow process of NO formation by this pathway [52].

However, in the case of ammonia combustion, the thermal-NO mechanism contributes to NO production even at low temperatures although its net contribution may be considered negligible [4]. Furthermore, the extended Zeldovich mechanism may be an important step for NO reduction due to the reverse reaction in $N_2 + O \rightleftharpoons NO + N$, favored by the presence of large quantities of NO and N. This pathway of NO reduction is particularly important and enhanced for rich flames [4].

2.2.4 Nitrous oxide mechanism

The N_2O-intermediate mechanism is also responsible for NO formation, with particular importance as an intermediate step for the Thermal DeNO$_x$ process. Reaction 2.10 expresses the production of N_2O through the reduction of NO by NH while Reaction 2.11 gives the main pathway for the large consumption of N_2O.

$$NH + NO \rightleftharpoons N_2O + H \tag{2.10}$$

$$N_2O + H \rightleftharpoons N_2 + OH \tag{2.11}$$

Keeping track of N_2O concentration levels is of great importance due to the fact that it has a greenhouse effect potential 298 times more effective than CO_2, the absence of which is precisely the biggest advantage of ammonia combustion.

2.2.5 Thermal DeNO$_x$ mechanism

The DeNO$_x$ thermal mechanism, found by Lyon [53], is a chemical process by which the addition of nitrogen-containing chemicals, such as urea or ammonia, into the flue gases is used to reduce NO$_x$, in the presence of oxygen.

It is known that the reaction of NO with NH_2 is the dominant NO reduction step, particularly in lean flames, which is modeled by Reactions 2.12 and 2.13.

$$NH_2 + NO \rightleftharpoons N_2H + OH \tag{2.12}$$

$$NH_2 + NO \rightleftharpoons N_2 + H_2O \tag{2.13}$$

The addition of ammonia in the flue gases may increase the concentration of NH_2 (Reaction 2.14), favoring the above reactions.

$$NH_3 + OH \rightleftharpoons NH_2 + H_2O \tag{2.14}$$

This process of NO_x reduction into N_2 and H_2O can be globally expressed by the chemical overall Reaction 2.15 [53].

$$4NO + 4NH_3 + O_2 \rightleftharpoons 4N_2 + 6H_2O \tag{2.15}$$

One aspect of paramount importance in this process is the fact that its efficiency is only for a specific temperature range and oxygen concentration [53].

A major advantage of this process is that it does not require the use of a catalyst, which is usually quite expensive. Its principal drawback is the production of the greenhouse effect molecule N_2O.

2.3 Chemical kinetics

Chemical kinetics is the fundamental study of the underlying chemical reactions taking place in a global chemical process, as is the combustion process. Understanding the chemistry is essential to determine species production and destruction and to predict some other combustion variables, such as ignition and extinction. In a chemical process the molecules existing in the gas, with different velocities and traveling by random paths, collide with each other, frequently breaking molecular bonds and creating a pool of radicals. These radicals will also crash with other radicals and molecules breaking and forming new bonds, and so, new species.

All these processes can be modeled by *elementary reactions* and respective *reaction rates*. An elementary reaction is each of multiple sequential processes involving interactions between intermediate species, occurring at the molecular level and unable to be broken down into smaller steps. The overall reaction of fuel with oxidant can be viewed as several underlying elementary reactions that occur over a specific period of time and can be modeled by Reaction 2.16.

$$A + B \rightleftharpoons C \tag{2.16}$$

Elementary reactions can be unimolecular, bimolecular or termolecular and they can react both in forward or reverse reaction directions, depending on some factors such as temperature, pressure and species concentrations. Sometimes a third body, M, is involved in the reaction and that expresses an inert molecule participating in the reaction, usually by absorbing or supplying energy.

$$A + B + M \rightleftharpoons C + M \tag{2.17}$$

The reaction rate constant, k, is usually approximated by an empirical Equation in a modified form of that proposed by Arrhenius [52] (the forward rate constant in Equation 2.18), where A, b and E_a are empirical parameters: pre-exponential factor, temperature exponent modifier, and activation energy respectively. T is the temperature and R is the gas constant. Particular reference can be made to the activation energy of the reaction, E_a, because it is the minimum amount of energy required for the chemical reaction to

occur.

$$k_f = AT^b e^{-E_a/RT} \tag{2.18}$$

The rate of reaction can be defined as the time rate at which a particular species is produced or consumed from a specific reaction or set of reactions. Reaction rates may be expressed by an empirical rate law (Equations 2.19 or 2.20) validated by experimental evidence, where the negative sign expresses the consumption of species A for the positive direction of the reaction, the [X_i] represents the molar concentration of species i, and the x_i represents the order of reaction with respect to X_i.

$$\frac{d[A]}{dt} = -k_f[A][B] \tag{2.19}$$

or

$$\frac{d[A]}{dt} = -k_f[A][B][M] \tag{2.20}$$

The reaction mechanism is a compilation of the sufficient number of elementary reactions needed to describe an overall reaction of fuel and oxidizer. An elementary reaction is a single step in a reaction mechanism and the latter can involve a few or several steps, depending on the complexity of the global reaction and the required accuracy. A current research challenge for combustion scientists is the mechanisms reduction, that is, the use of a minimum of elementary reactions that describe a given overall reaction with minimal loss of accuracy, which implies a great dominion and knowledge of the complex chemistry affecting combustion.

In a multi-step mechanism, compactly expressed by the general Reaction 2.21, each species j may be produced and consumed by various reactions i simultaneously occurring.

$$\sum_{j=1}^{N} x'_{ji} X_j \rightleftharpoons \sum_{j=1}^{N} x''_{ji} X_j \; for \; i = 1, 2, ..., M \tag{2.21}$$

Where x'_{ji} are the stoichiometric coefficients of reactants and x''_{ji} are the stoichiometric coefficients of products.

A net production rate must be considered for each species given by Equation 2.22.

$$\dot{w}_j = \frac{d[X_j]}{dt} = \sum_{i=1}^{M} x_{ji} (k_i^{(f)} \prod_{j=1}^{N} [X_j]^{x'_{ji}} - k_i^{(r)} \prod_{j=1}^{N} [X_j]^{x''_{ji}}) \tag{2.22}$$

where

$$x_{ji} = x''_{ji} - x'_{ji} \tag{2.23}$$

The upper indices f and r refer to the direction of the reaction, forward and reverse, respectively.

Equation 2.22 can be written in a different way (Equation 2.24), were concentrations $[X_j]$ are functions of time.

$$\frac{d[X_j]}{dt} = f_j([X_1], [X_2], ..., [X_N]) \tag{2.24}$$

By solving the N simultaneous Ordinary Differential Equations (ODEs) it is possible to calculate the time evolution of the chemical composition of the reactive system once the initial concentrations of the chemical species are known, with the addition that also the energy conservation Equation must be solved if the temperature is unknown. In the vast majority of cases this calculation can only be done by computer support.

2.4 Turbulence and flame stabilization

The vast majority of industrial and commercial applications of combustion deal with turbulent flames, characterized by very complex and unsteady shapes. Turbulence takes place when flow velocity reaches a maximum value above which the viscous forces become less preponderant and the instabilities raise, resulting in random fluctuations of velocity at each point of the flow. The turbulent characteristic of the flames has important implications on the efficiency of combustion as it greatly affects the blending of fuel and oxidizer and the heat transfer with surroundings. Although an analysis of turbulence flow in combustion is not within the scope of this thesis, it must be said, for a correct understanding of the assumptions presented later in this text, that it exists and plays an unavoidable role in the applications to which this work is directed and in the experimental data that support it (Turns [52]).

A relevant dimensionless parameter of combustion, related to the interaction of turbulence and chemistry, is given by the Damköhler number (Equation 2.25), which represents the ratio between a turbulence time-scale and a chemical time-scale.

$$Da = \frac{\text{reaction rate}}{\text{diffusion rate}} = \frac{\text{diffusion time}}{\text{reaction time}} = \frac{t_{flow}}{t_{chem}} \tag{2.25}$$

From this dimensionless number follows that for $Da << 1$ turbulence rates are faster than chemical rates and the combustion is limited by chemistry; for $Da >> 1$, chemical rates are faster and so the turbulence is the limiting factor.

Following what has been said, another important goal when dealing with turbulent flames is the attaining of a stabilized flame in the burner, which highly affects its performance and is an essential objective for a correct design. As being characterized by unsteadiness and instability, a turbulent flame frequently needs some support to be anchored at a specific point and cover an operating range without the risk of flashback (only for the case of premixed flame, when the flame speed exceeds the flow speed and the flame propagates backward in the flow mixture duct), liftoff (when the flow velocity is higher enough for the flame detach from the burner and sustain some distance above it), and blowoff (when, for a critical maximum flow speed, there is no enough residence time to chemical reactions occur and the flame simply extinguishes).

Some techniques can be used to promote the stabilization of flame. For the current work, the two most relevant techniques that are resumed below apply the principle of creating a region of low flow velocity, where the chemical reactions have enough time to occur.

Bluff-body stabilization (Figure 2.2) is an effective way of achieving a low-velocity zone in a flame. A body placed near the burner hole generates a strong recirculation zone in the flow downstream, a zone of low velocity when compared to the exterior flow but with high turbulence, which contains air, unburnt fuel and hot burned products, that due to the recirculation are very well mixed. The recirculation of these hot gases promotes the ignition of unburnt fuel present in this zone and the relatively long residence time in these zones contributes to the homogenization of the mixture composition and temperature. These recirculation zones are characterized by fast and efficient mixing due to high turbulence, where $Da << 1$ can be assumed. Thus they might be theoretically modelled by perfect-mixing reactors.

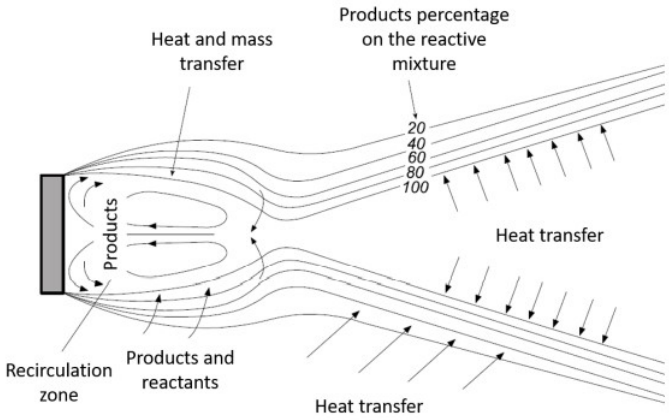

Figure 2.2: Bluff-body representation. Adapted from [54].

Swirl stabilization (Figure 2.3) is another technique for creating recirculation zones that consists of imposing a rotation on the incoming air around the axial direction, through the use of blades with a certain inclination placed at the burner mouth. This imposed rotation on the air results in the creation of a zone of low velocities in the vicinity of the burner axis. A recirculation zone arises if the rotation speed is high enough, and is greater the higher this speed is (Coelho and Costa [54]).

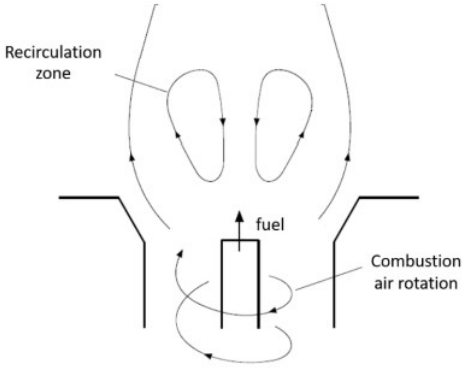

Figure 2.3: Swirl representation. Adapted from [54].

2.5 Strategies for NO_x reduction

The previous section was intended to lay out some of the current theoretical backgrounds on pollutant formation, especially the most crucial when it comes to the burning of nitrogen composite fuel. Regarding the formation of NO_x various methods and techniques have already been proposed and implemented in commercial combustion devices: most of these strategies are based on combustion modifications while a minority consists of post-combustion controls and are shown in Figure 2.4. All these techniques have been used for some years in different applications with successful results, depending on the operating conditions [52].

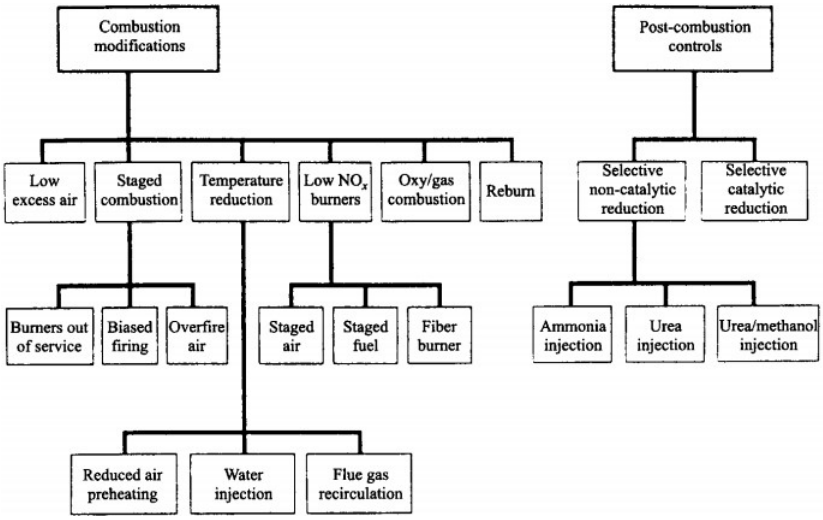

Figure 2.4: NO_x control techniques. Reprinted from [52].

For this work, two concepts may be described in more detail.

2.5.1 Selective Non-Catalytic Reduction (SNCR)

The Selective Non-Catalytic Reduction (SNCR) method is based on the Thermal DeNO_x mechanism and is a post-flame strategy for NO_x reduction by the addition of nitrogen-containing chemicals like urea or ammonia, being ammonia the reagent with major interest for the current text. For the case of the NH_3/H_2 flame study, this process is particularly relevant due to the fact that it occurs naturally by the very nature of the fuel, without the need for a supplemental addition of the nitrogenous chemical.

Especially in the lean-burn regime the conditions are generally favorable for the spontaneous realization of this process, due to the fact that the oxygen concentration is high as well as the temperatures, which are often within the temperature range that guarantees the efficiency for the NO_x reduction according to the limits of maximum allowable ammonia slip and the lowest possible NO_x, as it is illustrated in Figure 2.5.

Following on from the above, SNCR reactions are expected to occur in the Lean stage of an RQL

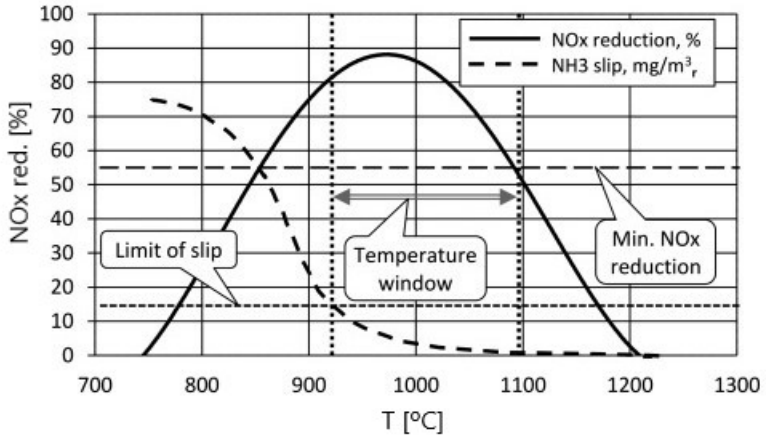

Figure 2.5: The SNCR system efficiency and the ammonia slip as a function of the flue gas temperature in the combustion of hydrocarbons. Adapted from [55].

combustor due to the presence of unburned NH_3 present in the effluent gases from the Rich stage, the high oxygen concentration resulting from the air injection in the Quench stage, as well as the high temperatures resulting from the combustion reactions that are generated in the Lean stage between the unburned NH_3 and the secondary air.

2.5.2 Rich-Quench-Lean combustor

As it was referred to earlier, the Rich-Quench-Lean combustor (RQL) concept emerged as an eminent strategy for NO_x reduction, specifically for stationary gas turbines. This concept consists fundamentally of a particular configuration of the gas turbine combustor to allow a staged air inlet, as shown in Figure 2.6.

A primary zone, operating at “rich-burn” condition, is created by introducing with both fuel (for this purpose, ammonia-hydrogen) and air, premixed or non-premixed, in the chamber with an equivalence ratio greater than one. As exposed in Section 2.1 the rich condition allows for low NO_x production due to lower temperatures and incomplete combustion. Furthermore, operating at rich conditions grants acceptable levels of flame speed and thus assures flame stability due to the production of energetic H_2 resulting from NH_3 dissociation [56].

The effluent hot gases from the primary zone move into the quenching, or quick-mix, zone where the air is quickly injected into the combustion products, promoting a very fast mixing. The speed of mixing should be such that reactions have no chance to occur and freeze for a very short time until they are reactivated in the Lean stage. In this way, it is possible to prevent reactions from occurring in the presence of a stoichiometric amount of air, which is the condition in which more NO_x is produced by the thermal route, precisely what we want to avoid. This stage is of a particularly challenging design since turbulence-chemistry interactions are quite complex and greatly influence the effectiveness of RQL [57]. The lean stage, immediately after the Quench zone, is where the last chemical reactions take place

and the existing H_2 and NH_3 are completely or almost completely consumed. It is expected that these reactions will result in an increase in NO_x concentration, due not only to the burning of NH_3 but also the temperature rise that promotes the thermal pathway. However, due to the presence of a considerable amount of ammonia at high temperatures, the SNCR process is also expected to occur in this zone, with a consequent decrease in the concentration of nitrogen oxides. Finally, it is worth mentioning that the RQL combustor concept has the attribute of good performance in processing fuels of varying composition [57], of which the ammonia-hydrogen blend is a proper example.

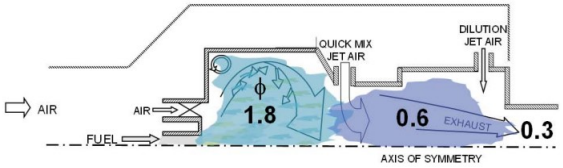

Figure 2.6: Rich-Quench-Lean combustor. Reprinted from [57].

2.6 Chemical Reactor Theory

A chemical reactor model can be defined as a method of coupling thermodynamic principles with chemical kinetics to compute the evolution of a thermodynamic reacting system from an initial state (reactants) to the final state (products), that may not necessarily be in chemical equilibrium. Hence, the state of the system can be calculated as a function of time, and so the temperature and species concentrations [52]. Thermodynamic equilibrium is assumed in the reactor at all instants of time. In a network of chemical reactors, single reactors are interconnected in a way that the contents of one reactor flow into the others. Besides mass interaction, connected reactors can also exchange heat and work. Some archetypal systems can be considered but for the present work only two will be presented and described in detail: Perfectly-Stirred Reactor (or Well-Stirred Reactor) and Plug-Flow Reactor.

2.6.1 Perfectly-Stirred Reactor

A Perfectly-Stirred Reactor (PSR), also referred to as Well-Stirred Reactor (WSR), Continuously Stirred Tank Reactor (CSTR), or Longwell Reactor is a single ideal reactor with constant volume, one or more inlets, and outlets, and where it is assumed to exist perfect mixing (and thus homogeneity in composition), steady-state and steady-flow (Figure 2.7). These assumptions are valid when the inlet jets have high velocity [52].

Mass conservation is assured by the following governing Equation 2.26:

$$(\frac{d\dot{m}}{dt})_{\text{PSR}} = \sum_{in} \dot{m}_{in} - \sum_{out} \dot{m}_{out} \tag{2.26}$$

Species concentration change in the reactor with time. The rate of change in mass for each species is

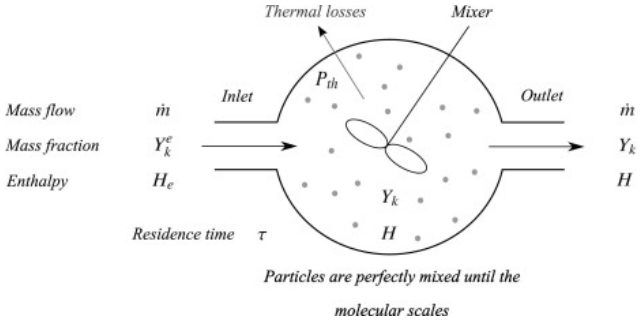

Figure 2.7: Schematic Perfectly Stirred Reactor under steady-state conditions. Reprinted from [33].

given by Equation 2.27 [58].

$$m\frac{dY_j}{dt} = \sum_{in} \dot{m}_{in}(Y_{j,in} - Y_j) + \dot{m}_{j,gen} \tag{2.27}$$

where Y is the mass fraction of species and

$$\dot{m}_{j,gen} = V\dot{w}_j W_j \tag{2.28}$$

is the rate at which species j are generated, being V the control volume and W the molecular weight of species.

The ideal gas state is another important assumption relevant to the present study, since the fuel used is gasified ammonia/hydrogen. Based on that, the energy conservation is given by Equation 2.29.

$$mc_p\frac{dT}{dt} = -\dot{Q} - \sum_j h_j\dot{m}_{j,gen} + \dot{m}_{in}\sum_j(h_{j,in}Y_{j,in} - h_{j,out}Y_{j,out}) \tag{2.29}$$

The heat rate $\dot{Q}$ (W) through a wall connecting reactors "left" and "right" can be expressed by Equation 2.30.

$$\dot{Q} = UA(T_{left} - T_{right}) + \epsilon\sigma A(T_{left}^4 - T_{right}^4) + Aq_0(t) \tag{2.30}$$

where U is an overall heat transfer coefficient $(W/(m^2K))$, A is the heat transfer area (m^2), ϵ is the wall emissivity, σ is the Stefan-Boltzmann radiation constant, and $q_0(t)$ is a time-dependent heat flux (W/m^2).

Residence time in a PSR can be calculated by Equation 2.31:

$$t_r = \rho V/\dot{m} \tag{2.31}$$

This reactor type is particularly interesting to approximate/model combustion in premixed turbulent flames and in stabilized flame recirculation zones (Coelho and Costa [54]), aforementioned in Section 2.5, characterized by almost assuring homogeneity and uniform properties at each point of the control volume.

2.6.2 Plug-Flow Reactor

A Plug-Flow Reactor (PFR) is an ideal steady-state reactor where an ideal gas flows through it in the axial direction and at steady-flow, i.e., at a constant mass flow rate. In the axial direction, there is no mixing and thus different states are obtained, neglecting the mass diffusion in this direction. At any cross-section, i.e., perpendicular to the flow, the gas is considered to be homogeneous and thus with uniform properties. The flow is assumed to be frictionless (Turns [52]).

The mass conservation in a PFR is given by Equation 2.32, where u is the axial velocity in m/s and A is the cross-sectional area in m^2 [58].

$$\frac{d(\rho u A)}{dz} = 0 \tag{2.32}$$

The continuity of species k is given by Equation 2.33 [58].

$$\rho u \frac{dY_j}{dz} = \dot{w}_j W_j \tag{2.33}$$

Energy conservation in the PFR is expressed in Equation 2.34, where U is the heat transfer coefficient in $W/(mK)$, P is the perimeter of the duct in m, and T_w is the wall temperature in K. Kinetic and potential energies are neglected [58].

$$\rho u A c_p \frac{dT}{dz} = -A \sum_j h_j \dot{w}_j W_j + UP(T_w - T) \tag{2.34}$$

An interesting conclusion that follows from the previous assumptions is that a PFR can be modeled by a linear chain of interconnected PSRs, where each PSR approximates a discrete axial distributed volume [58]. When dealing with stabilized flames, this type of reactor can be used for modeling the post-flame zone where there are no recirculation zones and the gas simply flows axially.

Chapter 3

Implementation

3.1 Experimental setup

The experimental apparatus of the swirl and bluff-body stabilized burner related to the numerical work proposed in this text is now exposed and described, as well as the methodologies used for the measurements in the previous studies where they were performed [35, 37]. It is important to mention that this reference to the experimental work is only intended to present the way this work was developed by the authors mentioned above, insofar as the values obtained by these authors served as validation support for the numerical model developed, since the focus of this thesis is a numerical modeling and not the experimental work, which was not developed in this thesis.

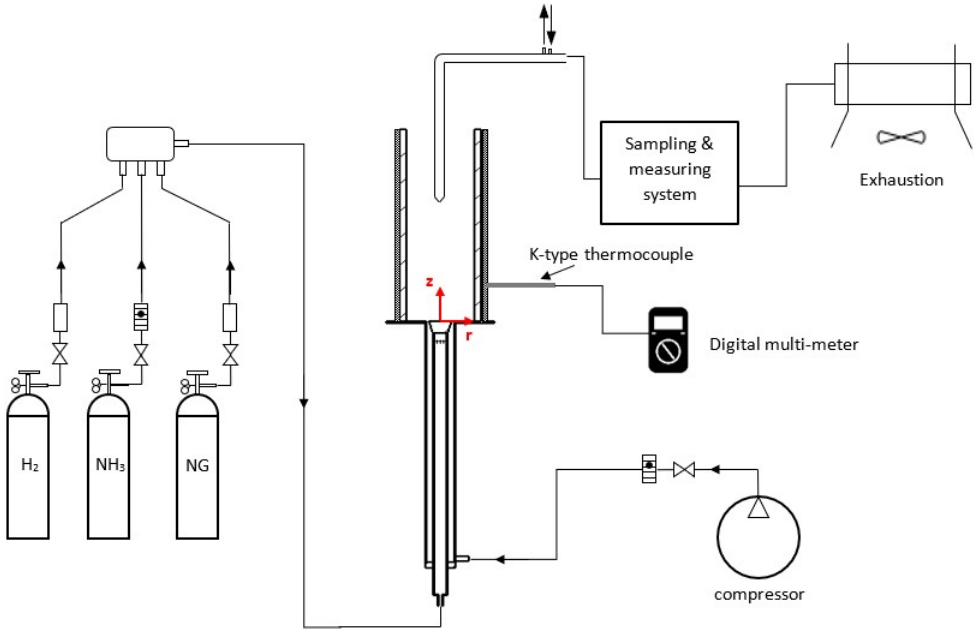

Figure 3.1: Schematic of the burner setup. Adapted from [59].

A schematic of the experimental rig is shown in Figure 3.1. It was introduced and developed by Franco et al. [35], whose work was already mentioned. From this layout three main parts can be distinguished: the air and fuel supply, the combustor itself, and the sampling and measuring instruments.

The fuel of interest consists of a mixture of NH_3 and H2, in proportions that can be variable. This system uses natural gas (NG) fuel for the initial ignition of the flame, and for an initial heating of the burner to later facilitate the ignition of the NH_3 present in the main fuel mixture. Both NH_3 and H_2 are initially stored in compressed cylinders, in which there is a pressure regulator at the outlet to handle the pressure at which each gas is supplied. NG is supplied from the common supply line in the building where the laboratory is located. The air is supplied through a compressor, and it is also possible to control the pressure at which it is supplied through a pressure controller. The flow rates of each fuel and air are controlled: for NH_3 and air, this control is done by means of fluctuating rotameters while for NG and for H_2 the control is done by means of digital flow meters. The transport of the various gases to the combustor is done through the respective Teflon tubes, being controlled by the mentioned flow controllers.

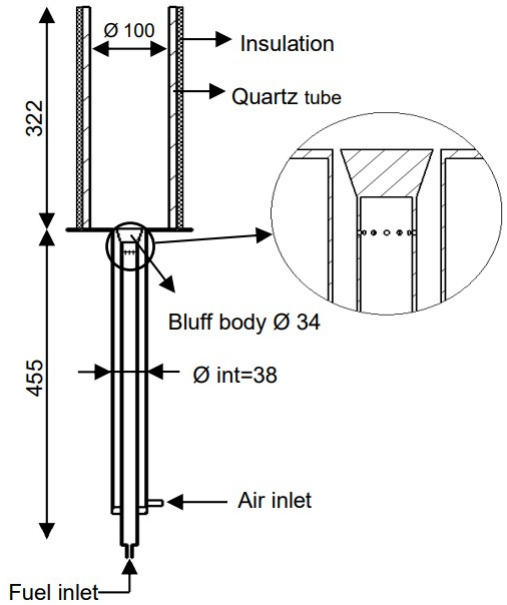

Figure 3.2: Schematic of the burner. Dimensions in mm. Reprinted from [59].

Upstream of the burner a duct composed of two concentric tubes makes the connection between the Teflon tubes and the burner, as shown in Figure 3.2. The inner tube has an outer diameter of 22 mm and is 2 mm thick, and the outer tube has an inner diameter of 38 mm. In the inner pipe flows the fuel flow, and the various constituent gases of the fuel mixture are mixed right at the entrance to this pipe. In the space between the inner and outer ducts flows the air flow, which is introduced tangentially to the duct in order to promote the swirl movement. At 13.5 mm upstream of the bluff-body the fuel mixture is injected radially into the airflow through 12 holes of 2 mm diameter, promoting partial premixing at a short distance from the burner mouth. The bluff-body placed exactly at the burner mouth is shaped like a truncated cone, with a height of 20 mm, a base diameter of 22 mm, and a top diameter of 34 mm. Its function is to impede the passage of air/fuel flow by creating a recirculation zone in the flame downstream of the burner mouth. From the level of the burner mouth a quartz tube confines the deflagrated flame. This quartz tube has an inner diameter of 100 mm, a thickness of 10 mm and a height of 322 mm, and is surrounded by a 20 mm lining of ceramic wool, which in turn is covered with reflective tape and finally by two stainless steel cylindrical layers with a thickness of 4 mm, to minimize heat losses.

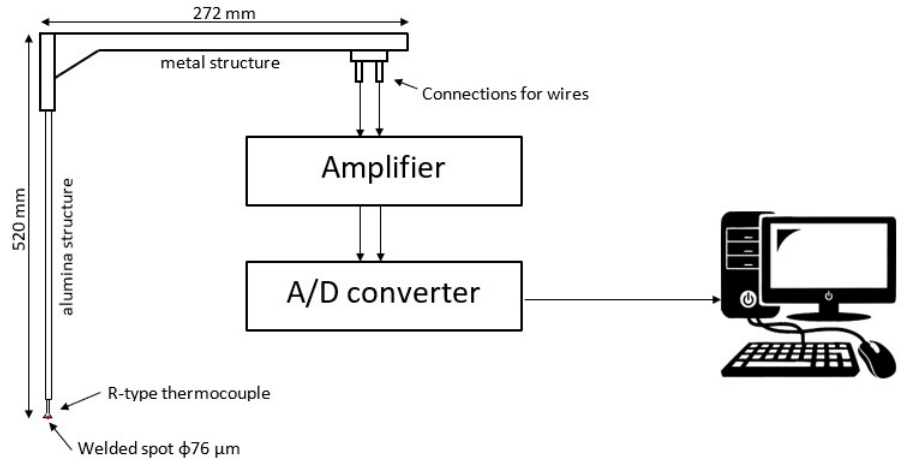

Figure 3.3: Schematic of temperature analyzer system. Adapted from [59].

Regarding the various measurements performed there were slight differences in some of the instruments or methods used for these measurements in lean or rich flames, studied by different authors. These minor differences will be identified in due course. The temperature measurement was performed along the central axis of the quartz tube (r = 0 mm, z = 30 - 300 mm), using a platinum/platinum-13% rhodium (Pt-Pt 13% Rh) thermocouple with a diameter of 76 μm at the *hot junction*, that can measure a range of values from -50 to 1760 ºC. The thermocouple is connected to a probe, protected by an aluminum jacket, which in turn is fixed to a metal frame that can be handled and allows movement in all three directions of a three-dimensional referential. This approach to perform temperature measurements was used by both rich and lean flames.

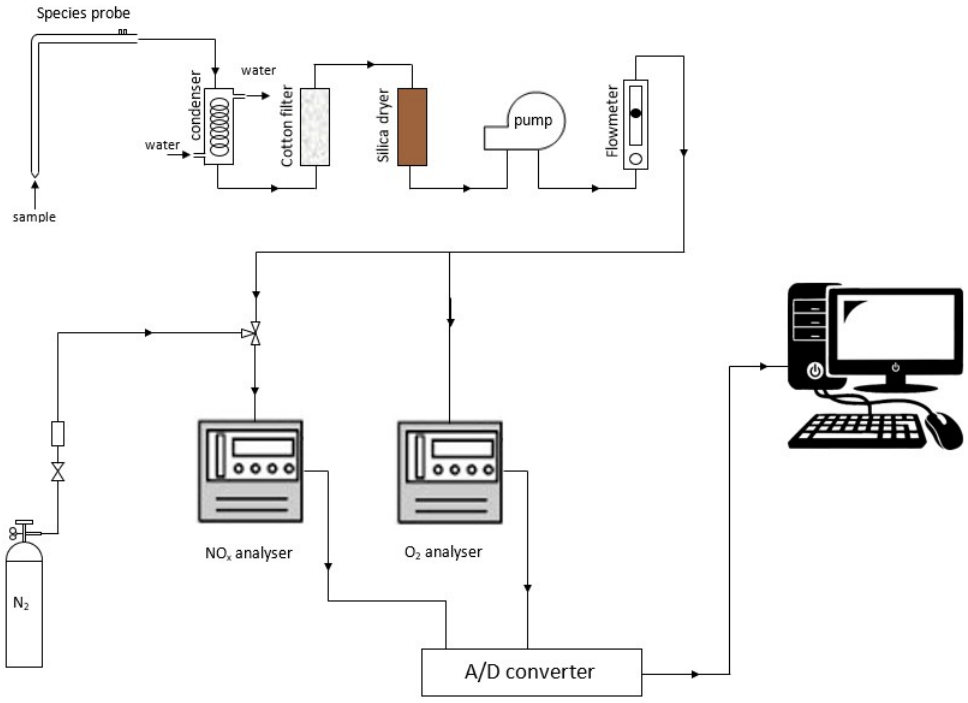

Figure 3.4: Schematic of sampling and gas analyzers system for NO_x and O_2. Reprinted from [59].

Regarding the measurement of the gas species two different methods were used: through gas analyzers

or through detection tubes GASTEC Co. The gas analyzers were used for the measurement of the mole fraction of NO_x and O_2 along the central axis of the combustor (r = 0 mm, z = 30 - 300 mm) for lean [35] flames, and in the measurement of the H_2 concentration only at the combustor exit (z = 300 mm) for rich [37] flames. For this there is a stainless steel water-cooled probe attached to the metallic structure already mentioned that collects the sample of combustion gases at a certain position, and these gases are conducted through a condenser, a cotton filter and a silica dryer to remove humidity and impurities, allowing gas analyzers to measure in a dry basis.

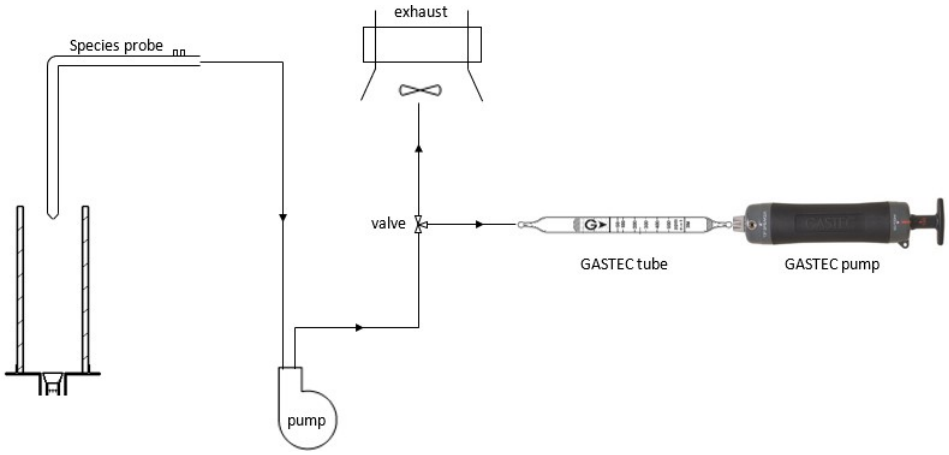

Figure 3.5: Schematic of measurement system for NH_3, NO_x and H_2. Reprinted from [59].

In measuring the mole fraction of NH_3 at the combustor exit (r = 0 mm, z = 300 mm) for lean [35] flames and in measuring the mole fractions of NH_3 and NO_x also at the combustor exit (z = 300 mm) for rich [37] flames, the aforementioned GASTEC detection tubes were used, supported by a hand pump. The gas samples are conducted by the sampling system shown in Figure 3.5.

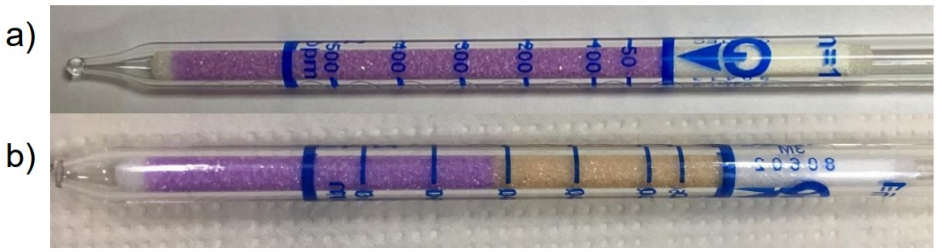

Figure 3.6: Gastec tubes 3M: a) unused tube b) used tube measuring slightly more than 300 ppm. Reprinted from [59].

The GASTEC tubes, shown in Figure 3.6, allow the molar fraction of species to be measured, in a simpler but less accurate manner, by changing the color of a particulate matrix containing a reagent that is sensitive to the presence of a particular chemical species. Depending on the scale range needed, the tubes used for NH_3 were 3M class (10-1000 ppm) and 3HM class (0.05-3.52%); for NO_x measurements tubes 11S (5-625 ppm) class and 11HA (50-2500 ppm) class were used.

Some experiments were performed for lean flames [35] and for rich flames [37]. The reported uncertainties for the measurements performed on the lean and rich flames are summarized in Table 3.1.

Table 3.1: Estimated uncertainties reported for measured values in lean flames [59] and stoichiometric and rich flames [37].

Parameter evaluated	Lean Flames	Rich Flames
x_{NH_3} (flow meter)	4.4 %	-
ϕ (flow meter)	2 %	-
Temperature	2 %	1 %
NO_x	18 %	-
O_2	14 %	13 %
NH_3	$\pm$ 50 ppm	20 %
H_2	-	5 %

For more detailed information on the experimental setup or on the conditions under which the experimental tests were carried out it is suggested to consult references [35, 37, 59].

3.2 Numerical Model

The model used in this thesis and that will be presented in the current chapter is based on some prior and fundamental assumptions that allow a simplified analysis of the actual complex processes that are occurring in a flame. The developed model aims to correctly represent the combustion occurring in the swirl and bluff-body stabilized burner developed at Instituto Superior Técnico by properly predicting in-flame temperatures, residence times, and species concentrations as well as overall combustion efficiency as outputs of the simulation.

There are some computational ways of performing a burning simulation. It must take into account the computational cost and the main objective of the simulation in order to do effective work. Chemical Reactor Network (CRN) modeling was the chosen approach to model combustion flame in the aforementioned burner of IST, for its already demonstrated ability to simulate combustion chemistry with consequently good emission prediction, requiring low computational power and little running time. The simplifying assumptions implied by this method have already been presented in Section 2.6, concerning the theory of chemical reactors.

3.2.1 Cantera package

To implement and perform the Chemical Reactor Networks simulations, Cantera open-source object-oriented software [58], with Python interface, was the chosen alternative. Cantera is a package of tools that allows an efficient modeling approach to problems involving chemical kinetic, thermodynamics and transport processes. Being object-oriented it allows a significant flexibility in shaping the reactor network and defining boundary conditions, as well as the managing and treatment of the output data. To integrate the system of stiff ODEs of the reacting system for the calculation of the temperature and species evolution with time (Section 2.2) Cantera uses CVODES solver from the Sundials package [60]. In this

work the steady-state solution of the reactor network was always used.

Being an open-source and relatively new tool, with still incomplete functionalities that are continuously being improved, programming in Cantera requires an additional learning effort, both in terms of implementing the desired models and of troubleshooting. Although fairly new, the Cantera suite has already demonstrated adequate results in recent combustion investigations reported by several authors [61–64], and is currently attracting the attention among the researchers in this area.

Regarding chemical modeling, Cantera uses .cti files as inputs, which contain all species and reaction parameters, as well as thermodynamic and transport data, specified for a given chemical kinetic mechanism available in the literature. Cantera provides a way to convert these files from the widely used Chemkin software [65] input files .inp, .dat and .trans.

3.2.2 Mechanism Selection

The first step for this campaign was to select the most appropriate chemical kinetic mechanism(s) that would be used in the process of modeling chemical reactions in combustion and thus perform simulations (Section 2.3). As it was mentioned in Section 1.2.2, some mechanisms have been proposed for the ammonia combustion modeling and, precisely, for ammonia-hydrogen combustion. Within this list presented, only two mechanisms will be chosen, preferably one that can bound NO_x production from above and one that can bound NO_x production from below, and it is expected that, in general, the detailed mechanisms will override NO_x production. The performance of the mechanisms reported in the available literature will also be a criterion for choice.

The Miller and Bowmann mechanism [38] was the first to be discarded due to its outdatedness and unsuitability to model the oxidation of ammonia under conditions different from those for which it was validated, as attested by the authors themselves, despite its importance in historical terms. The Konnov et al. mechanism [39] was also quickly sidelined due to the fact that it always greatly overproduces NO_x emissions, according to several authors [4, 66]. The Tian [25] and Song [44] mechanisms were the next to be discarded, mainly due to the fact that they were developed and validated for pressure conditions very different from the atmospheric pressure considered in this study.

The remaining mechanisms - Klippenstein et al. [42], Otomo et al. [45], Nakamura et al. [46], Li et al. [48], Glarborg et al. [47] and Stagni et al. [49] - were all tested with the current model. The Li et al. and Glarborg et al. mechanisms were the ones that, prominently, most predicted NO_x production, with Li et al. being the one that predicts in the most excess. On the other hand, for one of the modeled flames ($\phi = 0.7$ and $x_{NH_3} = 0.9$), only the mechanism of Glarborg at al. was able to predict the ignition of the fuel mixture at the burner inlet. The fact that this mechanism is particularly extensive is also advantageous in that it allows the performance of a fairly detailed kinetics model to be evaluated in the simulations

presented. Thus the mechanism of Glarborg et al. was one of those selected.

The mechanisms of Klippenstein et al., Otomo et al. and Nakamura et al. showed results for NO_x values still higher than the experimental ones but still well below those of Li et al. and Glarborg et al., with Otomo et al. giving results with the least overprediction. The Stagni et al. mechanism, the most recent and perhaps least known, was the one that gave lower NO_x production results and therefore closer to the experimental ones, as will be seen later. For this reason this was the second mechanism selected for demonstration and comparison of results. For simplicity, each of Glarborg et al. and Stagni et al. will sometimes be called the Glarborg mechanism and the Stagni mechanism, respectively.

3.2.3 Model implementation

The previous works of Franco et al. [35] and Rocha et al. [36] have already described some different lean flames through in-flame measurements of temperature and species concentrations and also through RANS simulations. Pacheco et al. [37] presented experimental results of both temperature and emissions for some stoichiometric and rich flames, as well as a first study using the CRN approach for species concentration prediction. These works were taken as starting point in the development of the model presented here.

CRN model architecture

It was described before in Section 2.6 that a stabilized flame can be modeled by a network of interconnected chemical reactors that represent specific zones of the flame with homogeneous properties. The network design had successive changes until its current layout. The interactions between the various reactors also had a progressive evolution until the final configuration. It would be too space-consuming and perhaps of little use to describe in this text the whole evolutionary process of the model. However, it is important to state that the main criterion for improving the model was conformity with known experimental data. All the previous versions of the model that have been surpassed for not faithfully predicting these data have provided, in a way, a deeper understanding of reality by the need to model it correctly.

Identifying the precise location of the different zones within the flame is the first and crucial step in modeling using a reactor network. A hypothesis for the division of several distinct zones of the flame, as shown in Figures 3.7 and 3.8, had been pointed out previously by Franco et al. [35] and Rocha et al. [36]. Through RANS simulations and by visualization of the flame it was possible to distinguish certain zones where gas recirculation was stronger mainly due to the swirl of the incoming reactant mixture and the bluff-body effect. Thanks to the strong recirculation in these zones there is rapid mixing of the fuel with the oxidizer and also with the gases resulting from combustion, already at high temperatures. The high mixing rates achieved in these zones lead to considerable uniformity of temperature, pressure, and species concentrations throughout their domain. Due to these characteristics, as exposed in Section 2.6 it is convenient to theoretically model these zones by perfect mixing reactors (PSRs). There are other

zones within the flame, distinct from the previous ones, where there is virtually no recirculation and the gases simply flow streamwise. These zones must be modeled by plug-flow reactors (PFR).

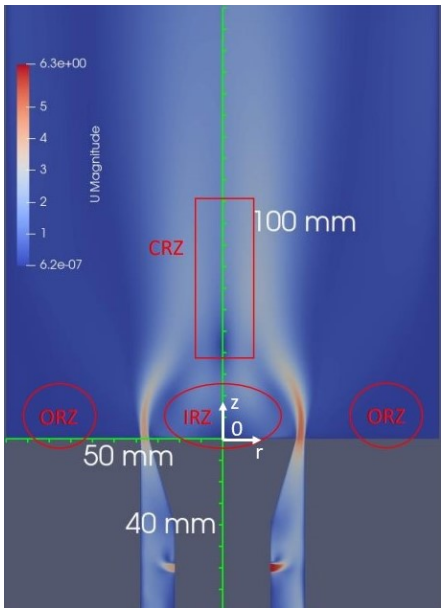

Figure 3.7: Isothermal velocity (magnitude): $\phi = 0.8$, $x_{NH_3} = 0.8$ (left) and $\phi = 1.0$, $x_{NH_3} = 0.8$ (right). Reprinted from [36].

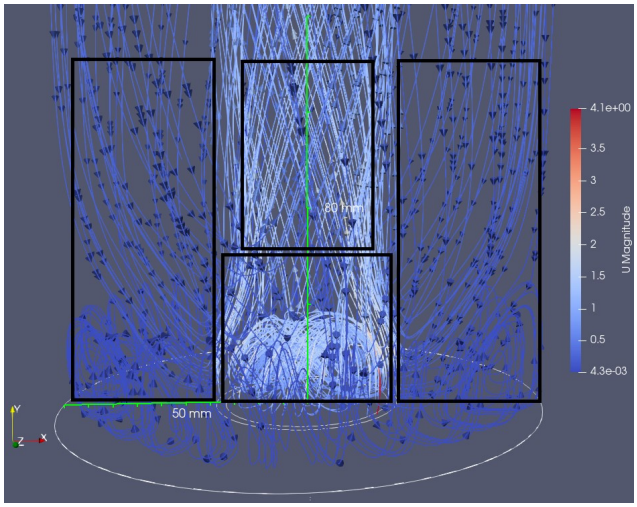

Figure 3.8: (3D) Streamlines with vectors for isothermal velocity: $\phi = 0.8$, $x_{NH_3} = 0.8$. Are indicated distinct regions of flow. Adapted from [36].

Resorting to images from RANS simulations previously performed by [36], the dimensions of each PSR reactor and the PFR reactor were estimated, as represented in Figure 3.9. All reactors are considered to be of constant volume, which corresponds to the solid or hollow cylinder whose profile section has the shape of the respective region, shown in Figures 3.9 and 3.10.

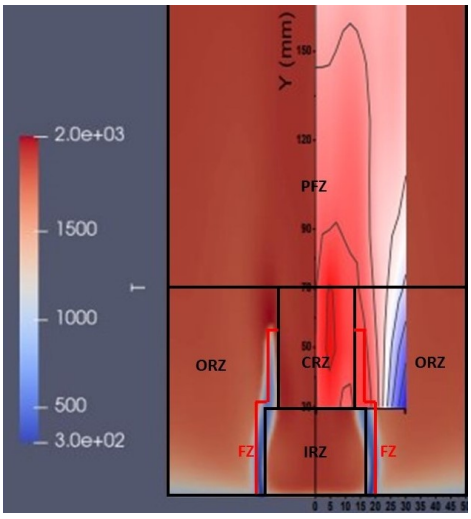

Figure 3.9: Reactors network based on the Temperature profile from RANS reacting simulation ($\phi = 0.8$, $x_{NH_3} = 0.8$). Adapted from [36].

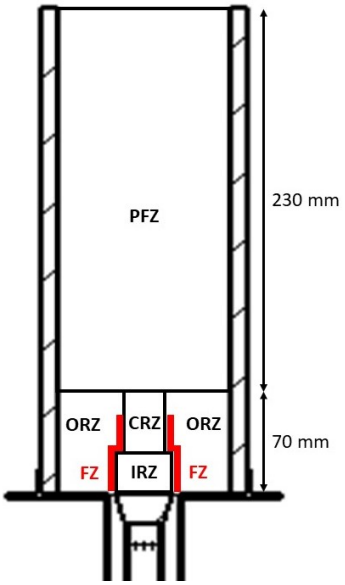

Figure 3.10: Schematic outline of reactors network for flame modeling in the burner.

According to what has already been explained, five distinct zones have been identified, which are rep-

resented in Figure 3.9. The region in the vicinity of the burner mouth was subdivided into four different flow regions, and their boundaries were defined approximately, without any strict criteria for this subdivision, and adjusted for a better reproduction of the experimental results. Those regions are modeled by PSRs. They are the Flame Zone (FZ), the Inner Recirculation Zone (IRZ), the Central Recirculation Zone (CRZ), and the Outer Recirculation Zone (ORZ). It is perhaps worth mentioning that other authors have proposed similar flame zones division [22, 28]. The remaining zone corresponds to the entire region of the flame beyond the region of greatest turbulence and is therefore modeled by a PFR. This zone is called the Post-Flame Zone (PFZ). It should be noted that although the PFZ is referred to as one PFR reactor, in fact, in its computational implementation it is made up of a linear chain of several PSR reactors, as many as is desired for more accurate modeling. A more detailed description of each of these zones might be useful.

Flame Zone (FZ) is, as the name implies, the reactor that is intended to model the flame front, where the fuel initially ignites in the presence of the oxidizer (in this case, air). All the fuel and most of the incoming air initially enters this zone. Because it is the area where ignition occurs, it is the area that reaches the highest temperatures. It is in contact with the other three recirculation zones IRZ, CRZ, and ORZ, with which it exchanges mass and heat.

Inner Recirculation Zone (IRZ) is the recirculation zone immediately downstream the burner mouth, generated by the bluff body. This zone receives the unburned or resulting combustion gases coming from the FZ, where they remain for a certain residence time which promotes quite intense mixing rates. Due to the in-flow velocity and due to the tendency of the upward movement of the hot gases it is expected that a larger fraction of gases leaving the IRZ goes directly to the CRZ although a smaller fraction may return to the FZ.

Central Recirculation Zone (CRZ) is immediately downstream of the IRZ and the FZ and is also in contact with the ORZ and upstream of the PFZ, i.e. interacting with all the flame zones considered. As it is downstream of the IRZ and FZ, it receives from these zones a considerable mass flow of hot gases that remain there for some time in recirculation and re-burning, after which they flow to the PFZ. A very residual flow may recirculate to some of the other zones. It has been verified through visualization of the flames in the laboratory that considerable flaring of unburned gases occurs in this recirculation zone.

Outer Recirculation Zone (ORZ) is the outer region of the flame that extends to the wall of the quartz tube of the burner. In this region, although some radical reactions are expected, no combustion reactions are expected to occur and therefore temperatures will be lower, with typically high oxygen concentrations due to the incoming atmospheric air. It is expected that atmospheric air and some hot combustion gases, coming from the FZ or CRZ, remain recirculating there during a long residence time. From the ORZ the recirculating gas mixture goes mostly to the PFZ, although it has been admitted that a small fraction may also enter the CRZ, and follow from there to the PFZ.

Post-Flame Zone (PFZ) is the last part of the flame, downstream of the recirculation zones already mentioned. In the modeling performed it was assumed that this region occupies the entire volume of the interior of the quartz tube above the recirculation zones, with the gases present in this zone in contact with the tube wall. The flow admitted in this region comes from the CRZ and ORZ. This region is characterized by a continuous and stationary flow of the gases resulting from combustion, without recirculation occurring. Several reactions are expected to take place here, particularly selective non-catalytic reduction (SNCR) reactions due to the large concentration of NO_x produced in the previous recirculation zones and the presence of unburned NH_3 as well as oxygen from the ORZ.

Figure 3.11 shows the schematic diagram of the final reactor network, closely linked with that of the Figure 3.9. This diagram shows the considered interactions between the various reactors. As laid out in this diagram the various interconnected reactors will interact with each other through mass and heat exchange, as predicted by chemical reactor theory. These two types of interaction were taken into account in the development of the model, which will be further described below.

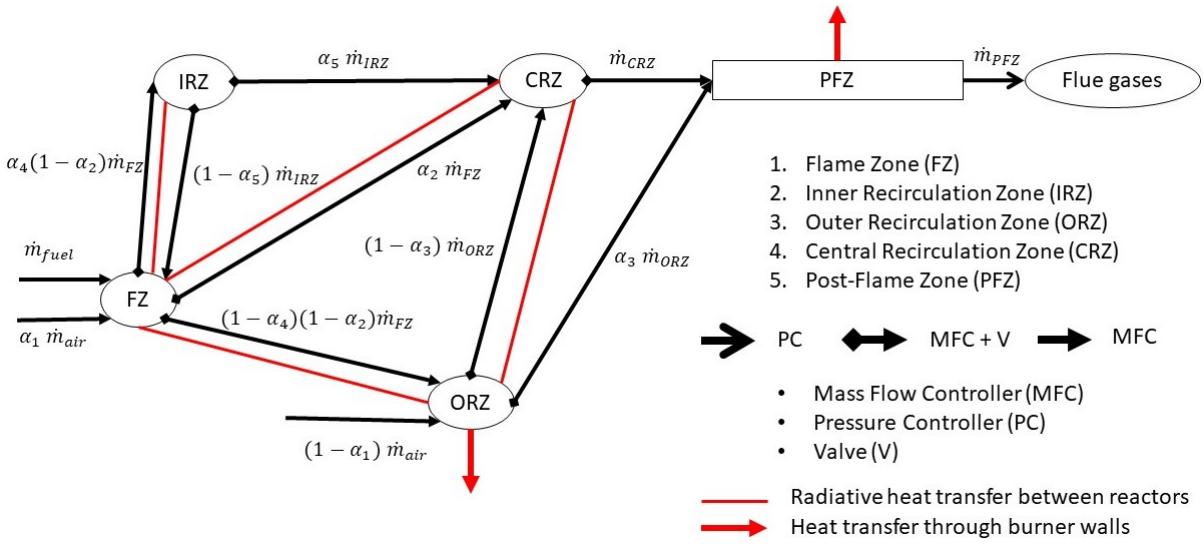

Figure 3.11: Diagram for the CRN model of a single-stage swirl and bluff-body burner type.

Mass transfer

Regarding the mass exchanges, we must first ensure mass conservation for all reactors considered, given by Equation 2.26, presented in Section 2.6. From this equation, it follows directly that the mass flow rate at the inlet of each reactor in the network must equal the mass flow rate at its outlet. Under this assumption it is possible to calculate the mass flow rates exchanged by the various connected reactors, assuming coefficients (α_1 to α_5) for the mass flow fractions leaving or entering a given chemical reactor. Logically these coefficients will have to be estimated in order for the modeling to be appropriate for each particular case, since flames with different inlet conditions may have different flow patterns. Starting from the scheme shown in Figure 3.11 the Equations 3.1 to 3.5 allow the mass flow rates in each reactor

to be calculated, as a function of the total mass flow rates of incoming air and fuel and the coefficients α_1 to α_5 ($0 < \alpha_i < 1$, for $i = 1, .., 5$).

$$\dot{m}_{FZ} = \alpha_1 \, \dot{m}_{air} + \dot{m}_{fuel} \tag{3.1}$$

$$\dot{m}_{ORZ} = (1 - \alpha_1) \, \dot{m}_{air} + (1 - \alpha_4) \, (1 - \alpha_2) \, \dot{m}_{FZ} \tag{3.2}$$

$$\dot{m}_{IRZ} = \alpha_4 \, (1 - \alpha_2) \, \dot{m}_{FZ} \tag{3.3}$$

$$\dot{m}_{CRZ} = \alpha_2 \, \dot{m}_{FZ} + \alpha_5 \, \dot{m}_{IRZ} + (1 - \alpha_3) \, \dot{m}_{ORZ} \tag{3.4}$$

$$\dot{m}_{PFZ} = \dot{m}_{air} + \dot{m}_{fuel} \tag{3.5}$$

The choice, implementation, and adjustment of these mass flow partition coefficients (α_1 to α_5) was a particularly time-consuming part of the model development process. Apart from some basic intuitions that came from the observation of the NH_3/H_2 flame and that allow us to give a general notion about the value of some of these coefficients, they are not known a priori. Thus, the procedure adopted was to perform successive tests of different combinations of these coefficients comparing the model results, for each combination, with the experimental results, by calculating the relative error as well as observing the trends of the results. The adjustment of the value of each coefficient thus followed this quantitative and qualitative method. The fact that a computer simulation of a CRN model can be relatively fast allows the parameters to be adjusted in a reasonable amount of time.

The coefficient α_1 represents the ratio of air mass flow rate that enters directly into the FZ and mixes with the fuel present there, where the initial ignition occurs. It was assumed that the remaining amount of incoming air that does not enter the FZ disperses into the ORZ, where it remains in recirculation for a considerable residence time. The α_1 fraction must be large enough to have the necessary amount of air in the FZ to enable combustion within flammability limits. The coefficient α_2 is the ratio of the mass flow rate of the gaseous mixture (unburned fuel and combustion products) present in the FZ that flows directly to the CRZ. It is expected that most of the mass flow out of the FZ will be fed into the CRZ, where flaring of unburned ammonia is likely to occur through recirculation of hot gases resulting from combustion. The coefficient α_3 is the ratio of gas mixture mass flow rate present in the ORZ that goes directly to the PFZ. The remaining fraction enters the CRZ where it recirculates with the other gases there. The coefficient α_4 is the ratio of the mass flow rate of the gas mixture present in the FZ entering the IRZ where it remains in recirculation. This fraction can be expected to be small since there doesn't seem to be any burning in this area. The coefficient α_5 is the ratio of the mass flow rate of the recirculating gas mixture in the IRZ that goes into the CRZ. This fraction can be expected to be quite large since it is most natural for the gases present in the IRZ to rise to the CRZ, and then enter the PFZ.

In terms of the Cantera implementation, there are three appropriated flow devices to model the mass transfer between 0-dimensional reactors: by using mass flow controllers (MFC), valves (V), or pressure

controllers (PC). These flow devices are considered in the diagram in Figure 3.11.

Mass flow controllers are characterized by allowing a specific mass flow rate into or out of each reactor, regardless of upstream and downstream conditions, an aspect that must be taken with care for proper use. Valves allow the transfer of a mass flow rate dependent on the pressure difference between the two reactors. This mass flow rate is given by Equation 3.6, where K_v $(kg/s/Pa)$ is a proportionality constant and $P_2 - P_1$ is the pressure difference between upstream (1) and downstream (2) reactors. This flow device can be used between two reactors to keep a minimum of pressure difference between them. To attain that K_v must be sufficient large, up to a limit associated with the stiffness of the EDOs system [58, 63]. Thus, the value of K_v was imposed to 1×10^{-6} $kg/s/Pa$, since for higher values the simulations often crashed. Used in parallel with the MFC, a Valve allows the correction of pressure peaks that have been generated by the forced mass transfer performed by the former.

$$\dot{m} = K_v(P_1 - P_2) \tag{3.6}$$

Pressure Controllers, typically used in series with a MFC, are installed at the outlet of a reactor and allow the flow rate specified by the upstream MFC, plus a small correction dependent on the pressure difference, which is given by Equation 3.7. This implies that the reactor in question has only one mass flow inlet and one mass flow outlet, which can be an important limitation knowing that in general reactors may have more than one inlet or outlet.

$$\dot{m} = \dot{m}_{MFC} + K_v(P_1 - P_2) \tag{3.7}$$

The way these flow controllers were used in the model is shown in Figure 3.11. In a first approach, only MFCs were used for imposing the flow rates in the reactors according to Equations 3.1 to 3.5. However, it was found that the pressure in certain reactors reached unreasonable values, an order of magnitude higher than atmospheric pressure. This was understood to be perhaps due to the high stiffness of that system, with all flow rates being imposed. So, to overcome this problem, a V was placed in parallel with each MFC, thus giving some slack to the system. The mass flow rates imposed by the MFCs were not changed. Thus, the expected pressure values have already been verified, very close to the atmospheric pressure and with very slight differences between the various reactors. The pressure in each reactor is calculated in the simulation (output), since the volumes of each reactor are constant and imposed.

Regarding the residence times of each reactor they are obtained by Equation 2.31. The mass flow rates are given by Equations 3.1 to 3.5, as seen, the volumes are known and constant, and the density is calculated by solving the ODEs of the reacting system, through Cantera. Thus, residence times are addressed as an output of the model, controlled by the mass flow rates, i.e., through the coefficients α_1 to α_5.

Heat transfer

It was settled that the temperature in each reactor should be calculated and given as an output of the simulation, rather than imposed and considered as an input. This option was taken considering that the need of a temperature profile as input data would limit the cases to be analyzed, in complete dependence on the availability of temperature measurements. The actual option seems to provide a more versatile model.

Due to the lack of available information on heat losses of the burner used as well as the still incipient information in the literature on the radiative heat emitted by ammonia flames some simplifications had to be made. The solution presented here is therefore based on certain simplifying assumptions that should be taken with care, leaving the more elaborate study of heat transfer modeling for future work, since it requires a more in-depth analysis that is beyond the focus of this work, although it can be very useful for improving the present model. The Cantera package allows establishing heat transfer between interconnected reactors according to the Equation 2.30, as described in Section 2.6. It is assumed that heat transfer only takes place in the radial direction. Due to the impossibility of quantifying the heat flux released by the flames the heat transfer must be approximated by estimating values for the overall heat transfer coefficient and emissivity.

It was first considered that there is considerable heat transfer between the inside of the quartz tube where the flame exists, and the outside, at room temperature (298 K), promoted through convection of the combustion gases and conduction through the tube wall. Radiation was considered negligible due to good burner insulation and materials used. It was assumed a constant overall heat transfer coefficient (U_{ovr}) throughout the entire burner wall. This U_{ovr} coefficient can be calculated by Equation 3.8.

$$U_{ovr} = \frac{1}{\frac{1}{h_{qt}} + \frac{r_{qt}}{k_{qt}} \ln\frac{r_{cw}}{r_{qt}} + \frac{r_{qt}}{k_{cw}} \ln\frac{r_{ss}}{r_{cw}} + \frac{r_{qt}}{k_{ss}} \ln\frac{r_{ext}}{r_{ss}} + \frac{r_{qt}}{r_{ext}} \frac{1}{h_{ext}}} \tag{3.8}$$

Using the dimensions of the various insulation layers of the mentioned burner and using typical values for the thermal conductivity of the materials used ($\kappa_{qt} = 1.38\ W/(mK)$, $\kappa_{cw} = 0.35\ W/(mK)$ and $\kappa_{ss} = 15\ W/(mK)$) [67–69] as well as for estimated heat convection coefficients for a sufficient wide range of values that may be reasonable for this case (interior forced convection: $h_{int} = 30 - 90\ W/(m^2K)$; exterior free convection: $h_{ext} = 10 - 15\ W/(m^2K)$) [70–72] it is possible to estimate that the value of U_{ovr} will most likely be within the range of 5-11 $W/(m^2K)$. In Large-Eddy Simulation (LES) performed previously, for lean flames at a thermal input of 1900 W, Franco et al. assumed a coefficient of 10 $W/(m^2K)$. This value was also taken into account as an initial estimate for the present model. In any case, these ranges of values served only as a reference since the values adopted in the model were those that allowed the best numerical results to be obtained.

Given the different conditions of each different flame, it is expected that for each flame the value of U_{ovr} will be different. One of the major obstacles in this process of obtaining a reasonable value of U_{ovr} was

to understand how this value could vary depending on the conditions of the flames considered. Some assumptions had to be made. Considering the studied flames, the coefficient U_{ovr} may vary especially depending on thermal input, equivalence ratio, and the volumetric fraction of ammonia in fuel, apart from other less relevant influences. The increase in the thermal input, as well as the proximity of the stoichiometry in terms of equivalence ratio, have the direct effect of increasing the flame temperature. Greater temperature differences between the inside of the burner and the outside lead to greater heat transfers and thus higher U_{ovr} coefficients. Increasing the NH_3/H_2 ratio implies decreased temperature due to the lower calorific value of NH_3 as well as its worse reactivity. Thus, it is expected that the lower temperature difference between indoor and outdoor translates into lower values of U_{ovr}. The difficulty arises when it is necessary to understand the preponderance of one of these factors over the others since it is necessary to compare coefficients for flames with varied thermal input, equivalence ratio, and NH_3/H_2 ratio.

Besides that, from the observation of the various experimental temperature profiles (r = 0 mm, z = 30 - 300 mm) in Figure 3.12 it is possible to verify that the slope of the temperature decrease along the burner is very similar for the various flames analyzed, which allows us to think that, approximately, the overall heat transfer coefficient will not be very different from one flame to the other. Thus, although it is very difficult with the available data, to estimate accurate values for the U_{ovr} some tests were conducted for different reasonable values and final numerical results compared with experimental ones to choose the most appropriate for each flame.

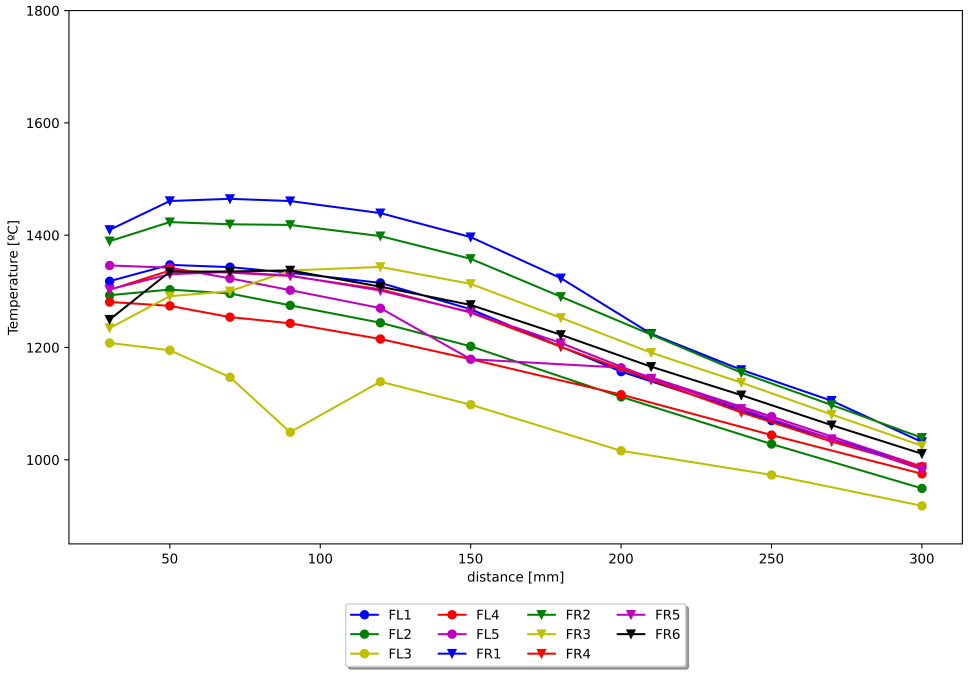

Figure 3.12: Experimental profile temperatures (r=0mm, z=30-300mm) for eleven flames analyzed, lean (FL) and stoich./rich (FR). Data from [35] and [37].

With respect to radiative heat transfer, other assumptions were carried out. As it was already mentioned, emission from hot flame gases to the exterior of the burner was considered negligible due to the burner

insulation. However, in order to model the heat transfer between the connected reactors it was considered that the sidewalls of each reactor would emit radiative heat to the other reactor with the same wall, by an emissivity coefficient equal to the flame gas emissivity. This modeling intends, in some way, to simulate the heat transfer between the various reactors by assuming heat radiation between the masses of hot gas contained in each of them. In this way, the various reactors inside the flame (recirculation zones) are approximated as radiant grey bodies. According to this reasoning, the FZ would exchange heat by radiation with the IRZ, the CRZ and the ORZ; the IRZ would exchange with the FZ only; the CRZ would exchange with the FZ and ORZ; the ORZ would exchange with the FZ and the ORZ. The PFZ was considered as not participating in these exchanges: it only exchanges heat with the outside through convection and conduction through the burner walls.

Some comments can be made to this hypothesis. On the one hand, gas radiation is a volumetric phenomenon [70] contrary to what happens in this modeling, where the intention is to simulate gas radiation by the radiation emitted by reactor walls, that is, considering it as a surface phenomenon. In addition, it is not possible to evaluate the validity of using typical values of emissivity of gases considering its radiation as a surface phenomenon. On the other hand, it seems reasonable to think that a chemical reactor that models a zone inside a flame exchanges heat with the neighbouring reactors. Although this approximation is relatively crude, a more in-depth study of the radiation phenomenon is not the focus of this work. Later on, in Section 3.2.4, it will be seen that this hypothesis was not abandoned due to the fact that it allows better results to be obtained.

The emissivity appears in Equation 2.30. As is known from the literature, the radiative emission of gases in combustion processes depends particularly on the chemical species CO_2 and H_2O. For the fuel considered in this thesis, only water vapor exists in the combustion products, so this is the main species contributing to the heat radiation of the flames studied. As we can see from Equation 2.3 of the overall reaction for the fuel in question, the mole fraction of water in the products increases with the increase of the mole fraction of ammonia in the NH_3/H_2 fuel mixture, resulting in higher radiation expected for flames with higher NH_3/H_2 ratio if nothing else would intervene in the radiative phenomenon. However, one cannot disregard the influence of temperature variation and the characteristic size of the flame [70], which are altered by varying the NH_3/H_2 ratio (as well as thermal input and equivalence ratio), and which also have an influence on the radiation of the gas. It is therefore very difficult to conclude on the variation of the emissivity value depending on the actual conditions of each flame analyzed. In comparison with other typical hydrocarbon flames, which have considerable amounts of CO_2 and soot in their products, NH_3/H_2 flames with similar characteristics will be less radiative, which was qualitatively proven in the laboratory.

Unfortunately, research on radiative heat transfer in ammonia or ammonia/hydrogen combustion is still incipient and the information available in the literature is still very scarce. Therefore, it is not possible currently to find precise values of radiative characteristics, such as emissivity, for this particular type of

flame. The alternative adopted to choose acceptable values for the emissivity of the flames was thus to consider intermediate values between typical emissivities for hydrogen flames and for hydrocarbon flames, particularly for biofuels, since it is expected that they have calorific value and vapor fraction in the products of combustion closer to those of NH_3/H_2 flames, at least when compared with other commonly used conventional hydrocarbons. Through a literature search, it was possible to arrive at the values of 0.1 for the emissivity of an H_2 flame (no other flame characteristics are specified) [73] and also the range of maximum flame emissivity values at 0.05 - 0.25, for a range of equivalence ratios of 0.71- 0.91, for volatilized biomass lean flames, presented by Yan et al. [74]. These authors reported that both emissivity and maximum temperature decreased with decreasing equivalence ratio. These ranges of values were used as a reference for the model developed, and the final emissivity values were adopted, again, after work to adjust the final results predicted by the model for various emissivities with the experimental results.

It remains to alert to the approximation, perhaps crude, that is made of the modeling of heat transfer between the various reactors in contact, in the initial and interior zone of the flame. It is not the intention here to make an in-depth analysis of the radiative phenomenon of gases but only to give some fundamental notions in order to understand what was intended to be done in the model and what uncertainties it incurs. Given all these factors there is no way to know exactly the variation of both the U_{ovr} and the ϵ coefficients. The main criterion considered was always the fit of the model results to the experimental ones, considering a priori that the values of the aforementioned coefficients should be within the reasonable ranges that were exposed here.

Rich-Quench-Lean implementation

As presented in Section 2.5.2 a combustor designed according to the RQL concept consists, essentially, of three stages: the first stage, where primary air and fuel mass flow rates enter in the burner and rich combustion takes place; the second stage, where the secondary air mass flow rate enters at high velocities promoting high mixing with the effluent gases coming from the first stage; and the lean stage, where new combustion reactions, as well as others (for example, SNCR), can take place due to the presence of enough air and unburned NH_3 and H_2 produced from NH_3 cracking, as well as relative high temperatures to assure those reactions.

Taking advantage of the model that was developed for the single-stage combustor, there is already a first stage, which will be the rich stage of the new RQL combustor. It only remains to add two additional stages: one for the Quench Zone (QZ) and the other for the Lean Zone (LZ). Figure 3.13 shows the layout for the new reactor network, this time an RQL-type system. The QZ, where the quick mixing of the incoming air and effluent gases occurs was modeled as a perfectly-stirred reactor with heat transfer with the exterior through quench stage walls and without chemical reactions taking place (in Cantera this can be implemented by setting *chemical_enable = False*), as no reactions are expected to occur in this zone [56, 57]. The LZ was modeled by a plug-flow reactor along which reactions occur, and with heat

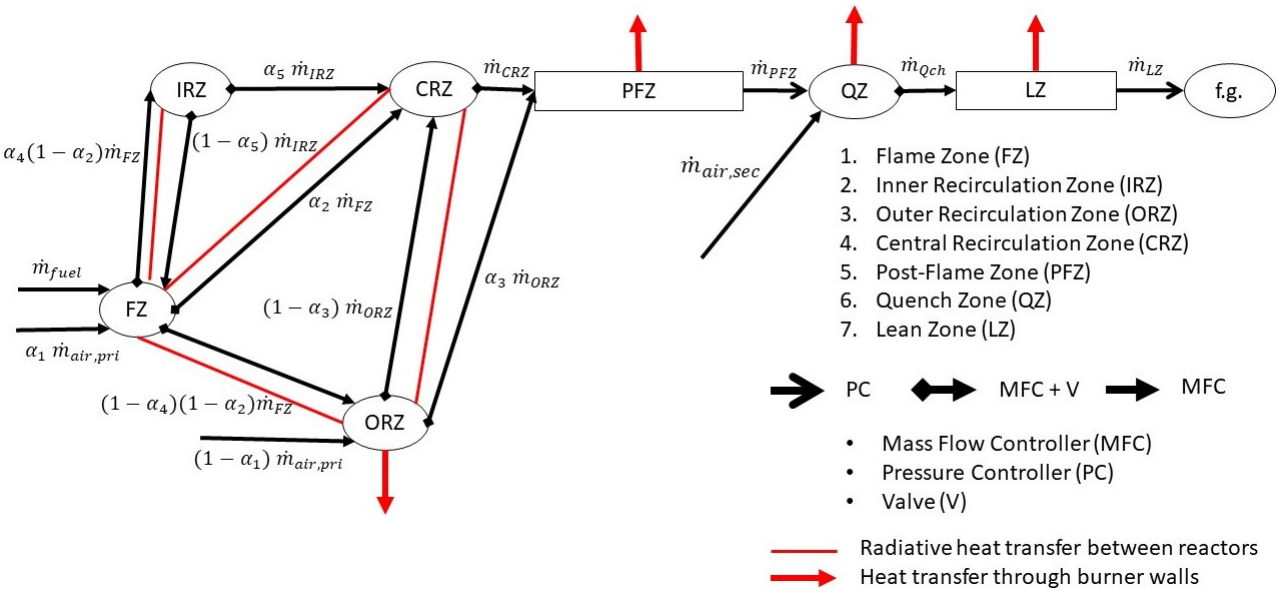

Figure 3.13: Diagram for the CRN model of a swirl and bluff-body burner adapted to RQL type combustor.

transfer with the exterior through lean stage walls. A simplified sketch of the RQL system geometry is shown in Figure 3.14.

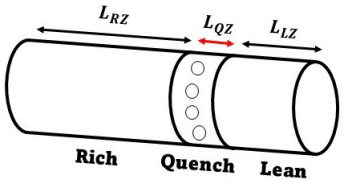

Figure 3.14: Basic design of the RQL combustor type.

The study of the RQL combustor concept requires the introduction of a parameter to estimate the length of the Quench, of particular interest for future practical implementation. This parametric study will be addressed in Section 4.4.4. For simplicity, a value for the Lean stage length was assumed at the outset. Other parameters related to RQL effectiveness were studied and are exposed in Section 3.2.5. The results for the RQL combustor model are presented and commented on in Section 4.4.

Model inputs

Regarding combustor geometry, all the relevant data are set out in Table 3.2.

The incoming air and fuel enter the burner at ambient temperature (298 K) and pressure (1 atm). The NH_3/H_2 fuel mixture is initialized with the respective molar fractions of each chemical species, respective to each flame. The values of the air and fuel (NH_3 and H_2) input mass flow rates were calculated using the equations presented below, depending on the desired thermal power, NH_3 molar fraction in fuel mixture and equivalence ratio. Thermal input or power input, TI, is given by Equation 3.9.

$$TI = \dot{m}_{fuel}\ LHV_{\text{fuel}} = \dot{m}_{\text{NH}_3}\ LHV_{\text{NH}_3} + \dot{m}_{\text{H}_2}\ LHV_{\text{H}_2} = \dot{m}_{fuel}\ (y_{\text{NH}_3}\ LHV_{\text{NH}_3} + y_{\text{H}_2}\ LHV_{\text{H}_2}) \quad (3.9)$$

Table 3.2: Geometric dimensions of reactors in flame model.

Reactor	D_i $[m]$	D_o $[m]$	L $[m]$	A_{sup} $[m^2]$	V $[m^3]$
FZ	0.034	0.038	0.06	7.16e-03	1.36e-05
IRZ	-	0.034	0.03	3.20e-03	2.72e-05
CRZ	-	0.025	0.04	3.14e-03	1.96e-05
ORZ	0.038	0.1	0.07	2.20e-02	4.89e-04
PFZ	-	0.1	0.23	7.23e-02	1.81e-03
QZ	-	0.1	L_{QZ}	$f(L_{QZ})$	$f(L_{QZ})$
LZ	-	0.1	0.2 - L_{QZ}	$f(L_{QZ})$	$f(L_{QZ})$

From which can be derived the Equation 3.10, allowing the calculation of the total fuel mass flow rate from the thermal input and fuel constituents properties.

$$\dot{m}_{fuel} = \frac{TI}{y_{\mathsf{NH_3}}\ LHV_{\mathsf{NH_3}} + y_{\mathsf{H_2}}\ LHV_{\mathsf{H_2}}} \tag{3.10}$$

Where y_i ($i = \mathsf{NH_3}\ and\ \mathsf{H_2}$), calculated by Equation 3.11 as function of species mole fraction x_i in the fuel, is the mass fraction of each component in the total fuel mixture and LHV_i ($i = \mathsf{NH_3}\ and\ \mathsf{H_2}$) is the Lower Heating Value of each one of the gaseous fuels considered.

$$y_i = \frac{M_i\ x_i}{M_i\ x_i + M_j\ x_j} \quad for \quad i,j = \mathsf{NH_3}\ and\ \mathsf{H_2} \quad and \quad i \neq j \tag{3.11}$$

Thus it is possible now to compute all the fuel mass flow rate values by Equation 3.12, assuming ideal gas state.

$$\dot{m}_i = y_i\ \dot{m}_{fuel} \quad for \quad i = \mathsf{NH_3}\ and\ \mathsf{H_2} \tag{3.12}$$

And also the volumetric flow rates as well, by Equation 3.13.

$$\dot{V}_i = \dot{m}_i\ \frac{R_i\ T}{p} \quad for \quad i = \mathsf{NH_3}\ and\ \mathsf{H_2} \tag{3.13}$$

In order to calculate the air mass flow rate for each equivalence ratio, ϕ, defined by Equation 3.14, the following equations will be useful.

$$\phi = \frac{(\frac{\dot{m}_{air}}{\dot{m}_{fuel}})_{st}}{(\frac{\dot{m}_{air}}{\dot{m}_{fuel}})} \tag{3.14}$$

Since the fuel mass flow rate remains constant during the operation with a specific flame, Equation 3.15 can be derived from the previous Equation 3.14.

$$\dot{m}_{air,i} = \frac{\dot{m}_{air,st}}{\phi_i} \quad for \quad i = pri,\ sec\ and\ ovr \tag{3.15}$$

Considering single-stage combustor Equation 3.15 directly gives the air mass flow rate, function of equivalence ratio. For the RQL system, some deductions are needed due to the air flow splitting in two stages, and are expressed by Equations 3.16 to 3.19.

$$\dot{m}_{air,ovr} = \dot{m}_{air,pri} + \dot{m}_{air,sec} \tag{3.16}$$

$$\dot{m}_{air,i} = \frac{\dot{m}_{air,j}\ \phi_j}{\phi_i} \Leftrightarrow \frac{\phi_i}{\phi_j} = \frac{\dot{m}_{air,i}}{\dot{m}_{air,j}} \quad for \quad i,j = pri,\ sec\ and\ ovr \quad and \quad i \neq j \tag{3.17}$$

$$\phi_{ovr} = \frac{\dot{m}_{air,st}}{\dot{m}_{air,ovr}} = \frac{\dot{m}_{air,st}}{\dot{m}_{air,pri} + \dot{m}_{air,sec}} = \frac{\dot{m}_{air,st}}{(\frac{\dot{m}_{air,st}}{\phi_{pri}}) + \dot{m}_{air,sec}} \tag{3.18}$$

$$\dot{m}_{air,sec} = \dot{m}_{air,st}\ (\frac{1}{\phi_{ovr}} + \frac{1}{\phi_{pri}}) \tag{3.19}$$

After a simple mathematical manipulation, from Equations 3.15 and 3.19 it can be obtained Equation 3.20, which expresses the $\dot{m}_{air,sec}$ as function of $\dot{m}_{air,pri}$, ϕ_{pri} and ϕ_{ovr}.

$$\dot{m}_{air,sec} = \dot{m}_{air,pri}\ (\frac{\phi_{pri}}{\phi_{ovr}} - 1) \tag{3.20}$$

After calculating values by this process, it was observed that there are slight differences between the values obtained through this calculation and the flow rates used in the laboratory tests [59]. For each flame, the calculated air mass flow rate is slightly higher than experimental air mass flow rate (around 2.5% difference from the experimental) and the calculated fuel mass flow rate is lower than the experimental fuel mass flow rate (for a difference ranging from 45-56% compared to the experimental). In the present work, theoretical values were chosen to be used rather than the ones exactly used in the laboratory. The choice to use the theoretical values was due to the fact that by using the experimental mass flow rates in the simulation the predicted results were not satisfactory. The initial conditions for the eleven flames studied are given in Table 3.3.

Table 3.3: Operating conditions theoretically obtained for each flame analized.

		Initial Conditions						
		$TI\ [W]$	x_{NH_3}	ϕ	$\dot{m}_{air}\ [kg/s]$	$\dot{m}_{NH_3}\ [kg/s]$	$\dot{m}_{H_2}\ [kg/s]$	$V\ [m/s]$
Flame 1	Lean	1900	0.7	0.8	7.539×10^{-4}	7.693×10^{-5}	3.911×10^{-6}	3.50
	Stoich.	2800	0.7	1.0	8.888×10^{-4}	1.134×10^{-4}	5.763×10^{-6}	4.33
Flame 2	Lean	1900	0.8	0.8	7.626×10^{-4}	8.575×10^{-5}	2.543×10^{-6}	3.52
	Rich	2800	0.7	1.1	8.080×10^{-4}	1.134×10^{-4}	5.763×10^{-6}	4.03
Flame 3	Lean	1900	0.9	0.7	8.809×10^{-4}	9.415×10^{-5}	1.241×10^{-6}	3.94
	Rich	2800	0.7	1.2	7.407×10^{-4}	1.134×10^{-4}	5.763×10^{-6}	3.78
Flame 4	Lean	1900	0.9	0.8	7.708×10^{-4}	9.415×10^{-5}	1.241×10^{-6}	3.53
	Stoich.	2800	0.8	1.0	8.990×10^{-4}	1.264×10^{-4}	3.747×10^{-6}	4.35
Flame 5	Lean	1900	0.9	0.9	6.851×10^{-4}	9.415×10^{-5}	1.241×10^{-6}	3.21
	Rich	2800	0.8	1.1	8.173×10^{-4}	1.264×10^{-4}	3.747×10^{-6}	4.04
Flame 6	Lean	-	-	-	-	-	-	-
	Rich	2800	0.8	1.2	7.492×10^{-4}	1.264×10^{-4}	3.747×10^{-6}	3.79

For the implementation in Cantera, it is necessary to somehow guarantee the ignition of the mixture. This was solved using the chemical equilibrium of the reactants for constant enthalpy and pressure as an initial guess, as suggested in Cantera's site [58].

Error analysis

The available experimental results can be divided into two main groups. On the one hand for poor flames there are profiles of temperature values and mole fraction values of NO_x and O_2 measured at various points along the central axis of the flame; for stoichiometric and rich flames only the temperature profile,

obtained also along the central axis of the flame, is available. On the other hand, for stoichiometric and rich flames there are only measurements of NO_x, H_2 and NH_3 emissions at the burner exit. Therefore, it was decided to calculate a relative average error (RAE) associated with the profiles, whenever they exist, and for all flames, to calculate the relative error of temperature and species mole fractions at the burner exit (z = 300 mm). Regarding the calculation of the error associated with the profiles, this was further divided into three parts, considering that in the modeling presented the profile values are taken from the IRZ (one point), CRZ (one point) and PFZ (N points). Thus, the error was calculated separately for these three zones. In the error calculation the experimental values are compared with the numerical values obtained by interpolation to the position of the respective experimental value, since the vectors of experimental and numerical values have different dimensions.

The relative error associated with the profiles is obtained by Equation 3.21, where x_i are the measure value at each position both for experimental (e) and numerical (n) profiles.

$$RAE_{profile}[\%] = \frac{\sum_i^N |x_i^{(e)} - x_i^{(n)}|}{N \times \overline{x}^{(e)}} \times 100 \tag{3.21}$$

The relative error (RE) for numerical results at the exit of the burner, as well as for IRZ and CRZ results, is given by Equation 3.22.

$$RE_{exit}[\%] = \frac{|x_{exit}^{(e)} - x_{exit}^{(n)}|}{x_{exit}^{(e)}} \times 100 \tag{3.22}$$

Since there is more than one experimental value associated with the CRZ, Equation 3.22 is used in it, but the experimental value considered is an average of the experimental values associated with that region.

3.2.4 Model coefficient fitting

In the adjustment with experimental data, some priorities were observed to reduce possible approximation errors. Temperatures and O_2 emissions, being the largest order of magnitude experimental data, must be predicted with a low relative error. The NO_x and NH_3 emissions, present in ppm-scale, are expected to present greater relative errors due to the higher precision required, even using very complete and detailed chemical kinetics mechanisms, such as those of Glarborg et al. and Stagni et al..

Successive tests performed for different combinations of model coefficients have shown that not all of them have a relevant impact on the flame characteristics analyzed, and thus could be set constant. Regarding the mass flow splitting coefficients the variation of α_1 showed more relevant changes on final profile results, particularly associated with the equivalence ratio. The changes introduced by the remaining flow coefficients were quite small for most of the species profiles analyzed. This can perhaps be explained by the fact that the various flames studied experimentally have relatively similar velocities; thus it is quite reasonable that the aerodynamics of the various flames are also similar, which explains that the coefficients mentioned are not be very different for each flame. As for the heat transfer param-

eters, for lean flames more satisfactory results were obtained by keeping both the overall heat transfer coefficient of each flame and the reactor emissivity in each flame constant. For the rich flames, the reactor emissivity was kept constant for all flames but in order to achieve satisfactory predictions it was necessary to change the overall heat transfer coefficient for each flame, mainly depending on the equivalence ratio.

In terms of plug-flow reactor modeling in Cantera, since the great advantage of a CRN model is the ease and speed of obtaining results with the low computational cost it is important to make the most of this possibility and so to use the minimum number of reactors (N_{PSR}) necessary without relevant precision loss. Taking this into account, N_{PSR} was reduced to a minimum number, keeping accuracy very similar to what is obtained using much greater numbers.

After the work of fitting the coefficients of the model, the values shown in Table 3.4, for each lean flame (1 to 5) and for each rich flame (1 to 6), respectively, were obtained for each of these parameters, which correspond to the best agreement with the experimental results that could be obtained.

Table 3.4: Model coefficients for the better fitting with experimental temperature and species concentrations profiles.

		Model Coefficients							
		U_{ovr}	ϵ	α_1	α_2	α_3	α_4	α_5	N_{PSR}
Flame 1	Lean	7.5	0.2	0.97	0.9	0.9	0.9	0.99	100
	Stoich.	11	0.2	0.99	0.9	0.9	0.9	0.99	100
Flame 2	Lean	7.5	0.2	0.99	0.9	0.9	0.9	0.99	100
	Rich	9.5	0.2	0.97	0.9	0.9	0.9	0.99	100
Flame 3	Lean	7.5	0.2	0.98	0.9	0.9	0.9	0.99	100
	Rich	8.5	0.2	0.97	0.9	0.9	0.9	0.99	100
Flame 4	Lean	7.5	0.2	0.98	0.9	0.9	0.9	0.99	100
	Stoich.	11.5	0.2	0.99	0.9	0.9	0.9	0.99	100
Flame 5	Lean	7.5	0.2	0.98	0.9	0.9	0.9	0.99	100
	Rich	10	0.2	0.97	0.9	0.9	0.9	0.99	100
Flame 6	Lean	-	-	-	-	-	-	-	-
	Rich	8.5	0.2	0.97	0.9	0.9	0.9	0.99	100

3.2.5 Parametric analysis procedure for Rich-Quench-Lean system

The purpose of the studies of the parameters mentioned here is to seek the best possible conditions for the implementation and operation of an RQL system in the burner currently existing in the laboratory. These studies are based on four main parameters: the equivalence ratio of the first stage (ϕ_{pri}), the global equivalence ratio (ϕ_{ovr}), the molar fraction of NH_3 in the fuel mixture (x_{NH_3}), and the length of the Quench stage (L_{QZ}), from which the Quench volume can be directly obtained. The total length of the RQL burner is assumed to be constant and thus the length and volume of the Lean stage are linked to L_{QZ}, as it was previously stated. These parameters were chosen because they are relevant to be used on the experimental apparatus, with RQL system implemented.

Since the first stage of this RQL system coincides with the single stage of the current burner (rich regime) and knowing that this stage is, in the modeling presented, dependent on some model coefficients, the coefficients adopted were those used in the modeling of the single-stage rich flames. Since these flow splitting coefficients shown similarity both in lean flames for 1900 W and rich flames for 2800 W, it is expected a fairly performance adopting those values.

The method adopted for defining the heat transfer coefficients of the model (U_{ovr} and ϵ) for the various cases of the parametric studies consists in using, depending on the thermal power considered (1900W or 2800W), the U_{ovr} values that were used for the same flame inputs in the single-stage cases analyzed. An extrapolation was made for the operation with equivalence ratios 1.3 and 1.4, not tested experimentally. For the two flames with these equivalence ratios was used the same U_{ovr} used in the flame with $\phi = 1.2$. For the case of the 1900 W thermal input, since only lean flames on the single-stage burner were analyzed the extrapolation is more uncertain. The U_{ovr} values (for 1900 W flames in the rich stage) were considered within the range of these same values that were obtained for the single-stage poor at 1900 W (i.e., 7.5 $W/(m^2K)$) but with the difference that a small change is introduced to account for the effect of the decrease in the U_{ovr} coefficient with increasing equivalence ratio in the rich regime. Regarding the emissivity of the indoor reactors, the values associated with each thermal power used in the single-stage analysis were used. All the model coefficients needed to perform the parametric study of the RQL system can be checked in Table B.1 in Appendix B.

For the Quench and Lean stages it was assumed a value for the overall heat transfer coefficient through the burner walls ($U_{ovr,\text{QL}}$). For consistency, the value of this coefficient will have to be lower than the value assumed for the same coefficient in the first burner stage, since the introduction of secondary air will always have the effect of decreasing temperatures and, consequently, decreasing heat transfer through the burner walls. It was found that for fairly low values of the coefficient $U_{ovr,\text{QL}}$ (i.e., for considerably low predicted heat losses in the Quench and Lean stages of the model) the simulation could not predict the ignition of the NH_3/H_2 present in the effluent coming from the rich stage for overall equivalence ratios where such ignition would be expected to exist, according to experimental flammability limits for both thermal inputs (Figure 1.12 and Figure 1.15). Varying $U_{ovr,\text{QL}}$ value it was verified that, for both thermal inputs, the increasing of $U_{ovr,\text{QL}}$, and thus the increasing of heat losses, has the effect on increasing the value of ϕ_{ovr} from which ignition starts, i.e., increasing low flammability limit and narrowing flammability range. This points to the importance of ensuring good insulation of the secondary stage of the RQL system to be implemented, in order to ensure re-ignition in that stage and flame stability. This will be further commented on the parametric study of ϕ_{ovr} in Section 4.4.3.

It was chosen to perform the study of each of the above parameters for each input power considered in the experimental measurements (1900 W and 2800 W), which also allows one to compare the results for two different powers (which, in a way, can be considered an additional parameter). In the analysis of

each parameter, which will be shown graphically later, each of the other parameters remains constant and equal to a reference value, which is chosen in advance. Table 3.5 shows the values chosen for each parameter in performing this study. Cases 1 - 3 refer to the study of the variation of x_{NH_3}; cases 1, 4 - 7 allow us to evaluate the influence of the variation of ϕ_{pri}; cases 1, 8 - 11 concern the study of the variation of ϕ_{ovr} and cases 1, 12 - 15 serve to show the influence of the variation of L_{QZ}. The results will be shown and commented on in Section 4. These results consist of the variation of species mole fractions at the combustor exit with each parameter.

Table 3.5: Cases for the parametric study with the modeled RQL combustor system.

	Parameters values					Cases used for Parametric studies			
	$TI\ [W]$	x_{NH_3}	ϕ_{pri}	ϕ_{ovr}	$L_{QZ}\ [mm]$	x_{NH_3}	ϕ_{pri}	ϕ_{ovr}	$L_{QZ}\ [mm]$
1	1900/2800	0.8	1.2	0.8	20	x	x	x	x
2	1900/2800	0.7	1.2	0.8	20	x			
3	1900/2800	0.9	1.2	0.8	20	x			
4	1900/2800	0.8	1	0.8	20		x		
5	1900/2800	0.8	1.1	0.8	20		x		
6	1900/2800	0.8	1.3	0.8	20		x		
7	1900/2800	0.8	1.4	0.8	20		x		
8	1900/2800	0.8	1.2	0.4	20			x	
9	1900/2800	0.8	1.2	0.5	20			x	
10	1900/2800	0.8	1.2	0.6	20			x	
11	1900/2800	0.8	1.2	0.7	20			x	
12	1900/2800	0.8	1.2	0.8	30				x
13	1900/2800	0.8	1.2	0.8	40				x
14	1900/2800	0.8	1.2	0.8	50				x
15	1900/2800	0.8	1.2	0.8	60				x

Finally, to evaluate the effectiveness of the RQL burner compared to the currently existing single-stage burner, the numerical results obtained for the RQL system under the most advantageous conditions were compared to the experimental and numerical results obtained for the single-stage burner, for the conditions under which it is possible to make that comparison. Thus, for the 2800 W thermal input the emission results at the output of the RQL system, for x_{NH_3} = 0.7 and 0.8, ϕ_{ovr} = 0.8 and ϕ_{pri} = 1.0, 1.1 and 1.2, were compared with the analogously experimentally and numerically obtained results for the rich single-stage model. For the 1900 W thermal power, the emissions at the exit of the RQL combustor were compared, for the same values of x_{NH_3}, ϕ_{pri} and ϕ_{ovr} as those used in the previous case, with the experimental and numerical results for single-stage lean flames.

Chapter 4

Results and Discussion

The present section presents the final results of the model with the most suitable coefficients for each flame to validate predictions for both lean and rich flames against the available experimental data, obtained previously by other authors [35, 37, 59]. In Appendix A the numerical results at the output of each reactor in the model are tabulated, for each flame analyzed.

4.1 Results from lean-burn

For the lean validation, experimental measurements on the flame obtained refer to five flames of different combinations of three different equivalence ratios and three different volume fractions of ammonia in the fuel mixture, as shown in the stability diagram of Figure 1.12, in Section 1.2. In this way, it is possible to compare the influence of the equivalence ratio and the volume fraction of NH_3 in the fuel on the temperatures and species mole fractions of the different flames. All measurements were made along the central axis of the tube, starting at 30 mm. from the burner mouth. For consistency with these measurements on the central axis, the values presented graphically with the results predicted by the developed model are captured from the IRZ (30 mm), CRZ (70 mm), and the various reactors that form the chain that models the PFZ (70 mm to 300 mm), as shown in Figure 4.1a.

Since the IRZ and CRZ regions are modeled by a PSR, the results in each are represented graphically by a point. For simplicity of representation, in the graphs that will be shown below, the points representing the results in these two zones are connected by a straight line, which is not intended to be an accurate representation of what is happening at the intermediate distance. Numerical results were obtained for the two selected chemical kinetics mechanisms, Glarborg and Stagni. The simulation carried out for the five flames predictions took 3 min.

4.1.1 Temperature profile

Figure 4.1a shows the temperatures of the three flames with the same ϕ and different x_{NH_3}, while Figure 4.1b shows the temperatures of the three flames with the same x_{NH_3} and different ϕ. As can be seen,

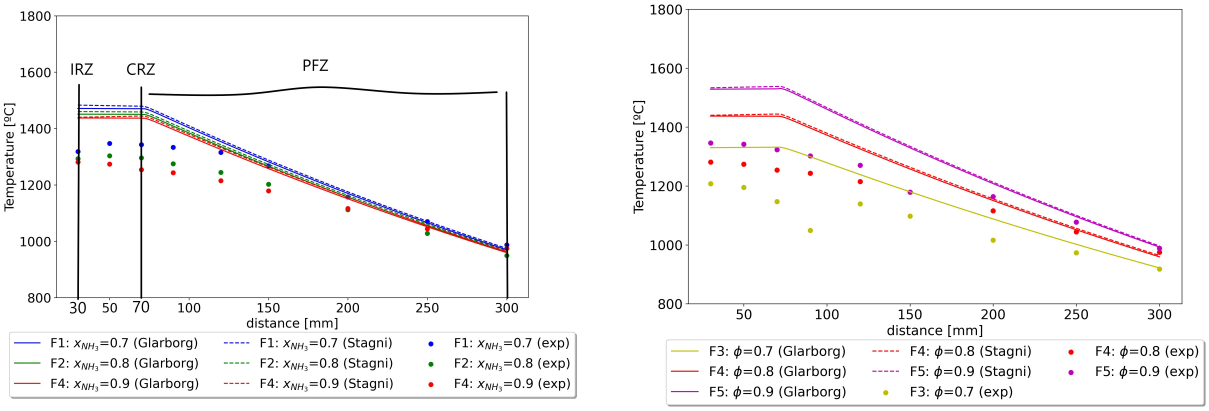

Figure 4.1: Temperature profiles for (a) $\phi = 0.8$ and (b) $x_{\mathrm{NH_3}} = 0.9$

the largest discrepancy between the numerical and experimental results occurs in the near burner region which is the zone modeled by the various PSRs. The higher predicted temperature in comparison with the experimental temperature, which is represented, is expected due to the perfect mixing reactor hypothesis.

Although it is not clear from the figures, the various profiles show a very slight decrease or increase in temperature from the IRZ to the CRZ, as can be confirmed by the values in the Tables A.1 to A.5 in Appendix A, although this variation is almost irrelevant. In the experimental profiles this variation is somewhat steeper, generally of decreasing temperature along the recirculation region (except for Flames 1 and 2). This difference may be due to some slight inaccuracy associated with the method of partitioning the mass flow rates entering the IRZ and CRZ. It can be noted that the slope of the numerical profiles in the PFZ is considerably steeper than that of the experimental profiles. This higher heat transfer through the walls than observed experimentally is based on a deliberate choice to use values of the overall heat transfer coefficient (U_{ovr}) slightly higher than what would be expected, in order to bring the numerical prediction of the burner outlet temperatures as close as possible to the experimental values.

The relationship between the experimental temperature profiles is captured by the model and the trends are confirmed. It is possible to check that the closeness of the temperature profiles shown in Figure 4.1a, closer together, versus those in Figure 4.1b, further apart, is well predicted by the model. Figure 4.1b shows that temperature increases with increasing equivalence ratio (lean regime) while Figure 4.1a allows one to see the decrease in temperature with increasing mole fraction of NH_3 in the fuel mixture. The two mechanisms provide practically coincident results and the relative error of the temperature at the end of the reactor, one of the relevant values, is quite small.

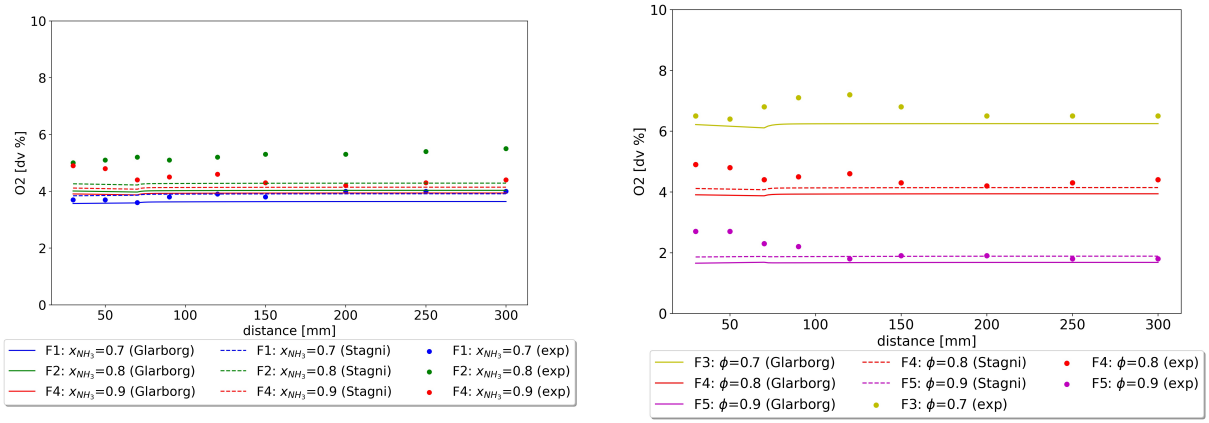

(a) (b)

Figure 4.2: O_2 profiles for (a) $\phi = 0.8$ and (b) $x_{NH_3} = 0.9$

4.1.2 O_2 profile

The O_2 profile for all the lean flames is shown in Figure 4.2. Except for the results obtained for Flame 2 ($\phi = 0.8$ and $x_{NH_3} = 0.8$), the numerical results are in good agreement with the experimental measurements and the trends are verified for all flames. It is not easy to find an explanation for the behavior of the Flame 2 profile because this is the only flame for which there is a relevant departure from the experimental measurements. However, although not very evident, the trends remain correct, and the O_2 profile for Flame 2 is the one with the highest values among the three flames with the same equivalence ratio. To better understand this, the mole fraction of O_2, x_{O_2}, was calculated for the ideal case of complete combustion, using Equation 4.1. It is thus understood that theoretically the value of x_{O_2} does not depend on x_{NH_3}, but only on ϕ. For $\phi = 0.7$, $x_{O_2} = 5.49$ %; for $\phi = 0.8$, $x_{O_2} = 3.60$ % and for $\phi = 0.9$, $x_{O_2} = 1.77$ %. Thus, the closeness of the numerical O_2 profiles for the same ϕ points to the hypothesis of a combustion prediction close to complete by the model.

$$x_{O_2} = \frac{(\frac{1}{\phi} - 1)(0.5 + \frac{x_{NH_3}}{4})}{(1 + \frac{x_{NH_3}}{2}) + (\frac{1}{\phi} - 1)(0.5 + \frac{x_{NH_3}}{4}) + \frac{3.76}{\phi}(0.5 + \frac{x_{NH_3}}{4})} = \frac{\frac{1}{\phi} - 1}{2 + (\frac{1}{\phi} - 1) + \frac{3.76}{\phi}} \tag{4.1}$$

Both mechanisms globally predict lower O_2 mole fractions inside the burner than those observed experimentally, which probably indicates a higher O_2 conversion than what happens in reality, because the model predicts more advanced combustion. The fact that the mole fraction of O_2 remains almost constant between IRZ and CRZ must be linked in part with mass flow splitting inaccuracy and in part with almost complete combustion from the first reactors in the model. Although not shown graphically most of the combustion predicted by the model takes place in the FZ (Tables A.1 to A.5), from which the flow then proceeds to the IRZ and CRZ. This explains also the almost constant O_2 mole fraction along the PFZ. Regarding the experimental profiles, the decrease in O_2 mole fraction seems to indicate that combustion is advancing along the burner, with a greater advance in the initial recirculation region. Nevertheless, it is worth mentioning the closeness of numerical and experimental O_2 profiles along the PFZ, with a quite accurate prediction of the O_2 mole fraction at the exit of the burner. The two mechanisms

predict quite similar values and the same trends.

4.1.3 NO_x profile

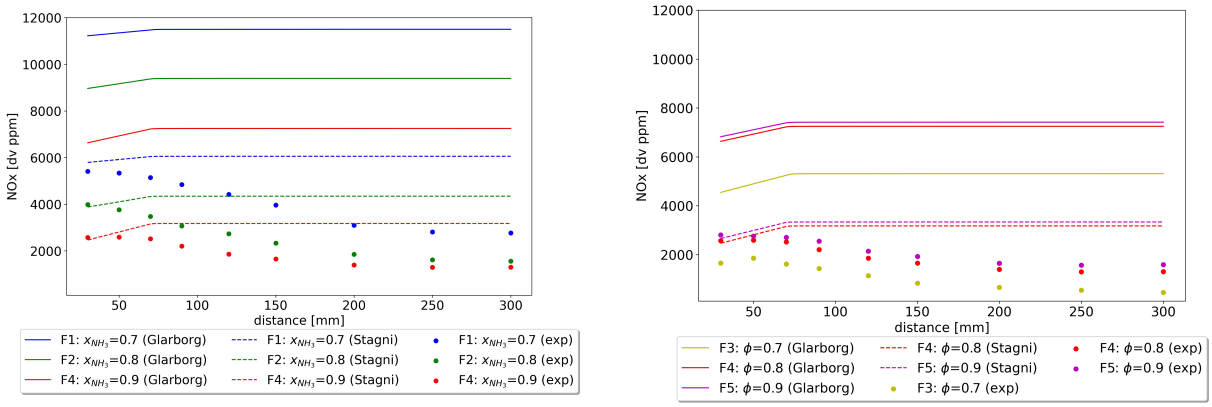

(a) (b)

Figure 4.3: NO_x profiles for (a) $\phi = 0.8$ and (b) $x_{NH_3} = 0.9$

Figures 4.3a and 4.3b show the NO_x profiles for each lean flame. As can be immediately observed, the results predicted by the model for NO_x mole fractions show a quite significant NO_x overproduction compared to the experimentally measured values, moreover with quite different predictions for the two mechanisms used. Furthermore, the inability to reproduce the gradual decrease in NO_x concentration along the Post-Flame Zone is also evident, as shown by the experimental results for all flames. Each of these aspects will need to be addressed in particular.

The discrepancy is much larger for the Glarborg mechanism than for the Stagni mechanism. The latter mechanism predicts NO_x values close to the maximum measured for each flame. Actually, as Rocha et al. have shown [66], the Glarborg et al. mechanism greatly over-predicts the flame velocity for NH_3/H_2 mixtures, particularly for equivalence ratios close to stoichiometry and for higher NH_3 mole fractions in the fuel, which necessarily implies an over-prediction of the ammonia reactivity and the consequent over-prediction of the NO_x mole fraction in the combustion products, mainly by the great enhancement of the fuel-NO pathway. The closer predictions of the Stagni mechanism may perhaps be linked to the fact that this mechanism was particularly designed to model conditions of NH_3 combustion in the presence of large O_2 concentrations [49], which is the case given the lean regime of these flames. However, the accuracy of the chemical kinetics mechanisms alone is not the only reason for the discrepancy in results.

Referring to the Section 2.6 it is fundamental at this point to be aware of the limitations that the theoretical model of perfect mixing reactors itself imposes on the results that are possible to achieve. Chemical reactor theory, which is at the foundation of the model developed, relies precisely on the premise that within the reactor there is infinitely fast chemistry and therefore perfect mixing so that combustion is also greatly enhanced and homogeneous. Turbulence is thus assumed to be very high but without being considered as a variable. As said before, this model can be a reasonable approximation of the recirculation

zone of a flame, where the residence time is generally higher and allow a more homogeneous mixing of reactants and products, although it does not consider enough other factors relevant to combustion, such as the different turbulence intensities, which lead to different mixing rates, with the consequent influence on combustion efficiency. Thus, as a matter of principle, combustion will always be more efficient in perfectly mixed reactors than in reality. This may be the main reason for the exaggerated numerical predictions for the NO_x mole fraction along with the burner and it is an important limitation of the developed reactor model, closely linked to the theoretical simplifications assumed by the theory of perfect-mixture chemical reactors. On the fact that the model fails to predict the decrease in NO_x along the PFZ, it is important to note that what was said above applies here as well.

Although not shown graphically, since it is not in the central region of the burner, the FZ is the zone where the NH_3 burning takes place first and foremost, with a large production of NO_x mainly by the fuel-NO pathway, with the resulting gases - NO_x, and unburnt NH_3 and H_2 - then going out in larger quantities to the CRZ and in smaller quantities to the IRZ (and in a residual quantity to the ORZ). It seems, from the evaluation of the predicted heat released rate (HRR) in FZ (Appendix A) compared with the HRR of the other zones, that a very advanced NH_3 burning occurs in this zone. The fact that the almost complete burning of the ammonia occurs too early in the model prevents a sufficient flow of ammonia from entering the IRZ, CRZ and PFZ, to enable the SNCR reactions, which mainly explains the decrease in NO_x along the respective regions in the experimental flame. This tendency for the NO_x concentration to remain constant along the post-flame zone has been previously verified by several authors, such as Brackmann et al. [75, 76] and Mashruk et al. [31].

In the current simulation, instead of SNCR reactions there seem to be along the PFZ some NO_x production reactions (from Tables A.1 to A.5 it can be verified a slight increase on NO_x mole fraction in PFZ), most likely induced by O_2 dissociation at high temperatures (thermal-NO pathway). The same seems to occur from IRZ to CRZ. Finally, it can be pointed out that the trends concerning the relative position of profiles are generally true. It is possible to verify that the relative distance between the profiles predicted by the Stagni mechanism is almost equal to the relative distance between the maximum NO_x values measured experimentally.

4.1.4 NH_3 profile

Figures 4.4a and 4.4b show the ammonia concentration along the burner. For this species, there are no experimental measurements along with the entire burner, but measurements were made at the burner exit for all five flames, consisting of values of 14, 16, 75, 13, and 15 ppm (dry volume @13% O_2) for flames 1 through 5, respectively. Both mechanisms coincide in predicting complete ammonia conversion at the burner exit, which is not exactly in agreement with the experimental, which shows some unburned ammonia remaining in the exhaust gas. It is important to emphasize that the overall values of unburned ammonia inside the burner predicted numerically (in the order of tens of ppm, in dry volume) are much

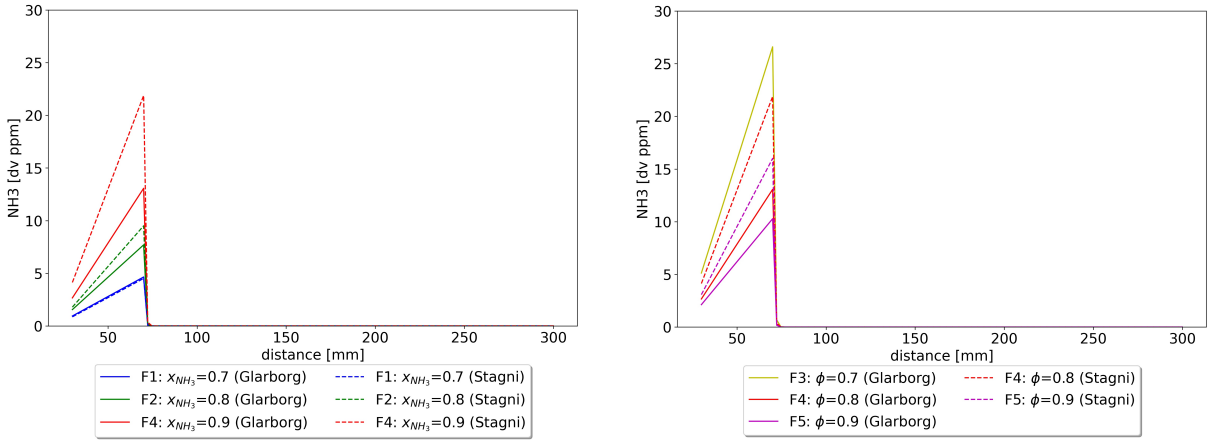

(a) (b)

Figure 4.4: NH_3 profiles for (a) $\phi = 0.8$ and (b) $x_{NH_3} = 0.9$

lower than what would be expected in reality, which may be largely due to the over-reactivity of ammonia predicted by both mechanisms, which leads to a faulty prediction of unburned ammonia.

It is of interest to note that the discrepancy between the NH_3 predictions of the two mechanisms increases with increasing ammonia present in the input fuel, as well as with increasing equivalence ratio. The Stagni et al. mechanism is the one that globally predicts a higher mole fraction of ammonia inside the burner for all flames except for Flame 1, for which the prediction is exactly the same considering both mechanisms. Flame 3 ($x_{NH_3} = 0.9$, $\phi = 0.7$) is the one for which the NH_3 mole fraction is highest up to the beginning of the PFZ, mainly due to the large fraction of ammonia present in the input fuel as well as the fact that it is the leanest flame considered, which implies a lower combustion temperature and therefore higher resistance to ammonia reactivity.

As expected, in the lean regime, as the equivalence ratio increases and approaches 1 the temperature will rise favoring ammonia cracking into hydrogen. Both mechanisms are also in agreement in showing the abrupt decrease in the NH_3 mole fraction upon entry to the PFZ (70 mm). This rapid decrease can be explained by the small amount of NH_3 (order of tens of ppm) and the above-mentioned over-reactivity of ammonia. The very fact that PFZ (plug-flow reactor) is simulated through a chain of perfectly-stirred reactors (it is the only modeling possibility in Cantera for a model with these characteristics) seems to be one of the main reasons for this very fast burning. For the conditions of Flame 3 ($\phi = 0.7$, $x_{NH_3} = 0.9$), the Stagni et al. mechanism did not allow the ignition of the fuel mixture in the FZ, so the results obtained were totally away from what would be intended; for better clarity, it was decided not to show the results predicted by this mechanism for this flame.

4.1.5 H_2 profile

The hydrogen mole fraction along the burner is shown in Figures 4.5a and 4.5b, without any experimental data for comparison. Recognizing that globally the trends of the relative position of profiles of

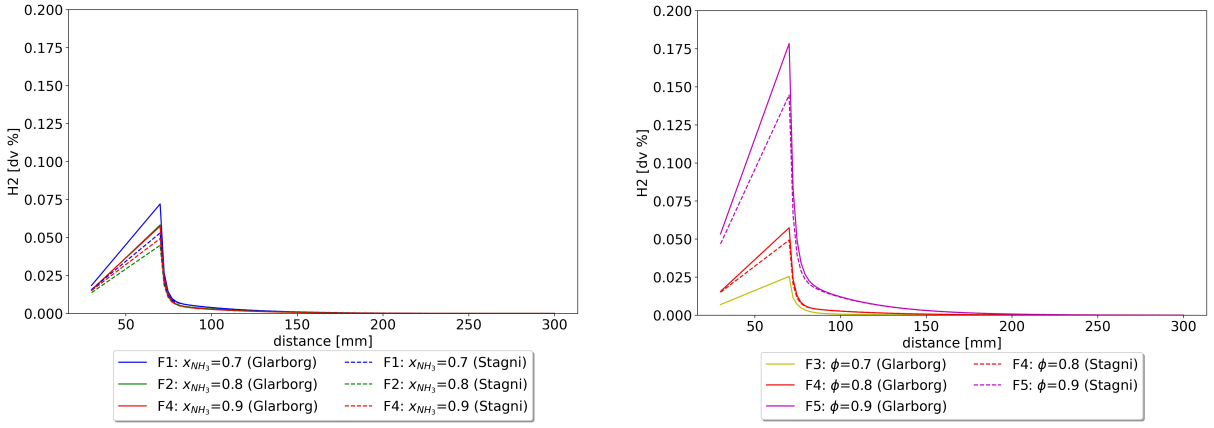

(a) (b)

Figure 4.5: H_2 profiles for (a) $\phi = 0.8$ and (b) $x_{NH_3} = 0.9$

the other species it is also expected that the H_2 profiles will also show appropriate trends of this kind. Similar to what was found for NH_3, the mole fraction of H_2 is also higher in the recirculation zone region, reaching a maximum in the CRZ region (70 mm) and then decreasing rapidly as it enters the PFZ. This decrease is milder than the one seen in the NH_3 profiles mostly because of the fact that NH_3 cracking in that zone contributes to H_2 production, and thus delaying its decrease in the PFZ. Both mechanisms agree almost perfectly showing this decreasing. It is notable that the increase in H_2 in the recirculation zones is particularly sensitive to the equivalence ratio, which can be explained by the combined effect of both thermal-NO pathway and NH_3 dissociation enhancement by the increasing temperature with the closeness to the stoichiometry. Flame 5 is the one that shows globally the highest amount of NH_3 inside the burner, which can be found as a consequence of the NH_3 cracking into H_2 since Flame 5 ($\phi = 0.9$, $x_{NH_3} = 0.9$) has the larger NH_3 molar fraction in the inlet fuel and the greater lean equivalence ratio considered, which highly enhances the mentioned dissociation reaction.

4.2 Results from stoichiometric/rich-burn

For the stoichiometric and rich regimes validation, the available experimental data refer to six flames with six different combinations of three different equivalence ratios and two different volume fractions of ammonia in the fuel mixture, as it is shown in Figure 1.15. It is important to note that for this set of experimental data, only the measurements relating to the temperature profiles were performed inside the flame, along the central axis of the tube. The emission measurements were performed at the exit of the burner tube. The simulation carried out for the six flames predictions took 4 min.

4.2.1 Temperature profile

The temperature inside the six rich flames analyzed is shown in Figures 4.6a and 4.6b. The overall evaluation of these profiles is very similar to that of the lean flames. The trends seem to hold for all six cases. Only the proximity between the various profiles is not represented very accurately. The difference

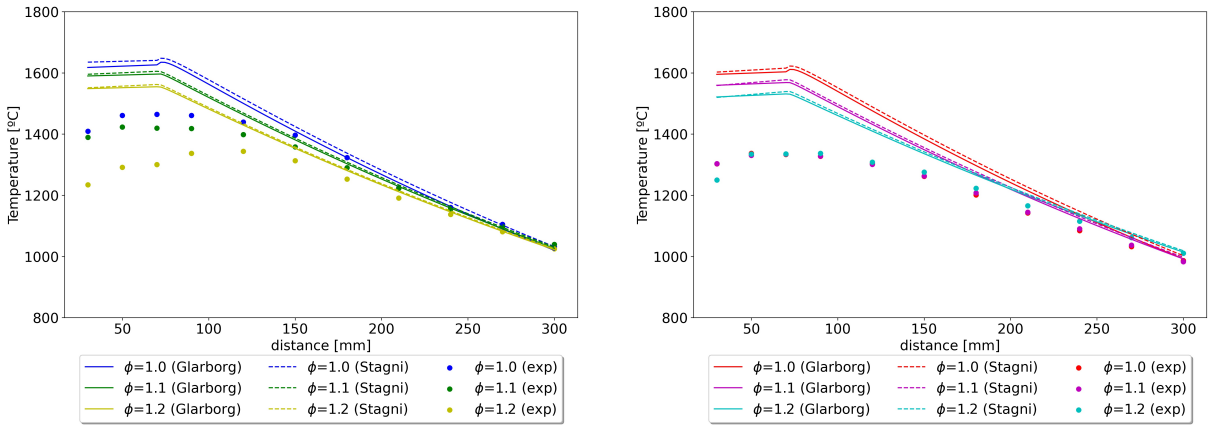

(a) (b)

Figure 4.6: Temperature profiles for (a) $x_{NH_3} = 0.7$ and (b) $x_{NH_3} = 0.8$

with the experimental results remains for the recirculation zone near the burner mouth, where the temperature predicted by the model is much higher than the real one. The slope of the numerical profiles remains higher than the experimental ones for the same reason pointed out regarding the respective lean flame profiles.

4.2.2 O_2 profile

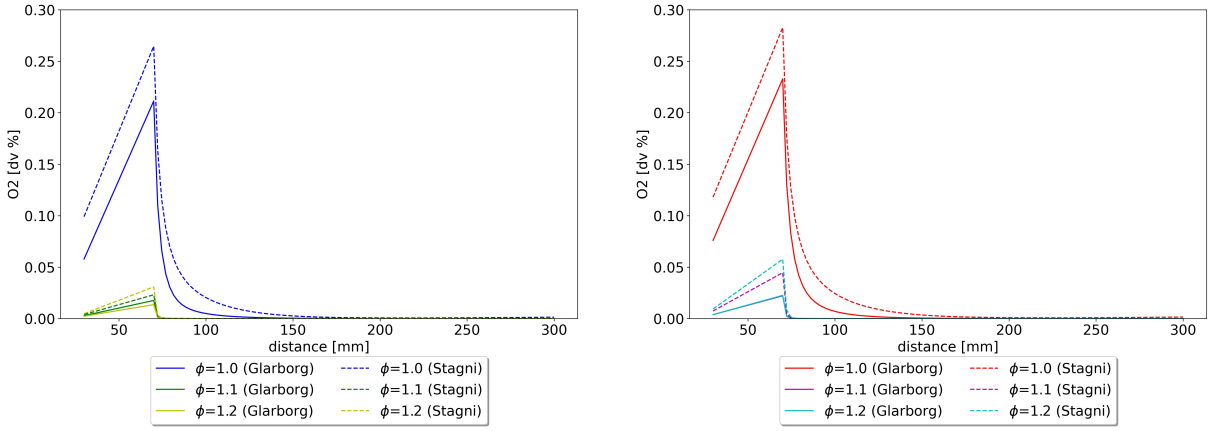

(a) (b)

Figure 4.7: O_2 profiles for (a) $x_{NH_3} = 0.7$ and (b) $x_{NH_3} = 0.8$

For the oxygen profiles, shown in Figures 4.7a and 4.7b, there are no experimental values to contrast. In any case, recognizing that in the rich regime the oxygen present in the reactants is in default, it is natural that all of it is consumed during combustion, and combustion is generally left for lack of oxygen. Thus, the very small amount of oxygen shown in these graphs seems to correspond to what is supposed to be expected. Flames 3 and 6, stoichiometric, are logically those with the highest O_2 mole fraction for the recirculation zones. The higher concentration of O_2 in the initial region of the burner, where the recirculation zones are located, seems to correspond to the higher dilution there. It can be noticed that for both profile comparisons in Figures 4.7a and 4.7b, the oxygen values for flames with ϕ equal to 1.1

and 1.2 are very similar.

4.2.3 NO_x profile

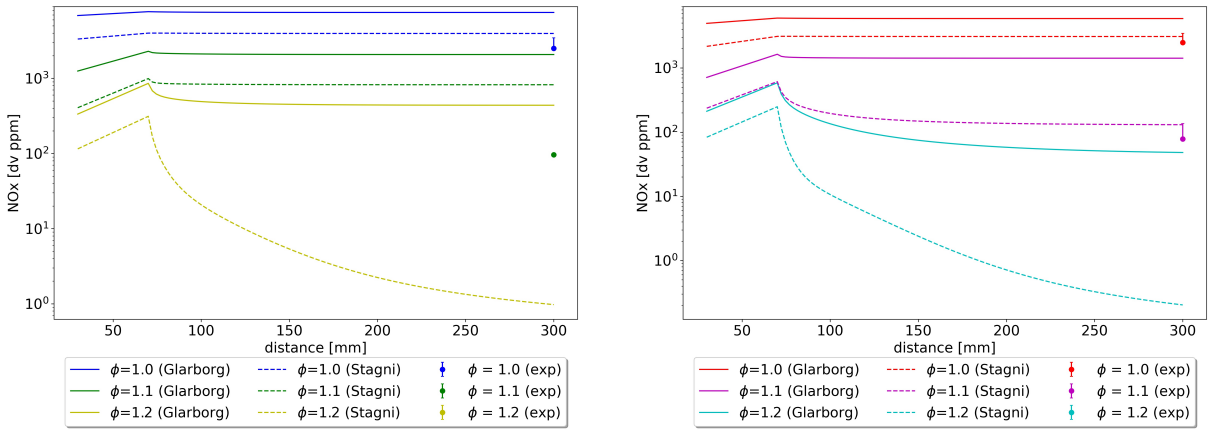

(a) (b)

Figure 4.8: NO_x profiles for (a) $x_{NH_3} = 0.7$ and (b) $x_{NH_3} = 0.8$.

The NO_x mole fractions for each rich flame along the burner are shown in Figures 4.8a and 4.8b. Both mechanisms generally predict excess NO_x compared to experimental tests, although the numerical results with the Stagni mechanism are particularly close to the experimental ones. Although not represented, due to the use of logarithmic scale, the experimental result of NO_x mole fraction for $\phi = 1.2$ is null for the two cases.

The increase in NO_x in the region of the recirculation zone may be particularly due to the initial burning of NH_3 present in the fuel in the FZ (Appendix A) with the consequent mainly promotion of the fuel-NO mechanism in that zone where more reactions of this type occur, as expected, with the consequent effluent of gases from FZ to CRZ (mostly), IRZ and ORZ. As CRZ receives more mass flow rate from FZ, the greater NO_x mole fraction shown in graph for this zone may be linked with that. The gradual decrease in NO_x that occurs from the entrance to the PFZ may be explained by the reactions of NO with N, NH and NH_2, and others also involved with SNCR processes at lower temperatures, as stated by Pacheco et al. [37].

By comparison with the NO_x profiles for the lean flames, where it was not possible to obtain this expected NO_x decrease, it can now be confirmed how the developed model is able to account for NO reduction reactions as long as the necessary conditions for them to happen are met, which are basically the presence of NO_x and sufficient amounts of unburned NH_3. This can be confirmed by the fact that it is possible to observe, by comparing the various profiles shown, that the decrease in NO_x is more pronounced the greater the amount of unburned ammonia present. However, the decrease that does occur is too rapid and too short for what would be expected, especially for the profiles given by the Glarborg mechanism, which always over-predicts ammonia reactivity (and thus under-predicts un-

burned ammonia) and NO_x production. The perfect-mix reactor assumption will always predict a more advanced burn-up than what actually happens. This rapid decrease in NO_x reaches a stationary value slightly after 100 mm.

Despite not being completely clear from Figures 4.8a and 4.8b, due to the logarithmic scale, it can be observed a predicted relevant increase of NO_x mole fraction for $x_{NH_3} = 0.7$ when compared to $x_{NH_3} = 0.8$. Although not being evident from experiments this prediction may be explained by the more enhanced fuel-NO and thermal-NO pathways for $x_{NH_3} = 0.7$, since the more H_2 present in the fuel leads to higher temperatures attained in flames.

4.2.4 NH_3 profile

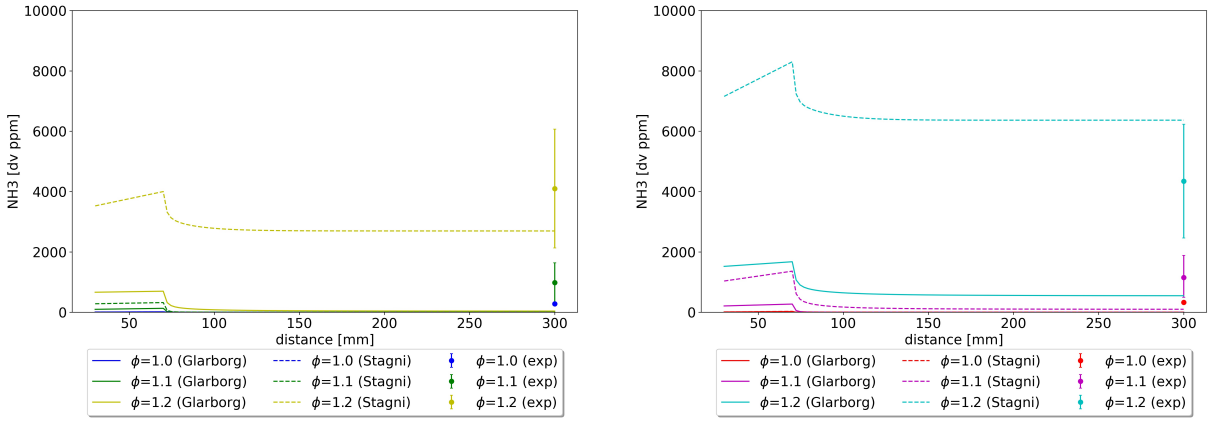

(a) (b)

Figure 4.9: NH_3 profiles for (a) $x_{NH_3} = 0.7$ and (b) $x_{NH_3} = 0.8$.

Figures 4.9a and 4.9b show the evolution of the NH_3 mole fraction over the various rich and stoichiometric flames. The Stagni mechanism is the one that makes the best predictions although for flames with $\phi = 1.1$ these predictions are less appropriate than for the cases of $\phi = 1.0$ and $\phi = 1.2$. The Glarborg mechanism predicts results less consistent with the experimental evidence, predicting complete ammonia burning where it should not happen. It is also worth noting the significant difference in prediction of both mechanisms for flames with $\phi = 1.2$, which shows the impact that the different emphasis given by each of the mechanisms on certain pathways of ammonia decomposition has. It is important to remember that Pacheco et al. [37], who published these experimental data, called attention to possible uncertainties in some measurements, especially for the flames with $\phi = 1.2$ (3 and 6), which they attributed to certain issues related to the sampling process, due to the instability of ammonia in the flue gases and to possible retention of part of the ammonia in the drying system.

4.2.5 H_2 profile

Figures 4.10a and 4.10b represent the H_2 profiles for the various rich flames. The H_2 mole fraction is over-predicted for all six flames by both mechanisms, with this divergence being increased with increas-

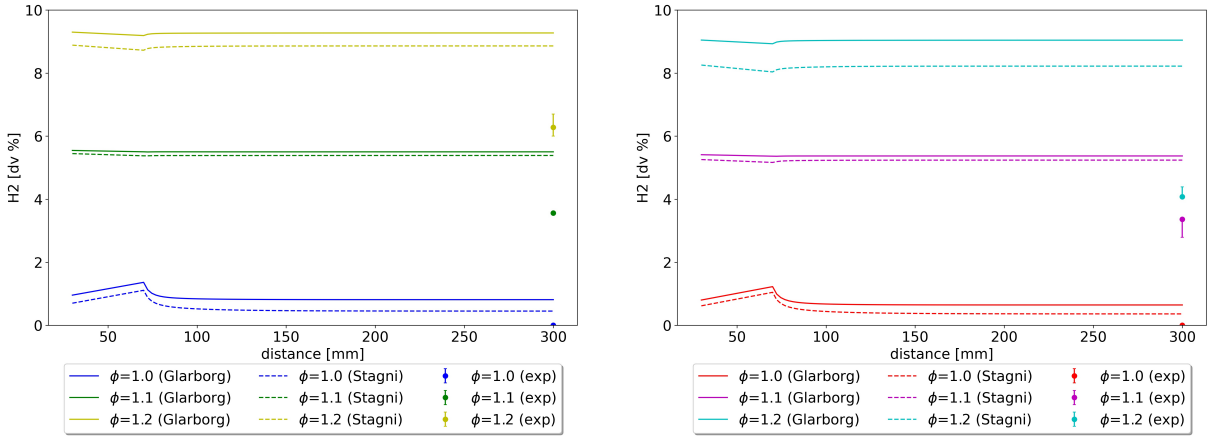

(a) (b)

Figure 4.10: H_2 profiles for (a) $x_{NH_3} = 0.7$ and (b) $x_{NH_3} = 0.8$

ing equivalence ratio and therefore greater for flames with $\phi = 1.2$. For the flames with this equivalence ratio, the mechanisms also show a greater difference in their respective predictions, most likely due to the greater presence of NH_3 in these flames with the consequent dissociation into H_2, a process that is addressed by each mechanism in a particular way.

Ammonia cracking into hydrogen for the richer flames is demonstrated by the slight increase in H_2 at the entrance to the PFZ (70 mm), exactly at the same point where a relatively sharp decrease was observed for the NH_3 profiles of the respective flames. For these richer flames, a slight decrease in H_2 is predicted in the recirculation zone, perhaps related to the rapid burning of H_2 in these initial zones, without this decrease being able to be compensated by the H_2 produced by NH_3 dissociation.

For the stoichiometric flames (1 and 4) the opposite behavior is observed, with the H_2 mole fraction increasing in the initial reactors (recirculation zone), suffering a considerable decrease after entering the PFZ. It is reasonable that this behavior is due to the fact that the larger amount of air present in these flames allows more efficient combustion of ammonia, thus promoting ammonia cracking into hydrogen in the recirculation zones. In this way, the mole fraction of unburned ammonia becomes residual, and the hydrogen produced in the meantime starts to be burned, mainly from the entrance to the PFZ, as can be observed.

Regarding the main trends, the model globally predicts, for both mechanisms, lower H_2 values for stoichiometric flames and higher values for the richer flames ($\phi = 1.2$; flames 3 and 6), which is consistent with the experimental evidence. Furthermore, by comparing both Figures 4.10a and 4.10b it can be distinguished that overall the H_2 profiles for flames with $x_{NH_3} = 0.7$ are slightly higher than those for flames with $x_{NH_3} = 0.8$, which is also true for laboratory measurements.

4.3 Error evaluation of model predictions

Table 4.1 shows the relative average error of the numerical profiles of temperature and NO_x and O_2 for the lean flames analyzed while Table 4.2 shows the relative average error of the numerical profiles of temperature and NO_x, NH_3 and H_2 for the stoichiometric and rich flames analyzed. These values were obtained as exposed in Section 3.2.3.

Table 4.1: Relative average error for profiles of temperature and species molar fractions along each lean flame. All values in %.

	Lean Flame 1 ($\phi = 0.8$ and $x_{NH_3} = 0.7$)						**Lean Flame 2** ($\phi = 0.8$ and $x_{NH_3} = 0.8$)					
	Glarborg			Stagni			Glarborg			Stagni		
	IRZ	CRZ	PFZ	IRZ	CRZ	PFZ	IRZ	CRZ	PFZ	IRZ	CRZ	PFZ
T	11.62	9.31	2.54	12.52	9.97	2.78	12.12	11.54	5.42	12.84	12.20	5.95
NO_x	107.48	118.79	215.02	7.09	15.24	65.89	125.94	160.02	330.15	2.08	20.23	99.10
O_2	3.55	1.69	7.24	3.78	5.72	2.02	18.09	21.40	22.53	13.00	16.55	17.74
	Lean Flame 3 ($\phi = 0.7$ and $x_{NH_3} = 0.9$)						**Lean Flame 4** ($\phi = 0.8$ and $x_{NH_3} = 0.9$)					
	Glarborg			Stagni			Glarborg			Stagni		
	IRZ	CRZ	PFZ	IRZ	CRZ	PFZ	IRZ	CRZ	PFZ	IRZ	CRZ	PFZ
T	10.11	13.73	8.67	-	-	-	12.21	13.67	5.91	12.41	14.26	6.27
NO_x	175.12	202.10	530.25	-	-	-	157.86	182.91	348.21	4.17	23.50	96.32
O_2	4.37	7.47	7.72	-	-	-	20.31	15.84	10.25	16.08	11.49	5.59

	Lean Flame 5 ($\phi = 0.9$ and $x_{NH_3} = 0.9$)					
	Glarborg			Stagni		
	IRZ	CRZ	PFZ	IRZ	CRZ	PFZ
T	13.56	14.81	7.75	13.92	15.42	8.16
NO_x	143.14	170.61	289.57	5.22	21.52	75.16
O_2	38.79	32.66	11.83	31.18	24.99	5.37

The better performance of Stagni mechanism in NO_x prediction is confirmed by the presented values. For lean flames it is found that as a general rule the mean relative error for NO_x prediction increases with increasing x_{NH_3} and decreases with increasing ϕ. For stoichiometric and rich flames it is found that the mean relative error for NO_x prediction increases with increasing x_{NH_3} and generally increases with increasing $x_{NH_3} = 0.7$ and decreases with increasing $x_{NH_3} = 0.8$.

Table 4.2: Relative average error for profiles of temperature and species mole fractions along each stoichiometric and rich flame. All values in %.

	Stoich. Flame 1: $\phi = 1.0$, $x_{NH_3} = 0.7$						**Stoich. Flame 4**: $\phi = 1.0$, $x_{NH_3} = 0.8$					
	Glarborg			Stagni			Glarborg			Stagni		
	IRZ	CRZ	PFZ	IRZ	CRZ	PFZ	IRZ	CRZ	PFZ	IRZ	CRZ	PFZ
T	14.78	11.18	2.51	16.01	12.18	3.12	22.46	20.10	8.50	23.03	21.00	9.50
	Rich Flame 2: $\phi = 1.1$, $x_{NH_3} = 0.7$						**Rich Flame 5**: $\phi = 1.1$, $x_{NH_3} = 0.8$					
	Glarborg			Stagni			Glarborg			Stagni		
	IRZ	CRZ	PFZ	IRZ	CRZ	PFZ	IRZ	CRZ	PFZ	IRZ	CRZ	PFZ
T	14.45	12.30	2.59	14.85	12.94	2.83	19.65	17.71	6.22	19.58	18.40	6.77
	Rich Flame 3: $\phi = 1.2$, $x_{NH_3} = 0.7$						**Rich Flame 6**: $\phi = 1.1$, $x_{NH_3} = 0.8$					
	Glarborg			Stagni			Glarborg			Stagni		
	IRZ	CRZ	PFZ	IRZ	CRZ	PFZ	IRZ	CRZ	PFZ	IRZ	CRZ	PFZ
T	25.45	19.99	3.70	25.67	20.56	3.98	21.75	14.69	4.43	21.61	15.28	4.89

Regarding the relative errors for the emissions to the burner for all the flames analyzed, all the values are presented in Table 4.3. These values summarize to some extent what has already been said throughout

this section, and give a quantitative notion of the quality of the predicted burner output values, which are also very relevant in terms of burner evaluation.

Table 4.3: Relative error for the predicted emissions with mechanisms Glarborg (G) and Stagni (S). ∞ means that experimental null value was considered.

		Flame 1					**Flame 4**				
		T	O_2	NO_x	NH_3	H_2	T	O_2	NO_x	NH_3	H_2
Lean	G	1.74	9.07	315.44	-	-	1.59	10.50	456.31	-	-
	S	1.25	2.24	118.77	-	-	1.11	5.86	143.67	-	-
Stoich.	G	1.12	-	201.16	100.00	∞	0.59	-	135.88	100.00	∞
	S	0.04	-	58.20	100.00	∞	1.62	-	23.86	100.00	∞
		Flame 2					**Flame 5**				
		T	O_2	NO_x	NH_3	H_2	T	O_2	NO_x	NH_3	H_2
Lean	G	1.22	25.28	504.24	-	-	0.46	6.69	366.23	-	-
	S	1.75	20.65	179.67	-	- -	0.86	4.68	109.63	-	-
Rich	G	1.19	-	2061.09	99.92	54.53	0.94	-	1714.57	99.91	71.60
	S	0.78	-	756.34	99.88	51.29	1.49	-	67.31	91.52	67.37
		Flame 3					**Flame 6**				
		T	O_2	NO_x	NH_3	H_2	T	O_2	NO_x	NH_3	H_2
Lean	G	0.42	3.90	1080.24	-	-	-	-	-	-	-
	S	-	-	-	-	-	-	-	-	-	-
Rich	G	0.27	-	∞	99.08	47.17	0.36	-	∞	87.42	115.31
	S	0.05	-	∞	34.29	40.64	0.80	-	∞	46.52	95.69

4.4 Results for Rich-Quench-Lean

In the previous section, the predictions of the single-stage model were compared with the experimental results obtained in the laboratory. The predictions were obtained using two different detailed chemical kinetics mechanisms. In general, the Stagni mechanism was the one that, for the conditions considered, showed results closest to the experimental ones. In this section the parametric studies for the modeled RQL system will be presented and analyzed, hoping through this numerical study to predict the best range of operating conditions for such a system with a view to its implementation in the single-stage burner currently used in the laboratory.

4.4.1 Parametric analysis of x_{NH_3}

Figure 4.11 show the numerical prediction of the variation of NO_x emissions at the exit of the RQL combustor with the variation of x_{NH_3}, for the two thermal operating powers, 2800 W and 1900 W, and $\phi_{pri} = 1.2$, $\phi_{ovr} = 0.8$ and $L_{QZ} = 20\ mm$. Both mechanisms coincide, for all cases considered, in predicting zero level of NH_3 and H_2 in the flue gases exiting the RQL system, which implies that a full conversion of both species has occurred. So there is no need to represent the latter values graphically. The general trend is that NO_x emissions increase with increasing value of x_{NH_3}, except for the case of $x_{NH_3} = 0.9$ and $TI = 1900\ W$, where the results obtained for each mechanism show opposite tendencies. Considering Figure 4.11a, for 2800 W, one can observe the Stagni mechanism predicts a steeper increase in NO_x emissions from x_{NH_3} = 0.7 to x_{NH_3} = 0.8, then maintaining the increase but now slight from x_{NH_3} = 0.8 to x_{NH_3} = 0.9. In contrast, the Glarborg mechanism predicts nearly equal output NO_x levels for x_{NH_3} = 0.7 and x_{NH_3} = 0.8, with a steeper increase for x_{NH_3} = 0.9. The Stagni mechanism

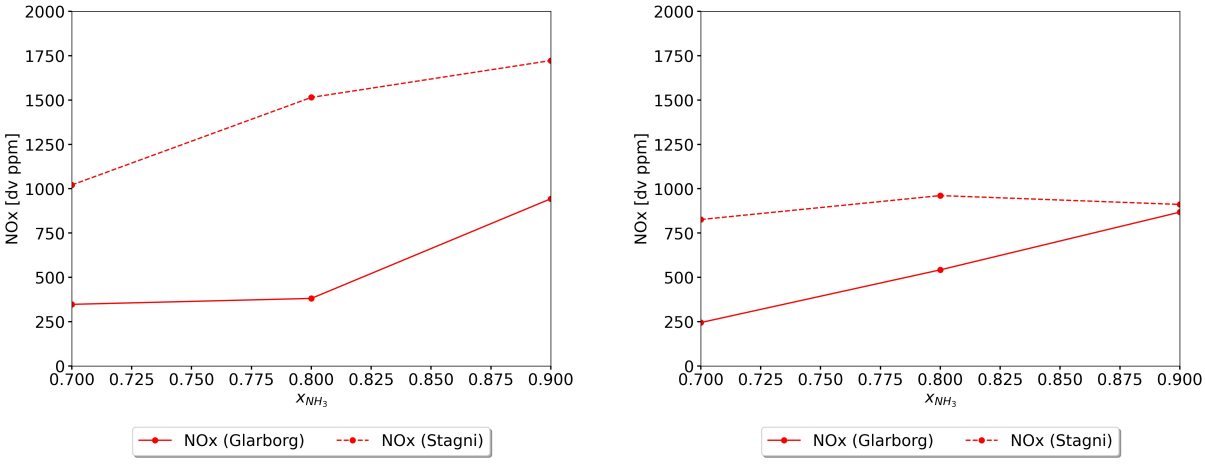

(a) (b)

Figure 4.11: Emissions for $\phi_{pri} = 1.2$, $\phi_{ovr} = 0.8$, $L_{QZ} = 20\ mm$. TI: (a) 2800 W and (b) 1900 W.

predicts, for all cases, higher exit NO_x levels than those predicted by the Glarborg mechanism.

It is important to note that, as shown in Section 4.2, the predictions of the Glarborg mechanism always indicated lower amounts of unburned NH_3 at the exit of the rich stage than the Stagni mechanism, the latter being closer to the experimental one. One can thus think that the prediction given by the Stagni mechanism is the most reliable, since it is the one that best reflects what happens in the first stage. Logically, the lower the mole fraction of unburned NH_3 at the exit of the rich stage and at the entrance of the lean stage, the less the fuel-NO pathway will be favored in the lean stage.

The increase in the mole fraction of NH_3 in the fuel (x_{NH_3}) will increase the mole fraction of unburned NH_3 of the rich stage and therefore also at the entrance of the poor stage. In this stage there is combustion of the remaining NH_3 and H2, with a corresponding favoring of the fuel-NO pathway, as well as the promotion of SNCR reactions. In addition, it is expected that the decrease in temperature associated with the increase in x_{NH_3} also has some effect, although it is not easy to evaluate its relevance, since the thermal-NO pathway is not the most predominant one. Thus, one can observe, especially for the graphs of the Stagni mechanism, how the increase of NO_x for higher x_{NH_3} can reflect the predominance of NO_x production via fuel-NO and how, starting from x_{NH_3} = 0.8, the slightest increase of NO_x for 2800 W as well as the slight decrease for 1900 W already show an important effect of the decrease of NO_x via SNCR reactions. The results predicted by the Glarborg mechanism seem to have a ”delay” when compared to those of Stagni, most likely due to the fact that only with higher values of x_{NH_3} that mechanism is able to make predictions that would be expected for lower values of x_{NH_3}, were it not for the exaggerated conversion of NH_3 always assumed by this mechanism.

As for the effect of thermal input, it is notable from the graph of the Stagni mechanism that the increase in power is related to the increase in NO_x in the flue gases, an increase that is more pronounced for higher values of x_{NH_3}. For the Glarborg mechanism the results are inconclusive about this effect. Taking all this

into account and from a point of view of reducing pollutant emissions, it is expected that, of the cases analyzed, the one with x_{NH_3} = 0.7 is the most favorable. This decision will have to be made depending on the objectives that are intended with the operation of the RQL burner.

4.4.2 Parametric analysis of ϕ_{pri}

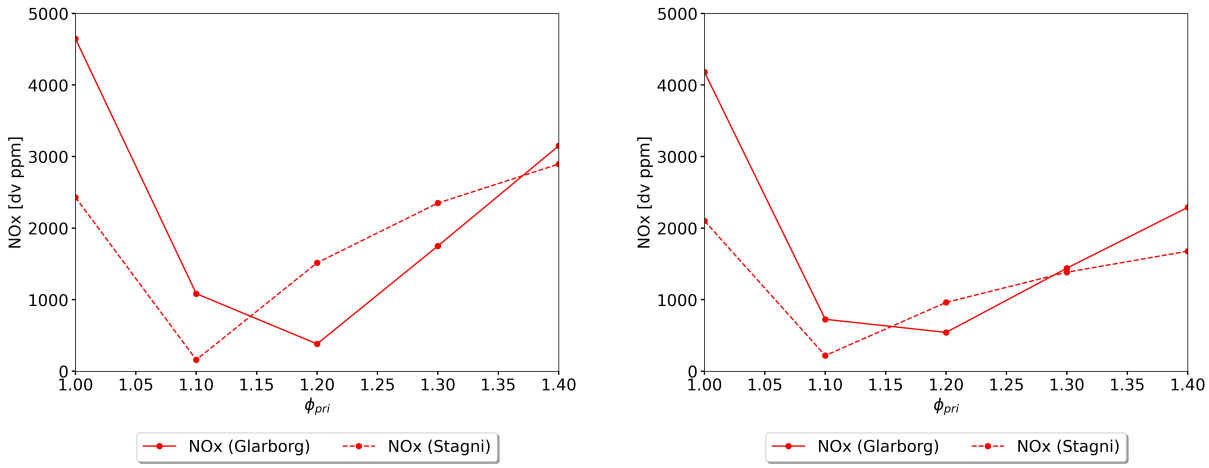

(a) (b)

Figure 4.12: Emissions for $x_{NH_3} = 0.8$, $\phi_{ovr} = 0.8$, $L_{QZ} = 20\ mm$. TI: (a) 2800W and (b) 1900W.

Figure 4.12 presents the impact of varying the ϕ_{pri} parameter on the main pollutant emissions for $x_{NH_3} = 0.8$, $\phi_{ovr} = 0.8$ and $L_{QZ} = 20\ mm$ and the two thermal inputs of 2800 W and 1900 W. Both mechanisms agree on predicting zero NH_3 and H_2 emissions at the burner exit, implying their full conversion, and thus these values are not shown graphically. Both mechanisms point to a minimum, and therefore optimal among those considered, level of NO_x emissions for relatively close values of ϕ_{pri}: 1.1 for the Stagni mechanism and 1.2 for the Glarborg mechanism. The sharp decrease of NO_x in the combustion products for small values of equivalence ratio in the rich regime has to do with the fact that the worse ammonia conversion efficiency, for increasing equivalence ratio in the considered regime, results in lower NO_x production in the rich stage as well as a higher mole fraction of unburned NH_3 to be converted in the lean stage by the fuel-NO pathway and the SNCR reactions. For equivalence ratios close to stoichiometric, it is notable from the figures that the NO_x production in the rich stage is dominant in terms of the overall NO_x production in the burner, this decreasing mainly with increasing equivalence ratio, which will decrease the NH_3 conversion efficiency. From a certain equivalence ratio, it can be seen how the NO_x production particularly occurs in the lean stage, through the conversion of unburnt NH_3 via the fuel-NO pathway, and thus increasing the NO_x level with the increasing equivalence ratio. Regarding SNCR reactions, it can also be pointed out the these reactions may be a main reason for the observed concave downward curve of NO_x emissions with the increasing of the equivalence ratio, since the increasing of unburnt mole fraction of NH_3 in lean stage may enhance those reactions for the NO_x reduction. Comparing the cases for the two different thermal inputs, it is notable that the optimum points predicted by both mechanisms remain unchanged, with an overall decrease in NO_x for increasing

equivalence ratio for larger thermal inputs.

Due to the already known track record of the Glarborg mechanism in the predictions of this model, we are led to consider that the Stagni mechanism prediction will be the closest to reality. Furthermore, the same ”delay” that was noticeable in the NO_x profile of the Glarborg mechanism prediction for the previously studied parameter (x_{NH_3}) is noticeable for this case as well. Thus, it can be concluded from the results presented here that $\phi_{pri} = 1.1$ seems to be the most satisfactory equivalence ratio for the first stage. It is worth recalling that other authors [28, 30] have also pointed, for their respective operating conditions, to values of ϕ_{pri} equal to 1.1 and 1.2.

4.4.3 Parametric analysis of ϕ_{ovr}

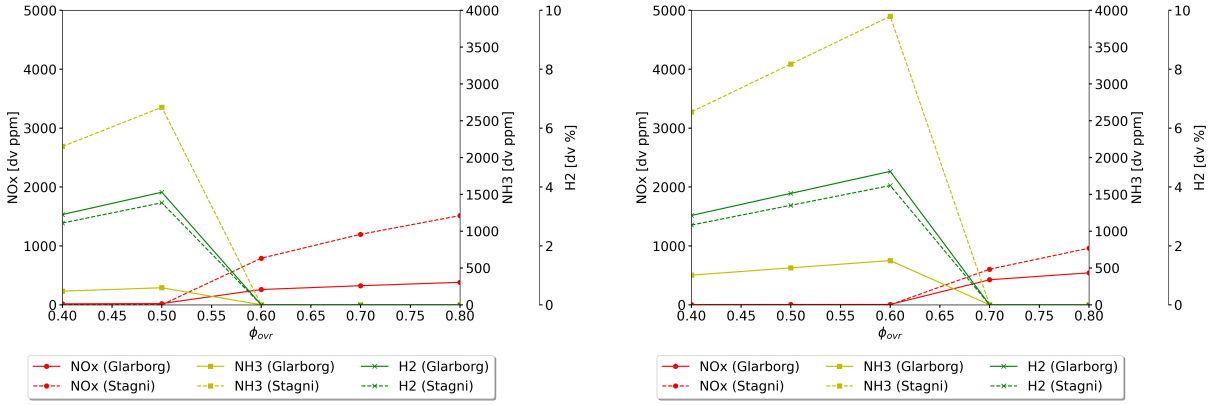

(a) (b)

Figure 4.13: Emissions for $x_{NH_3} = 0.8$, $\phi_{pri} = 1.2$, $L_{QZ} = 20\ mm$. TI: (a) 2800 W and (b) 1900 W.

The predicted impact of the ϕ_{ovr} parameter on the emissions at the exit of the RQL system can be analyzed using Figures 4.13a and 4.13b, for $x_{NH_3} = 0.8$, $\phi_{pri} = 1.2$ and $L_{QZ} = 20\ mm$ and the two thermal inputs of 2800 W and 1900 W. The first aspect that stands out is the large mole fractions of NH_3 and H_2 present at the combustor exit for smaller values of ϕ_{ovr}. This appears to be due to non ignition of unburnt NH_3 and H_2 in the LZ caused by the greater amount of air - for decreasing equivalence ratio - entering the QZ, which is at relative low (room) temperature. Thus, the large NH_3 and H_2 mole fractions at the combustor exit, as well as the almost zero NO_x emissions. Experimental tests have shown that the low flammability limit decreases for lower thermal inputs [37, 59]. Despite that, it seems from these predictions that the ignition takes place for lower values of ϕ_{ovr} with greater thermal input, apparently counteracting the latter empirical statement. A possible reason for this result can be advanced: since the ignition being considered takes place in the second stage, the conditions at the entrance of this stage will be those imposed by the combustion performance in the first stage. For the same ϕ_{pri} and x_{NH_3} and different thermal inputs, it is expected that for the higher thermal input there will be a higher temperature at the exit of the first stage, due to the higher initial amount of H_2 and NH_3 in the fuel. Thus, the higher temperature, for a higher thermal input, at the entrance of the second stage will facilitate the ignition of unburned NH_3 and H_2 for lower ϕ_{ovr} values, since the higher temperatures prevent the heat loss rate.

From the predicted value of ϕ_{ovr} at which ignition occurs, both mechanisms agree in predicting increasing NO_x concentration in the flue gas for increasing equivalence ratio, with the Stagni mechanism being the one that predicts higher values, as has already been a constant in previous studies. This increase seems to be especially associated with the temperature increase that occurs as the stoichiometry approaches, so that the main pathway of NO_x production should be the thermal-NO mechanism. Both mechanisms also coincide in predict zero NH_3 and H_2 emissions when combustion is attained at lean stage. Although not shown graphically here, it may be interesting to note that in preparing this particular study it was noted how the value of U_{ovr} considered for QZ and LZ has a relevant impact for the ϕ_{ovr} at which ignition starts. That is, for different values of the U_{ovr} used for this case, ignition can happen for higher or lower values of ϕ_{ovr}. The coefficient values used are tabulated in the Appendix B. Thus, for the reasons given, it seems logical to consider as the most satisfactory value the minimum ϕ_{ovr} for which there is ignition in the secondary stage, that is, 0.6 for 2800 W and 0.7 for 1900 W, according to the predicted values.

4.4.4 Parametric analysis of L_{QZ}

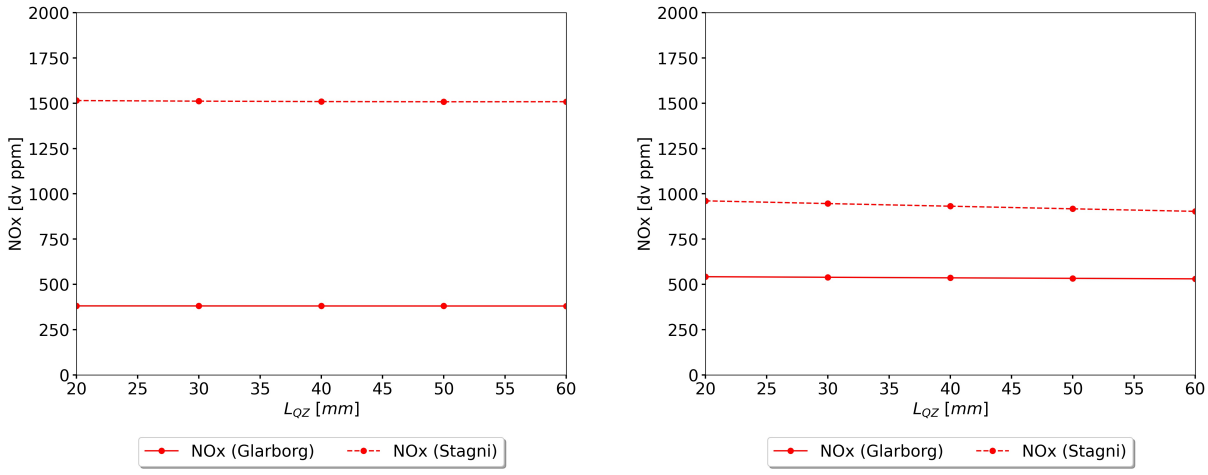

(a) (b)

Figure 4.14: Emissions for $x_{NH_3} = 0.8$, $\phi_{pri} = 1.2$, $\phi_{ovr} = 0.8$. TI: (a) 2800 W and (b) 1900 W.

Figure 4.14 show the influence of varying the parameter L_{QZ}. As can be seen, this parameter does not have much impact on the burner emissions as predicted by the model using both the Glarborg and Stagni mechanisms, although for increasing L_{QZ} it appears to decrease the emissions slightly, perhaps due to the increased residence time in the Quench stage, which allows for better dilution and decreased temperature, resulting in a very residual decrease in NOx. The model predicts complete conversion of NH_3 and H_2 for all values of L_{QZ} tested.

Comparing the results for the two thermal inputs we can see that NO_x emissions decrease with the decreasing of the thermal input when predicted by the Stagni mechanism, although the opposite happens

if the Glarborg mechanism is used. For the Stagni mechanism, the explanation may lie in the fact for an increasing thermal input, due to the larger NH_3 quantity present and the typical high temperatures it is likely to suppose an increasing NO_x emissions level, promoted by both thermal and fuel-NO pathways. On the other hand, for the Glarborg mechanism, the global increase of NO_x with the decrease of the thermal input can be associated with the prediction of a larger quantity of unburned NH_3 for a lower calorific value, which will promote more NO_x in the second stage through the fuel-NO pathway. As stated before, given the best prediction of the Stagni mechanism for the previous studies, the predictions of this mechanism were also considered to be the most reliable in this case.

4.4.5 RQL system validation

As described in Section 3.2.5, the method used in the theoretical validation of the RQL system consists of confronting its predictions with the numerical results for the single-stage model as well as with experimental results that are appropriate for comparison. The conditions under which this comparison can be made in a more reliable way were also specified in the mentioned Section. The results obtained can be seen in Figures 4.15 and 4.16, for thermal inputs of 2800 W (and single rich stage) and 1900 W (and single lean stage), respectively.

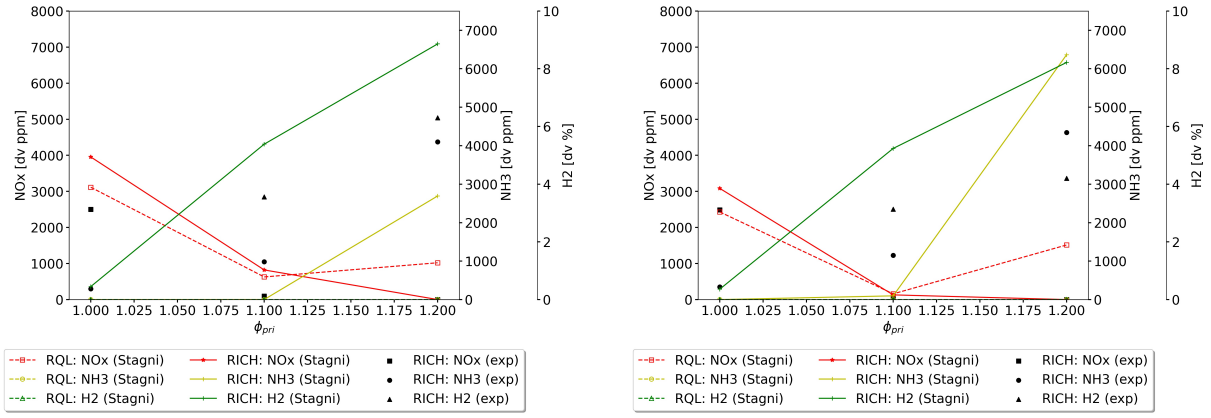

(a) (b)

Figure 4.15: Emissions for experimental and numerical single rich stage versus RQL. $TI = 2800\ W$, $\phi_{ovr} = 0.8$ and x_{NH_3} of (a) 0.7 and (b) 0.8.

It can be observed how the trends for both x_{NH_3} values considered are according with the variation that was previously analyzed on the x_{NH_3} parametric study. Considering now the comparison of the predicted emissions for the RQL burner and the experimental and predicted emissions for the single-stage rich burner (Figure 4.15), it can be observed how predicted NO_x emissions for RQL model are smaller than those predicted for single rich stage model, using both mechanisms, but always higher than experimental NO_x. This is expected due to the fact that NO_x at the exit of a single rich stage is generally smaller than at the exit of an RQL system, due to the NH_3 and H_2 combustion taking place on second stage, unless an higher NH_3 conversion than expected is predicted in the rich stage, as what is actually happening for the single rich stage predictions. This means that, for a proper NH_3 conversion predic-

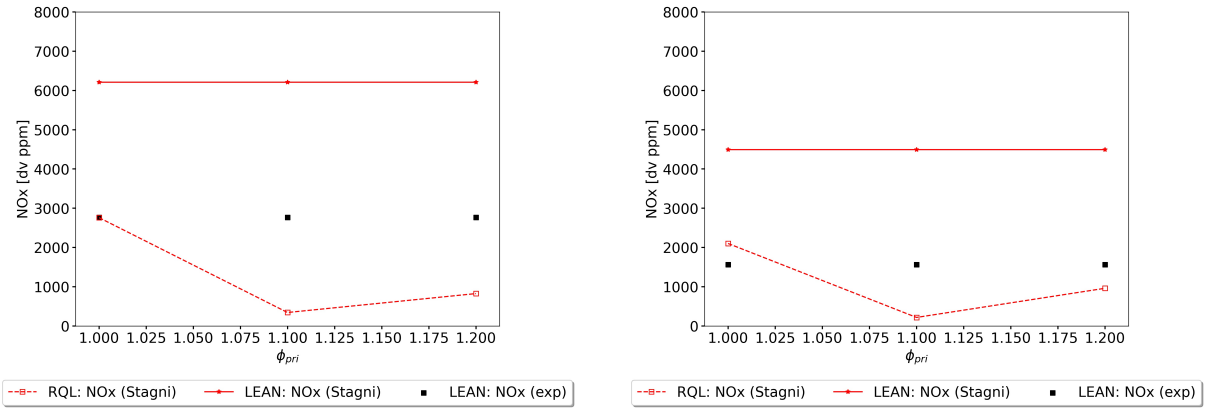

(a) (b)

Figure 4.16: Emissions for experimental and numerical single lean stage versus RQL. $TI = 1900\ W$, $\phi_{ovr} = 0.8$ and x_{NH_3} of (a) 0.7 and (b) 0.8.

tion in rich stage, NO_x emissions at the single rich stage exit would be smaller than those exiting RQL system. In terms of unburnt NH_3 and H_2 at the exit of the RQL system, zero emissions are predicted for all conditions, which confirms one of the main advantages of RQL system and shows an improved combustion efficiency.

Regarding the comparison between predicted RQL flue gas results with those for the numerical and experimental single lean stage (Figure 4.16) - that, in an overall perspective, has the same conditions (ϕ_{ovr}) - one can conclude that the prediction values seems to corroborate the effectiveness of the RQL system in terms of pollutant emissions reduction. Predicted NO_x from RQL system flue gas is much lower than that predicted from single lean stage model and considerably lower than experimental, except for the stoichiometric burning in the first stage. Even considering the underlying model uncertainties, the predicted NO_x emissions for the RQL system are sufficiently lower than the experimental ones for the single lean stage combustor, thus allowing a good margin for uncertainty without affecting the verification of the effectiveness of the RQL system. The continued trend in over-prediction of NO_x can serve in this case as an advantageous safety coefficient for this predicted value of NO_x at the exit of the RQL combustor.

Finally it might be interesting to indicate that the simulation of the first four parametric studies together had a duration of approximately 112 minutes, without any effort on the computational efficiency of the simulation and at a normal computer operation. The simulation generating the shown data for the RQL validation against experiments and single-stage model took approximately 30 minutes. This is quite relevant since the fast results are one of the major advantages of the CRN approach over CFD simulations. For the latter ones, it would be almost unthinkable to develop this kind of parametric studies in due time.

Chapter 5

Closure

5.1 Conclusions

Throughout this thesis, a numerical CRN model was proposed, developed and analyzed, based on the theory of perfect-mixture chemical reactors and using two detailed chemistry validated mechanisms, in order to study the main pollutant emissions from a swirl and bluff-body stabilized burner fueled by NH_3/H_2 blend. A theoretic prediction of the implementation and operation of a RQL system in that burner was also developed, through the addition of two additional stages, Quench and Lean. The main emission trends caused by the variation of several available parameters were also analyzed, as well as their relevance. Having accomplished this, some conclusions can be drawn from this work and are summarized below.

Regarding the chemical reactor model developed:

- The chemical reactor network model developed proved to correctly predict the trends of all profiles with the variation of ϕ, x_{NH_3} and TI, in accordance with the same trends presented in the experimental. This allows to evaluate the impact of different initial conditions for each flame.

- The model have frequently shown over-predicted values of NH_3 conversion, leading to over-prediction of NO_x mole fractions as well as H_2 mole fraction from NH_3 cracking. This was justified mainly because of (1) the theoretic assumption of perfect mixing, in which chemical reactor models are grounded, leading to almost complete combustion earlier than expected; (2) the yet overall over-prediction of NH_3 reactivity by the chemical kinetic mechanisms available on literature and used in this work; (3) some inaccuracy of the flow splitting method; and (4) slight difference in test conditions between experimental and numerical works;

- The developed CRN model proved to correctly simulate the NO_x reduction along the PFZ for richer flames but not for stoichiometric or lean flames. This result suggests the difficulty of modeling NO_x abatement, especially through the SNCR reactions, most likely due to the fact that the perfect-mix reactor assumption accelerates the consumption of ammonia, which is less available for the aforementioned reactions.

- For all flames tested numerically and compared with experimental values the Stagni mechanism proved to be the one that best reflected the expected values and trends, in contrast to the Glarborg mechanism that always over-predicted the reactivity of NH_3 as well as the amounts of NO_x present in the flame. For each mechanism predictions and for each different set of measurements an relative average error was calculated.

- Having performed CRN simulations in Cantera software (Python interface) with two detailed chemical kinetic mechanisms, Glarborg et al. [47] (151 species and 1397 reactions) and Stagni et al. [49] (31 species and 203 reactions), the time required for those simulations has proven to be quite low, even for parametric studies that required that that a flame simulation was performed for each different set of test conditions. This confirms the efficiency and speed of using a CRN model.

Regarding the implementation of Rich-Quench-Lean strategy:

- According to the developed model, the implementation of a Rich-Quench-Lean system in the current burner would be advantageous regarding the reduction of NO_x, NH_3 and H_2 emissions, for the best predicted conditions of $x_{NH_3} = 0.8$, $\phi_{ovr} = 0.7$, $\phi_{pri} = 1.1 - 1.2$.

- The effectiveness of using the RQL combustor concept with respect to pollutant emissions depends mainly on the parameter ϕ_{pri}, with emissions being minimal for a specific value of this parameter, which is confirmed by the literature. According to the predictions of the developed model this value is close to 1.1.

- In order for the implementation of the two new stages - Quench and Lean - to be successful, it must be taken into account the maximum heat losses reduction in these stages as much as possible, so as to ensure that in the Lean stage the effluent gases from the first stage are re-ignited. The model predicted lower NO_x emissions for lower ϕ_{ovr}, and thus near the low flammability limit.

- The best ϕ_{ovr} to be used in the RQL system for minimizing pollutant emissions is the minimum value from which ignition in the Lean stage can be guaranteed. This ϕ_{ovr} value is predicted to be lower the higher the thermal input, most likely due to the fact that the higher temperatures are a support for the re-ignition of unburned fuels in the secondary stage.

5.2 Future Work

The first and most relevant suggestion for future work is the development and implementation of a second stage (Quench and Lean) for the NH_3/H_2 burner currently existing in the IDMEC laboratory, using some of the conclusions predicted by this work as a reference, and thereby also testing its validity.

To improve CRN modeling it is necessary to come up with alternatives that allow more accurate modeling of zones in the flame where combustion is not complete, perhaps through the combined use of reactors

with and without activated chemical reactions (which could be an approximation to the Partially-Stirred Reactor (PaSR) model, not yet available in Cantera package), or modeling the Flame Zone through a Plug-Flow Reactor, where the residence time in each reactor is quite small. New ways of implementation in Cantera should be studied and developed as the currently existing ones do not allow easy modeling of these interconnected zones.

In relation to the developed modeling certain practical issues can also be further developed. The mass transfer modeling could be generated in a more efficient way, by defining an objective function for a routine that could find the best combination of flow splitting coefficients (α_1 to α_5). The objective function could be defined as function of the relative average error, which equation was presented in this work.

A rate of production analysis would also be very useful for a better knowledge of the underlying chemical processes predicted by the used mechanisms in each of the reactors in the CRN and for a better evaluation of some of the explanatory hypotheses raised throughout this text.

Also the heat transfer in the flames could be further studied for the improvement of this simulation, perhaps through measurements of the heat flux leaving the combustor or with better modeling of the heat transfer that exists between the various reactors that model the flame.

References

[1] International Energy Agency - IEA, 2021. URL https://www.iea.org/. Consulted on: 27/10/2021.

[2] X.-L. YUE and Q.-X. GAO. Contributions of natural systems and human activity to greenhouse gas emissions. *Advances in Climate Change Research*, 9(4):243–252, 2018.

[3] Global Carbon Project (GCP): Homepage. URL https://www.globalcarbonproject.org/. Consulted on: 3/11/2021.

[4] H. Kobayashi, A. Hayakawa, K. Somarathne, and E. C. Okafor. Science and technology of ammonia combustion. *Proceedings of the Combustion Institute*, 37(1):109–133, 2019.

[5] Z. Wan, Y. Tao, J. Shao, Y. Zhang, and H. You. Ammonia as an effective hydrogen carrier and a clean fuel for solid oxide fuel cells. *Energy Conversion and Management*, 228:113729, 2021.

[6] A. Valera-Medina, F. Amer-Hatem, A. K. Azad, I. C. Dedoussi, M. de Joannon, R. X. Fernandes, P. Glarborg, H. Hashemi, X. He, S. Mashruk, J. McGowan, C. Mounaim-Rouselle, A. Ortiz-Prado, A. Ortiz-Valera, I. Rossetti, B. Shu, M. Yehia, H. Xiao, and M. Costa. Review on ammonia as a potential fuel: From synthesis to economics. *Energy & Fuels*, 35(9):6964–7029, 2021.

[7] W. Henry. Experiments on ammonia, and an account of a new method of analyzing it, by combustion with oxygen and other gases. *Philosophical Transactions of the Royal Society of London*, 99:430–449.

[8] E. Krock. Ammonia: A fuel for motor buses. *Journal of the Institute of Petroleum*, 31:213–223, 1945.

[9] W. Cornelius, L. W. Huellmantel, and H. R. Mitchell. Ammonia as an engine fuel. *SAE International*, February .

[10] U. Army. Discussion of papers 650050 (p. 274), 650051 (p. 281). and 650052 (p. 300). URL http://www.alternatewars.com/Fiction/SF_Tech/SP-263_Discussion.htm.

[11] E. S. Starkman and G. S. Samuelsen. Flame-propagation rates in ammonia-air combustion at high pressure. *Symposium (International) on Combustion*, 11(1):1037–1045, 1967.

[12] D. T. Pratt. Performance of ammonia-fired gas-turbine combustors. *Technical Report No. 9, University of California*, 1967.

[13] F. J. Verkamp, M. C. Hardin, and J. R. Williams. Ammonia combustion properties and performance in gas-turbine burners. *Symposium (International) on Combustion*, 11(1):985–992, 1967.

[14] A. J. Reiter and S. C. Kong. Demonstration of compression-ignition engine combustion using ammonia in reducing greenhouse gas emissions. *Energy & Fuels*, 22(5):2963–2971.

[15] A. J. Reiter and S.-C. Kong. Combustion and emissions characteristics of compression-ignition engine using dual ammonia-diesel fuel. *Fuel*, 90(1):87–97, January 2011.

[16] C. Mørch, A. Bjerre, M. Gøttrup, S. Sorenson, and J. Schramm. Ammonia/hydrogen mixtures in an SI-engine: Engine performance and analysis of a proposed fuel system. *Fuel*, 90(2):854–864, 2011.

[17] K. Ryu, G. E. Zacharakis-Jutz, and S.-C. Kong. Performance enhancement of ammonia-fueled engine by using dissociation catalyst for hydrogen generation. *International Journal of Hydrogen Energy*, 39(5):2390–2398, 2014.

[18] D. C. Dayton and T. D. Foust. Chapter nine - optimized biofuels for high-efficiency, low-emission engines. In D. C. Dayton and T. D. Foust, editors, *Analytical Methods for Biomass Characterization and Conversion*, Emerging Issues in Analytical Chemistry, pages 129–145. Elsevier, 2020. ISBN 978-0-12-815605-6.

[19] T. Meyer, P. Kumar, M. Li, K. Redfern, and D. Diaz. Ammonia combustion with near-zero pollutant emissions. NH3 Congress: Iowa, USA, Iowa State University 2011.

[20] N. Iki, O. Kurata, T. Matsunuma, T. Inoue, M. Suzuki, T. Tsujimura, and H. Furutani. Micro gas turbine firing kerosene and ammonia. 8: Microturbines, Turbochargers and Small Turbomachines; Steam Turbines, June 2015.

[21] O. Kurata, N. Iki, T. Matsunuma, T. Inoue, T. Tsujimura, H. Furutani, H. Kobayashi, and A. Hayakawa. Performances and emission characteristics of NH_3–air and NH_3/CH_4–air combustion gas-turbine power generations. *Proceedings of the Combustion Institute*, 36(3):3351–3359, 2017.

[22] A. Hayakawa, Y. Hirano, E. C. Okafor, H. Yamashita, T. Kudo, and H. Kobayashi. Experimental and numerical study of product gas characteristics of ammonia/air premixed laminar flames stabilized in a stagnation flow. *Proceedings of the Combustion Institute*, 38(2):2409–2417, 2021.

[23] A. Valera-Medina, M. G. Božo, H. Xiao, D. Pugh, A. Giles, B. Goktepe, R. Marsh, and P. Bowen. Premixed ammonia/hydrogen swirl combustion under rich fuel conditions for gas turbines operation. *International Journal of Hydrogen Energy*, 44(16):8615–8626, 2019.

[24] A. Valera-Medina, D. Pugh, P. Marsh, G. Bulat, and P. Bowen. Preliminary study on lean premixed combustion of ammonia-hydrogen for swirling gas turbine combustors. *International Journal of Hydrogen Energy*, 42(38):24495–24503, 2017.

[25] Z. Tian, Y. Li, L. Zhang, P. Glarborg, and F. Qi. An experimental and kinetic modeling study of premixed $NH_3/CH_4/O_2$/ar flames at low pressure. *Combustion and Flame*, 156(7):1413–1426, 2009.

[26] S. A. Mosier and R. M. Pierce. Advanced combustor systems for stationary gas turbine engines, phase i. review and preliminary evaluation. Contract 68-02-2136 Volume I, U.S. Environmental Protection Agency, 1 1980.

[27] A. S. Feitelberg and M. A. Lacey. The GE rich-quench-lean gas turbine combustor. *Journal of Engineering for Gas Turbines and Power*, 120(3):502–508, 07 1998.

[28] K. D. Somarathne, S. Hatakeyama, A. Hayakawa, and H. Kobayashi. Numerical study of a low emission gas turbine like combustor for turbulent ammonia/air premixed swirl flames with a secondary air injection at high pressure. *International Journal of Hydrogen Energy*, 42(44):27388–27399, 2017.

[29] O. Kurata, N. Iki, T. Inoue, T. Matsunuma, T. Tsujimura, H. Furutani, M. Kawano, K. Arai, E. C. Okafor, A. Hayakawa, and H. Kobayashi. Development of a wide range-operable, rich-lean low-NO_x combustor for NH_3 fuel gas-turbine power generation. *Proceedings of the Combustion Institute*, 37 (4):4587–4595, 2019.

[30] E. C. Okafor, K. D. Somarathne, A. Hayakawa, T. Kudo, O. Kurata, N. Iki, and H. Kobayashi. Towards the development of an efficient low-no$_x$ ammonia combustor for a micro gas turbine. *Proceedings of the Combustion Institute*, 37(4):4597–4606, 2019.

[31] S. Mashruk, H. Xiao, and A. Valera-Medina. Rich-quench-lean model comparison for the clean use of humidified ammonia/hydrogen combustion systems. *International Journal of Hydrogen Energy*, 46(5):4472–4484, 2021.

[32] A. A. Perpignan, A. G. Rao, and D. J. Roekaerts. Flameless combustion and its potential towards gas turbines. *Progress in Energy and Combustion Science*, 69:28–62, 2018.

[33] V. Fichet, M. Kanniche, P. Plion, and O. Gicquel. A reactor network model for predicting nox emissions in gas turbines. *Fuel*, 89(9):2202–2210, 2010.

[34] S. Trespi, H. Nicolai, P. Debiagi, J. Janicka, A. Dreizler, C. Hasse, and T. Faravelli. Development and application of an efficient chemical reactor network model for oxy-fuel combustion. *Energy & Fuels*, 35(9):7121–7132, 2021.

[35] M. C. Franco, R. C. Rocha, M. Costa, and M. Yehia. Characteristics of NH_3/H_2/air flames in a combustor fired by a swirl and bluff-body stabilized burner. *Proceedings of the Combustion Institute*, 38(4):5129–5138, 2021.

[36] R. C. Rocha, G. P. Pacheco, M. A. A. Mendes, E. C. Fernandes, P. J. Coelho, and X. S. Bai. Numerical and experimental characterization of partially premixed NH_3/H_2/air flames on a laboratory scale combustor.

[37] G. P. Pacheco, R. C. Rocha, M. C. Franco, M. A. A. Mendes, E. C. Fernandes, P. J. Coelho, and X.-S. Bai. Experimental and kinetic investigation of stoichiometric to rich NH_3/H_2/air flames in a swirl and bluff-body stabilized burner. *Energy & Fuels*, 35(9):7201–7216, 2021.

[38] J. A. Miller and C. T. Bowman. Mechanism and modeling of nitrogen chemistry in combustion. *Progress in Energy and Combustion Science*, 15(4):287–338, 1989.

[39] A. A. Konnov and J. de Ruyck. Kinetic modeling of the thermal decomposition of ammonia. *Combustion Science and Technology*, 152(1):23–37, 2000.

[40] A. A. Konnov and J. de Ruyck. A possible new route for no formation via n_2h_3. *Combustion Science and Technology*, 168(1):1–46, 2001.

[41] A. A. Konnov. Implementation of the ncn pathway of prompt-no formation in the detailed reaction mechanism. *Combustion and Flame*, 156(11):2093–2105, 2009.

[42] S. J. Klippenstein, L. B. Harding, P. Glarborg, and J. A. Miller. The role of NNH in NO formation and control. *Combustion and Flame*, 158(4):774–789, 2011.

[43] J. A. Miller and P. Glarborg. Modeling the thermal De-NO_x process: Closing in on a final solution. *International Journal of Chemical Kinetics*, 31(11):757–765, 1999.

[44] Y. Song, H. Hashemi, J. M. Christensen, C. Zou, P. Marshall, and P. Glarborg. Ammonia oxidation at high pressure and intermediate temperatures. *Fuel*, 181:358–365, 2016.

[45] J. Otomo, M. Koshi, T. Mitsumori, H. Iwasaki, and K. Yamada. Chemical kinetic modeling of ammonia oxidation with improved reaction mechanism for ammonia/air and ammonia/hydrogen/air combustion. *International Journal of Hydrogen Energy*, 43(5):3004–3014, 2018.

[46] H. Nakamura, S. Hasegawa, and T. Tezuka. Kinetic modeling of ammonia/air weak flames in a micro flow reactor with a controlled temperature profile. *Combustion and Flame*, 185:16–27, 2017.

[47] P. Glarborg, J. A. Miller, B. Ruscic, and S. J. Klippenstein. Modeling nitrogen chemistry in combustion. *Progress in Energy and Combustion Science*, 67:31–68, 2018.

[48] R. Li, A. A. Konnov, G. He, F. Qin, and D. Zhang. Chemical mechanism development and reduction for combustion of NH_3/H_2/CH_4 mixtures. *Fuel*, 257:116059, 2019.

[49] A. Stagni, C. Cavallotti, S. Arunthanayothin, Y. Song, O. Herbinet, F. Battin-Leclerc, and T. Faravelli. An experimental, theoretical and kinetic-modeling study of the gas-phase oxidation of ammonia. *React. Chem. Eng.*, 5:696–711, 2020.

[50] J. A. Miller, M. D. Smooke, R. M. Green, and R. J. Kee. Kinetic modeling of the oxidation of ammonia in flames. *Combustion Science and Technology*, 34(1-6):149–176, 1983.

[51] J. Zeldovich. The oxidation of nitrogen in combustion and explosions. *European Physical Journal A. Hadrons and Nuclei*, 21:577–628, 1946.

[52] S. R. Turns. *An Introduction to Combustion: Concepts and Applications*. Mechanical Engineering Series. 1996.

[53] R. K. Lyon. Thermal deno$_x$ controlling nitrogen oxides emissions by a noncatalytic process. *Environmental Science & Technology*, 21(3):231–236, 1987.

[54] P. Coelho and M. Costa. *Combustão*. 2ª edição revista edition, 2 2012. ISBN 978-972-8620-10-3.

[55] M. Pronobis. Chapter 4 - Reduction of nitrogen oxide emissions. In *Environmentally Oriented Modernization of Power Boilers*, pages 79–133. Elsevier, 2020. ISBN 978-0-12-819921-3.

[56] R. C. Rocha, M. Costa, and X.-S. Bai. Combustion and emission characteristics of ammonia under conditions relevant to modern gas turbines. *Combustion Science and Technology*, 193(14):2514–2533, 2021.

[57] G. Samuelsen. 3.2.1.3 - Rich burn, quick-mix, lean burn (rql) combustor. In R. Dennis, editor, *The Gas Turbine Handbook*, pages 227–233. U.S. Department of Energy, 2006.

[58] D. G. Goodwin, R. L. Speth, H. K. Moffat, and B. W. Weber. Cantera: An object-oriented software toolkit for chemical kinetics, thermodynamics, and transport processes.

[59] M. A. C. Franco. Ammonia combustion on a swirl and bluff body stabilized burner. Master's thesis, Instituto Superior Técnico, ULisboa, December 2020.

[60] Sundials: Suite of nonlinear and differential/algebraic equation solvers. URL `https://computing.llnl.gov/projects/sundials`.

[61] R. C. Rocha, C. F. Ramos, M. Costa, and X.-S. Bai. Combustion of NH_3/CH_4/air and NH_3/H_2/air mixtures in a porous burner: Experiments and kinetic modeling. *Energy & Fuels*, 33(12):12767–12780, 2019.

[62] C. F. L. Ramos. Ammonia combustion: Experiments and modelling. Master's thesis, Instituto Superior Técnico, December 2018.

[63] B. Rosati. Prediction of emissions from combustion systems using 0d and 1d reacting flow models - chemical reactor network modeling. Master's thesis, Delft University of Technology, December 2015.

[64] C. M. Madrid. Chemical reactor network for LDI combustor. CRN development and analysis of different fuels. Master's thesis, Delft University of Technology, July 2017.

[65] Ansys Chemkin-Pro — Chemical kinetics simulation software. URL `https://www.ansys.com/products/fluids/ansys-chemkin-pro`.

[66] R. C. da Rocha, M. Costa, and X.-S. Bai. Chemical kinetic modelling of ammonia/hydrogen/air ignition, premixed flame propagation and NO emission. *Fuel*, 246:24–33, 2019.

[67] Technical Glass Products, Inc.: Properties of fused quartz, 2021. URL `https://technicalglass.com/technical_properties/`.

[68] *Superwool Technical Manual*. Morgan - Advanced Materials. URL https://www.morganthermalceramics.com/media/1518/2_lower_thermal_conductivity_sept_14.pdf.

[69] Thermtest. Thermal conductivity of steel, May 2021. URL https://thermtest.com/thermal-conductivity-of-steel. Consulted on: 2/11/2021.

[70] F. Incropera, D. Dewitt, T. Bergman, and A. Lavine. *Fundamentals of Heat and Mass Transfer*. Sixth edition edition, 2007.

[71] P. S. Veloo and J. G. Quintiere. Convective heat transfer coefficient in compartment fires. *Journal of Fire Sciences*, 31(5):410–423, 2013.

[72] B. W. Butler. Characterization of convective heating in full scale wildland fires. VI International Conference on Forest Fire Research, 2010.

[73] L. M. Das. On-board hydrogen storage systems for automotive application. *International Journal Hydrogen Energy*, 21(9):789–800, 1996.

[74] W. Yan, K. Li, X. Huang, L. Yu, C. Lou, and Y. Chen. Online measurement of the flame temperature and emissivity during biomass volatile combustion using spectral thermometry and image thermometry. *Energy & Fuels*, 34(1):907–919, 2020.

[75] C. Brackmann, V. A. Alekseev, B. Zhou, E. Nordström, P.-E. Bengtsson, Z. Li, M. Aldén, and A. A. Konnov. Structure of premixed ammonia + air flames at atmospheric pressure: Laser diagnostics and kinetic modeling. *Combustion and Flame*, 163:370–381, 2016.

[76] C. Brackmann, E. J. K. Nilsson, J. D. Nauclér, M. Aldén, and A. A. Konnov. Formation of NO and NH in NH_3-doped CH_4+N_2+O_2 flame: Experiments and modelling. *Combustion and Flame*, 194: 278–284, 2018.

Appendix A

Additional numerical data

Reactor		P [Pa]	RT [s]	HRR [W]	T $[°C]$	O_2 $[\%]$	NO_x $[ppm]$	NH_3 $[ppm]$	H_2 $[\%]$	H_2O $[\%]$
FZ	G	101325.66	2.97e-03	1846.28	1465.1	3.60	11636.2	651.18	0.44	36.2
	S	101325.66	2.95e-03	1869.23	1478.1	3.85	6157.2	745.29	0.36	36.5
IRZ	G	101325.53	6.61e-02	5.33	1471.2	3.57	11222.3	0.94	0.02	37.4
	S	101325.53	6.57e-02	4.36	1483.0	3.84	5792.3	0.86	0.02	37.4
CRZ	G	101325.39	4.32e-03	43.49	1470.2	3.59	11471.2	4.65	0.07	37.0
	S	101325.39	4.30e-03	36.02	1479.1	3.86	6041.8	4.51	0.05	37.1
ORZ	G	101325.33	3.38e+00	0.64	1325.9	16.88	2701.5	0.02	0.00	8.8
	S	101325.33	3.35e+00	0.52	1340.1	16.95	1409.5	0.02	0.00	8.8
PFZ	G	101325.00	4.57e-01	15.39	969.8	3.64	11499.4	0.00	0.00	37.3
	S	101325.00	4.55e-01	12.84	974.7	3.91	6055.6	0.00	0.00	37.3

Table A.1: Predicted results at the outlet of each reactor for lean Flame 1. Species in dry volume.

Reactor		P [Pa]	RT [s]	HRR [W]	T $[°C]$	O_2 $[\%]$	NO_x $[ppm]$	NH_3 $[ppm]$	H_2 $[\%]$	H_2O $[\%]$
FZ	G	101325.690	2.91e-03	1849.31	1445.0	3.99	9549.7	950.13	0.35	35.2
	S	101325.690	2.89e-03	1865.36	1454.8	4.27	4354.9	1414.66	0.33	35.3
IRZ	G	101325.552	6.46e-02	5.00	1450.8	4.01	8963.6	1.55	0.02	36.2
	S	101325.552	6.43e-02	4.62	1460.2	4.26	3878.7	1.79	0.01	36.2
CRZ	G	101325.414	4.23e-03	40.43	1450.3	3.97	9371.0	7.70	0.06	36.0
	S	101325.414	4.21e-03	38.13	1458.8	4.22	4328.8	9.51	0.04	36.0
ORZ	G	101325.345	6.30e+00	0.62	1315.8	12.70	4338.0	0.03	0.00	17.7
	S	101325.345	6.25e+00	0.58	1326.7	12.83	1782.4	0.04	0.00	17.7
PFZ	G	101325.000	4.54e-01	14.35	961.5	4.03	9395.1	0.00	0.00	36.3
	S	101325.000	4.52e-01	12.58	966.5	4.28	4344.2	0.00	0.00	36.3

Table A.2: Predicted results at the outlet of each reactor for lean Flame 2. Species in dry volume.

Reactor		P [Pa]	RT [s]	HRR [W]	T $[°C]$	O_2 $[\%]$	NO_x $[ppm]$	NH_3 $[ppm]$	H_2 $[\%]$	H_2O $[\%]$
FZ	G	101325.78	2.80e-03	1840.32	1321.9	6.14	5392.1	2150.03	0.23	30.7
IRZ	G	101325.63	6.19e-02	5.92	1330.1	6.22	4544.9	5.13	0.01	31.5
CRZ	G	101325.47	4.05e-03	47.28	1331.7	6.11	5246.0	26.60	0.03	31.4
ORZ	G	101325.39	4.21e+00	0.74	1166.0	16.22	1281.1	0.25	0.00	10.2
PFZ	G	101325.00	4.22e-01	15.43	921.9	6.25	5311.1	0.00	0.00	31.5

Table A.3: Predicted results at the outlet of each reactor for lean Flame 3. Species in dry volume.

Reactor		P [Pa]	RT [s]	HRR [W]	T $[°C]$	O_2 $[\%]$	NO_x $[ppm]$	NH_3 $[ppm]$	H_2 $[\%]$	H_2O $[\%]$
FZ	G	101325.70	2.90e-03	1847.81	1431.1	3.91	7378.8	1482.06	0.34	35.3
	S	101325.70	2.90e-03	1844.53	1432.4	4.29	2854.8	3213.26	0.42	35.0
IRZ	G	101325.56	6.45e-02	5.23	1437.4	3.90	6634.7	2.66	0.02	36.3
	S	101325.56	6.44e-02	6.37	1439.9	4.11	2465.7	4.13	0.02	36.3
CRZ	G	101325.42	4.22e-03	42.18	1436.8	3.87	7225.4	13.07	0.06	36.0
	S	101325.42	4.21e-03	54.37	1444.2	4.07	3154.1	21.87	0.05	36.1
ORZ	G	101325.35	4.38e+00	0.64	1293.4	15.48	2173.1	0.06	0.00	11.7
	S	101325.35	4.37e+00	0.77	1295.9	15.55	758.0	0.12	0.00	11.7
PFZ	G	101325.00	4.48e-01	14.69	959.5	3.94	7248.8	0.00	0.00	36.3
	S	101325.00	4.46e-01	13.65	964.1	4.14	3175.0	0.00	0.00	36.3

Table A.4: Predicted results at the outlet of each reactor for lean Flame 4. Species in dry volume.

Reactor		P [Pa]	RT [s]	HRR [W]	T $[°C]$	O_2 $[\%]$	NO_x $[ppm]$	NH_3 $[ppm]$	H_2 $[\%]$	H_2O $[\%]$
FZ	G	101325.63	3.01e-03	1837.11	1521.9	1.93	7477.7	1463.68	0.73	39.4
	S	101325.63	3.01e-03	1839.54	1526.2	2.33	2874.9	3173.63	0.77	39.2
IRZ	G	101325.50	6.71e-02	6.33	1528.6	1.65	6822.4	2.12	0.05	41.1
	S	101325.50	6.69e-02	6.90	1533.4	1.86	2659.6	3.08	0.05	41.1
CRZ	G	101325.38	4.38e-03	49.07	1529.8	1.68	7393.0	10.28	0.18	40.7
	S	101325.38	4.37e-03	56.98	1538.0	1.88	3320.1	16.01	0.14	40.7
ORZ	G	101325.31	4.57e+00	0.76	1398.1	14.77	2413.9	0.03	0.00	13.2
	S	101325.31	4.55e+00	0.82	1403.5	14.84	1018.9	0.04	0.00	13.2
PFZ	G	101325.00	4.71e-01	21.91	992.6	1.68	7417.7	0.00	0.00	41.2
	S	101325.00	4.70e-01	19.04	996.5	1.88	3335.2	0.00	0.00	41.2

Table A.5: Predicted results at the outlet of each reactor for lean Flame 5. Species in dry volume.

Reactor		P [Pa]	RT [s]	HRR [W]	T $[°C]$	O_2 $[\%]$	NO_x $[ppm]$	NH_3 $[ppm]$	H_2 $[\%]$	H_2O $[\%]$
FZ	G	101325.82	2.17e-03	2600.12	1604.4	0.77	8027.7	1315.66	2.38	41.9
	S	101325.82	2.15e-03	2640.34	1623.1	0.91	3985.5	1794.11	2.17	42.3
IRZ	G	101325.65	4.83e-02	14.85	1617.6	0.06	6851.5	4.32	0.96	45.1
	S	101325.65	4.79e-02	13.70	1635.0	0.10	3334.8	3.23	0.70	45.5
CRZ	G	101325.49	3.14e-03	102.03	1626.2	0.21	7714.4	12.84	1.36	44.1
	S	101325.49	3.12e-03	93.31	1640.8	0.26	3997.3	11.13	1.11	44.6
ORZ	G	101325.41	4.87e+00	2.40	1446.9	10.66	3858.8	0.02	0.00	22.5
	S	101325.41	4.81e+00	2.08	1467.7	10.75	1951.5	0.02	0.00	22.5
PFZ	G	101325.00	3.45e-01	64.12	1020.2	0.00	75.29	0.01	0.81	45.4
	S	101325.00	3.42e-01	69.29	1032.1	0.00	3954.9	0.00	0.45	46.0

Table A.6: Predicted results at the outlet of each reactor for stoich. Flame 1. Species in dry volume.

Reactor		P [Pa]	RT [s]	HRR [W]	T $[°C]$	O_2 $[\%]$	NO_x $[ppm]$	NH_3 $[ppm]$	H_2 $[\%]$	H_2O $[\%]$
FZ	G	101325.74	2.36e-03	2377.37	1581.2	0.42	3186.6	3264.86	5.95	41.3
	S	101325.74	2.36e-03	2383.34	1586.5	0.61	1613.6	6201.14	5.76	41.2
IRZ	G	101325.59	5.26e-02	9.31	1589.9	0.00	1250.6	95.25	5.55	43.2
	S	101325.59	5.24e-02	9.57	1595.4	0.00	406.5	279.89	5.45	43.4
CRZ	G	101325.44	3.42e-03	79.20	1596.0	0.02	2290.3	128.78	5.50	43.0
	S	101325.44	3.41e-03	88.58	1605.1	0.02	992.7	319.28	5.38	43.2
ORZ	G	101325.37	2.89e+00	4.77	1430.4	15.41	1233.7	0.05	0.00	12.2
	S	101325.37	2.88e+00	4.74	1437.1	15.43	859.4	0.06	0.00	12.2
PFZ	G	101325.00	3.67e-01	21.11	1026.8	0.00	2074.7	0.77	5.50	43.3
	S	101325.00	3.66e-01	16.84	1031.1	0.00	822.1	1.16	5.39	43.5

Table A.7: Predicted results at the outlet of each reactor for rich Flame 2. Species in dry volume.

Reactor		P [Pa]	RT [s]	HRR [W]	T $[°C]$	O_2 $[\%]$	NO_x $[ppm]$	NH_3 $[ppm]$	H_2 $[\%]$	H_2O $[\%]$
FZ	G	101325.69	2.54e-03	2169.52	1541.1	0.38	1780.8	5666.40	9.24	39.7
	S	101325.69	2.55e-03	2167.76	1543.1	0.59	1018.0	12287.84	8.65	39.5
IRZ	G	101325.55	5.65e-02	7.37	1548.5	0.00	334.5	661.75	9.30	41.1
	S	101325.55	5.65e-02	8.14	1551.2	0.00	115.2	3523.82	8.88	41.3
CRZ	G	101325.41	3.68e-03	68.60	1554.6	0.01	857.3	695.93	9.19	41.0
	S	101325.41	3.68e-03	80.82	1562.0	0.03	312.3	3998.89	8.72	41.3
ORZ	G	101325.34	3.18e+00	6.94	1401.9	14.90	1133.6	0.11	0.00	13.4
	S	101325.34	3.18e+00	6.99	1405.0	14.92	852.9	0.15	0.00	13.4
PFZ	G	101325.00	3.91e-01	15.01	1022.2	0.00	438.4	37.52	9.27	41.2
	S	101325.00	3.91e-01	11.18	1025.5	0.00	1.0	2692.82	8.86	41.4

Table A.8: Predicted results at the outlet of each reactor for rich Flame 3. Species in dry volume.

Reactor		P [Pa]	RT [s]	HRR [W]	T $[°C]$	O_2 $[\%]$	NO_x $[ppm]$	NH_3 $[ppm]$	H_2 $[\%]$	H_2O $[\%]$
FZ	G	101325.83	2.15e-03	2604.00	1581.2	0.87	6155.1	2137.98	2.25	41.5
	S	101325.83	2.15e-03	2610.15	1587.5	1.20	2665.1	4196.72	2.24	41.3
IRZ	G	101325.67	4.79e-02	15.19	1595.1	0.08	4938.8	7.03	0.80	44.8
	S	101325.67	4.78e-02	16.49	1602.5	0.12	2165.4	7.69	0.62	45.1
CRZ	G	101325.50	3.12e-03	103.98	1603.5	0.23	5969.2	22.14	1.23	43.8
	S	101325.50	3.10e-03	118.89	1615.5	0.28	3097.2	27.67	1.05	44.1
ORZ	G	101325.42	4.89e+00	2.35	1412.8	10.65	2919.9	0.06	0.00	22.4
	S	101325.41	4.87e+00	2.38	1421.1	10.73	1311.4	0.07	0.00	22.4
PFZ	G	101325.00	3.44e-01	66.08	992.4	0.00	5871.0	0.00	0.64	45.1
	S	101325.00	3.42e-01	71.48	1002.6	0.00	3082.9	0.00	0.36	45.6

Table A.9: Predicted results at the outlet of each reactor for stoich. Flame 4. Species in dry volume.

Reactor		P [Pa]	RT [s]	HRR [W]	T $[°C]$	O_2 $[\%]$	NO_x $[ppm]$	NH_3 $[ppm]$	H_2 $[\%]$	H_2O $[\%]$
FZ	G	101325.76	2.36e-03	2363.17	1549.6	0.54	2484.8	5234.55	5.76	40.7
	S	101325.76	2.37e-03	2345.71	1546.5	0.88	1324.3	11558.58	5.39	40.1
IRZ	G	101325.60	5.24e-02	10.08	1559.4	0.00	711.0	207.59	5.41	42.8
	S	101325.60	5.25e-02	12.24	1558.5	0.01	235.9	1033.47	5.26	42.9
CRZ	G	101325.45	3.41e-03	88.90	1568.3	0.02	1631.5	269.28	5.36	42.5
	S	101325.45	3.39e-03	117.54	1577.6	0.04	611.9	1360.41	5.16	42.8
ORZ	G	101325.38	2.92e+00	4.87	1387.0	15.37	1138.5	0.12	0.00	12.2
	S	101325.38	2.93e+00	5.09	1385.6	15.39	781.2	0.19	0.00	12.2
PFZ	G	101325.00	3.68e-01	19.60	992.0	0.00	1415.4	1.06	5.37	42.8
	S	101325.00	3.67e-01	17.81	997.4	0.00	130.5	97.39	5.24	43.0

Table A.10: Predicted results at the outlet of each reactor for rich Flame 5. Species in dry volume.

Reactor		P [Pa]	RT [s]	HRR [W]	T $[°C]$	O_2 $[\%]$	NO_x $[ppm]$	NH_3 $[ppm]$	H_2 $[\%]$	H_2O $[\%]$
FZ	G	101325.70	2.53e-03	2150.25	1512.9	0.50	1451.3	8943.43	8.85	39.0
	S	101325.70	2.56e-03	2131.32	1508.5	0.86	925.4	20762.07	7.80	38.4
IRZ	G	101325.56	5.62e-02	8.13	1521.3	0.00	211.1	1518.96	9.05	40.7
	S	101325.56	5.65e-02	10.66	1519.6	0.01	83.3	7153.78	8.25	40.9
CRZ	G	101325.42	3.66e-03	78.07	1531.2	0.02	585.6	1672.80	8.93	40.6
	S	101325.42	3.66e-03	104.65	1538.9	0.06	248.4	8300.70	8.04	40.8
ORZ	G	101325.35	3.20e+00	7.08	1370.4	14.85	1141.2	0.21	0.00	13.3
	S	101325.35	3.20e+00	7.31	1367.5	14.87	785.4	0.36	0.00	13.3
PFZ	G	101325.00	3.87e-01	14.69	1014.3	0.00	48.2	546.53	9.04	40.8
	S	101325.00	3.87e-01	12.84	1018.8	0.00	0.2	6364.73	8.22	41.0

Table A.11: Predicted results at the outlet of each reactor for rich Flame 6. Species in dry volume.

Appendix B

Model Coefficients

		RQL Model Coefficients									
		α_1	α_2	α_3	α_4	α_5	U_{ovr_R}	$U_{ovr_{QL}}$	ϵ	$N_{PSR_{PFZ}}$	N_{PSR_L}
1	2800	0.99	0.9	0.9	0.9	0.99	8.5	5.5	0.2	100	100
	1900	0.99	0.9	0.9	0.9	0.99	7.5	5	0.2	100	100
2	2800	0.99	0.9	0.9	0.9	0.99	8.5	5.5	0.2	100	100
	1900	0.99	0.9	0.9	0.9	0.99	7.5	5	0.2	100	100
3	2800	0.99	0.9	0.9	0.9	0.99	8.5	5.5	0.2	100	100
	1900	0.99	0.9	0.9	0.9	0.99	7.5	5	0.2	100	100
4	2800	0.97	0.9	0.9	0.9	0.99	11.5	8.5	0.2	100	100
	1900	0.97	0.9	0.9	0.9	0.99	8.5	6.0	0.2	100	100
5	2800	0.99	0.9	0.9	0.9	0.99	10	7.0	0.2	100	100
	1900	0.99	0.9	0.9	0.9	0.99	8	5.5	0.2	100	100
6	2800	0.99	0.9	0.9	0.9	0.99	8.5	5.5	0.2	100	100
	1900	0.99	0.9	0.9	0.9	0.99	7.5	5	0.2	100	100
7	2800	0.99	0.9	0.9	0.9	0.99	8.5	5.5	0.2	100	100
	1900	0.99	0.9	0.9	0.9	0.99	7.5	5	0.2	100	100
8	2800	0.99	0.9	0.9	0.9	0.99	8.5	5.5	0.2	100	100
	1900	0.99	0.9	0.9	0.9	0.99	7.5	5	0.2	100	100
9	2800	0.99	0.9	0.9	0.9	0.99	8.5	5.5	0.2	100	100
	1900	0.99	0.9	0.9	0.9	0.99	7.5	5	0.2	100	100
10	2800	0.99	0.9	0.9	0.9	0.99	8.5	5.5	0.2	100	100
	1900	0.99	0.9	0.9	0.9	0.99	7.5	5	0.2	100	100
11	2800	0.99	0.9	0.9	0.9	0.99	8.5	5.5	0.2	100	100
	1900	0.99	0.9	0.9	0.9	0.99	7.5	5	0.2	100	100
12	2800	0.99	0.9	0.9	0.9	0.99	8.5	5.5	0.2	100	100
	1900	0.99	0.9	0.9	0.9	0.99	7.5	5	0.2	100	100
13	2800	0.99	0.9	0.9	0.9	0.99	8.5	5.5	0.2	100	100
	1900	0.99	0.9	0.9	0.9	0.99	7.5	5	0.2	100	100
14	2800	0.99	0.9	0.9	0.9	0.99	8.5	5.5	0.2	100	100
	1900	0.99	0.9	0.9	0.9	0.99	7.5	5	0.2	100	100
15	2800	0.99	0.9	0.9	0.9	0.99	8.5	5.5	0.2	100	100
	1900	0.99	0.9	0.9	0.9	0.99	7.5	5	0.2	100	100

Table B.1: Model coefficients estimated for RQL modeling.